INVERSION LAYER SOLAR CELL FABRICATION AND EVALUATION

Midway Report

by

R. L. Call, Principal Investigator
Electrical Engineering Department
The University of Arizona
Tucson, Arizona 85721

December 1972

JPL Contract No. 953461

to

Jet Propulsion Laboratory
California Institute of Technology

TABLE OF CONTENTS

ABSTRACT

Silicon solar cells operating with induced junctions rather than diffused junctions have been fabricated. Induced junctions were created by forming an inversion layer near the surface of the silicon by supplying a sheet of positive charge above the surface. This charged layer was supplied through three mechanisms:

1. supplying a positive potential to a transparent electrode separated from the silicon surface by a dielectric,

2. contaminating the oxide layer with positive ions, and

3. forming donor surface states that leave a positive charge on the surface.

A movable semi-infinite shadow delineated the extent of sensitivity of the cell due to the inversion region. Measurements of the response of the inversion layer cell to light of different wavelengths indicated it to be more sensitive to the shorter wavelengths of the sun's spectrum than conventional cells. The greater sensitivity occurs because of the shallow junction and the strong electric field at the surface. Theory of the conductance of the inversion layer vs. strength of the inversion layer was compared with experiment and found to match. Theoretical determinations of junction depth and inversion layer strength was made as a function of the surface potential for the transparent electrode cell.

SUMMARY

This report relates experimental and theoretical work done to demonstrate that an induced junction, formed by creating an inversion layer at the surface of a semiconductor, can be used to separate hole-electron pairs created by photons and thus can be used as a device to convert solar radiation to electrical energy.

The results of the increase in output when the inversion region is induced by a transparent electrode separated by an insulator is described. An opaque knife edge drawn across the face of the cell delineated sensitive portions of the cell and showed the area of sensitivity to increase as the inversion layer grew. The inversion layer cell was found to be more sensitive to the shorter wavelengths in the sun's spectrum than a conventional cell due to the shallower junction and the strong electric field that exists at its surface.

Cells were fabricated by contaminating the oxide layer on the cell with positive ions and thereby inducing an inversion layer in the semiconductor. Results similar to the transparent electrode cell were obtained. A decrease in cell response was found as the oxide was incrementally etched away.

Attempts to fabricate a cell using surface states as the source of positive charge were made and the results reported.

A match of theory vs. experimental results was made between the conductance of the inversion layer and the magnitude of the inversion layer. A study of the inversion region as a p-n junction and its action as a photovoltaic cell was also made.

The V-I characteristic of the inversion layer cells shows a small curve factor and therefore a low efficiency. This is due to a high constant resistance and high reverse reduction current. Both of these are not inherent in the operation of the device and can be remedied.

I. INTRODUCTION

A metallurgical p-n junction with a built-in electric field across

the depletion region can act as a collecting medium for hole-electron pairs

created by photons. The unlike charges gather on either side of the

junction and cause a potential difference across the diode. A current can

be extracted from the device at a reasonable potential difference and

therefore the device is capable of delivering power to an outside load.

Maximum power can be drawn from the diode or photovoltaic cell by adjusting

the load for maximum power transfer. Very low internal impedance is needed

to minimize the internal power consumption and raise the efficiency of the

cell. Figure 1 shows a typical V-I curve for a photovoltaic cell.

If the cell is used to convert the sun's radiation to electrical

power, the efficiency will depend on the band gap of the semiconductor

with respect to the photon energy spectrum of the sun. The efficiency will

also depend on the collection efficiency of the p-n junction, that is, the

probability of a hole-electron separation by the field at the depletion

region before recombination takes place. The collection efficiency, then,

will depend on the distance of the junction from the places of hole-electron

creation, as well as the diffusion length of the charge carriers in the semi-

conductor. A conventional p-n solar cell configuration is found in Fig. 2.

The cross section of the device is shown in the drawing with the electric

field as shown.

To obtain maximum power from the cell, certain factors arise

that require trade-offs to occur. For instance, to obtain a low internal

resistance for the n layer, and therefore little internal power loss in this

layer, a rather thick layer would be desirable. However, a thick layer

means the field of the junction is deep into the top surface and hole-electron pairs created at the surface by the short wavelength rays from the sun will have a greater chance of recombining before being collected. So the junction depth is adjusted as a compromise between the two needs.

Another similar adjustment is between the need for a heavily doped n layer for low resistance and a lightly doped n layer for a long diffusion length. Again considering the plight of the pairs produced at the surface by the short wavelength portion of the sun's spectrum.

Solar cells made in quantity for earth distances from the sun can reach efficiencies around 12%. A junction depth of .5μ and a doping of $10^{18}/cm^3$ is used to produce these cells.

Another type of p-n junction exists, however, besides the metallurgical junction. This junction is an induced junction formed by attracting electrons to the surface of a p type semiconductor and converting the surface to n type. In the metallurgical junction the p and the n are created by impurity dopants in the silicon but in the induced junction, the n is created in the p semiconductor by capacitor action. A positively charged layer is formed close to the surface but isolated from it. This positive layer will attract electrons to the surface and fill the p holes until they are all filled and the electrons left over are free electron carriers creating an n layer. A thin layer at the surface has been inverted from p to n and is therefore called the inversion layer. Thus, a transition from n to p appears at the surface. This induced p-n junction has a built-in field and a depletion region as has the metallurgical junction. Therefore, this junction should be capable of separating photon produced hole-electron pairs and, therefore, act as a photovoltaic cell or solar cell.

The inversion layer cell has a distinct advantage over the conventional cell, however. Whereas the electric field of the conventional cell exists only at the junction, which might be comparatively deep beneath the surface so that no field exists at the surface, the field of the inversion layer cell originates outside the surface so the field is maximum at the surface. Thus, free charges created at the surface by ultraviolet photons are found in a high field and are aided by the force of the field on the carriers separating them faster than in the conventional cell. Therefore, the inversion cell should produce more power from the short wavelength part of the sun's spectrum because more pairs created at the surface are collected before they recombine than in the conventional cell. A cross section of the inversion layer cell is found in Fig. 3. To collect the electrons, it is necessary that n diffusions be connected to the inversion layer as shown.

The p type part of the cell below the junction is the same in both types of cells and, if the two are fabricated from the same resistivity wafer and the same thickness, the response to the long wavelength part of the sun's spectrum will be the same.

There is enough additional power in the short wavelength part of the radiation output of the sun to warrant an interest in investigating the possibility of obtaining a more efficient solar cell with the use of the induced junction. This report considers experiments performed to investigate this possibility.

The amount of additional power that might be available at the shorter wavelengths can be considered by observing the power spectrum from the sun shown in Fig. 4a. Conventional solar cells convert very little of the shorter wavelengths to useful power. Figure 4b shows the spectral response of a conventional cell. The poor response at the shorter wavelengths is due to the fact that these wavelengths create hole-electron pairs at the surface of the cell and must diffuse to the junction to be collected.. Most of them are lost by

recombination while travelling to the junction and therefore contribute nothing to the output current.

The inversion layer solar cell differs in several ways from the conventional cell with respect to the collection of hole-electron pairs created at the surface by photons from the sun in the short wavelength part of the spectrum. Most of the effective part of an inversion region is found within .1 μm of the surface and therefore represents a very shallow junction so carriers generated at the surface can be collected before recombination. Because an inversion region is formed by charges outside the surface, a high electric field exists at the surface and extends into the silicon. This field tends to aid the carrier drift to the junction and therefore shorten the time for collection. Thus, most of the holes and electrons created at the surface should be collected. If we assume that all of them are collected in the shorter wavelength region, we can add that part of the spectrum to the power converted by the inversion region solar cell.

If this is so, the response vs. spectrum curve (for equal energy input) might look like the dotted portion of Fig. 4b, where an increase in response in the shorter wavelengths as compared with the response of the conventional cell is evident. (These are not data points but an estimation of the response.) The output of both types when exposed to the energy from the sun is shown in Fig. 5. The dotted curve represents the inversion layer cell and the solid curve the conventional cell. The increase in power output for this estimated determination is roughly 10%. Thus, qualitatively, it can be seen that a greater response of the cell in the shorter wavelengths will yield a greater overall output power of the cell.

In order to induce an inversion layer in a semiconductor surface, a sheet of positive charge must be formed near the surface but isolated from it.

This can be accomplished in several ways. An obvious way is by creating a capacitor on the surface with the semiconductor as the bottom electrode. The insulator must be transparent and the top electrode must be somewhat conductive and also transparent.

Silicon oxide (quartz) is transparent over the spectrum of the sun and can be grown easily on the surface of a silicon wafer by thermal oxidation. Other insulators and other methods can be used to form a dielectric on the surface, but thermally grown SiO_2 will be used in the experiments described here.

Transparent conductors exist, but they are not of very low resistivity. Since the transparent electrode is not in the power circuit of the cell, it is not necessary that this electrode be very low resistance. A material such as tin oxide will suffice.

A positive bias applied to the transparent electrode with respect to the p semiconducting wafer of sufficient magnitude will cause an inversion layer to grow at the surface. This is one way of obtaining an induced junction and was used in fabricating cells.

Another method of obtaining positive charges above the surface is to supply ions to the SiO_2 layer on the silicon surface, either as it is growing or forcing it through the oxide surface after an oxide layer has been grown. No transparent electrode is necessary because the ions will be the source of positive charge.

Mixing a vapor strongly contaminated with a sodium compound with the oxidizing vapors such as oxygen and water vapor used to grow SiO_2 on silicon will produce an oxide rich in Na atoms and some will be ionized. Other substances can be used but Na was employed in the experiments reported here. This is another way of producing an induced junction and is part of this report.

Yet another way of obtaining a charged layer is to treat the silicon surface such that a large density of donor surface states are created. The surface represents a drastic change to the ordered crystal structure inside the bulk material and states with energies within the forbidden gap are possible if the interaction with the outside atoms and the silicon surface presents the proper properties. If these states yield an electron to the silicon bulk at the surface, a positive charge is left at the surface, the electron is trapped at the surface, and an inversion layer is formed.

Experiments on cells fabricated to bring out this means of creating an inversion region are part of this report.

A theoretical analysis of the induced junction as a solar cell will be reported. Fundamental equations normally applied to p-n junctions will be used. The boundary conditions and detailed equations peculiar to the induced junction will be applied to the fundamental equations to yield results compatible with the experimental findings.

II. TRANSPARENT ELECTRODE CELL

A drawing of the transparent electrode cell is found in Fig. 6. The positive layer is formed by applying a bias between a transparent conducting film and the silicon wafer. The conducting film and the surface of the silicon are separated by a layer of oxide thermally grown on the silicon surface.

In order to fabricate a transparent electrode cell, a method of depositing a transparent conductor had to be developed.

A. Transparent Electrode

Not many transparent substances that afford electrical conduction exist. Tin oxide is one such substance. It can be deposited as a thin film by passing fuming stannic chloride across a hot substrate in the presence of oxygen. Nitrogen is allowed to flow through a beaker containing the stannic chloride and oxygen is allowed to pass through a water bubbler before both are mixed and channelled to flow down the reaction tube. The center of the furnace tube is maintained at a temperature of 530°C. A diagram of the apparatus is shown in Fig. 7.

The wafer to be coated is inserted into the tube on a quartz carrier and positioned in the center where the reaction takes place. After a half hour pre-heat, the gas flow is initiated and the wafer subsequently coated. At the present flowrates, a five minute deposition time gives a sheet resistivity of 450 ohm/sq. A plot of deposition time vs. sheet resistivity is shown in Fig. 8.

Several slides were coated with a film of SnO_2 and subsequently, the film etched from half of each slide. Tungsten light was used to illuminate a conventional solar cell through the side of the glass slide with the tin oxide coating and then the side free of the oxide. Short circuit current ratios of .8-.9 were obtained. Thus, the light attenuation of the thin layer of tine oxide is not serious.

Since there is interest in the shorter wavelength sensitivity of the inversion layer solar cell, there should be interest in the transmission of the tin oxide in this region as well as the longer wavelengths. C. W. Morrison in his article in Applied Optics (Vol. 6, No. 3, Mar. 67, p. 573) presents a curve of transmission vs. wavelength for a deposited film of SnO_2. This curve is reproduced in Fig. 9. It is obvious that although there is some attenuation, the response of the cell will not be greatly affected in the short wavelength region.

Two solutions are used to etch the transparent conductor. One is an active HCl etch and the other is an HF solution. The HCl is made active by

adding zinc to the 1:1 H_2O - HCl solution. The etching takes place while the zinc is reacting with the HCl. This etch is selective so only the SnO_2 is removed leaving the Si or SiO_2 untouched beneath it.

The HF etch is a 6:1 solution. This will also etch SiO_2 and is, therefore, useful when both layers need to be etched together. Both of these etches are compatible with photoresist masking.

The effect of temperature on the formation of SnO_2 on Si wafers is shown in Fig. 10. The formation of a significant layer does not occur either at too low or too high temperatures. An operating temperature of 530°C was chosen because this temperature represents a somewhat flat minimum that would allow some temperature variation for consistent results.

B.   Transparent Electrode Cell

1. Large area cell

Transparent electrode inversion layer solar cells were fabricated using the standard processing techniques of the Solid State Engineering Laboratory at The University of Arizona. An outline of this process is found in Appendix I. An oxide was thermally grown and selectively etched for diffusion of n type impurities in areas shown in Fig. 11. The dimensions of this finger pattern are similar to the contact pattern of a conventional solar cell. An oxide was grown during the diffusion process. The oxide was covered with a transparent conducting coating of 450 ohm/sq. SnO_2.

Contact to the diffused areas has to be made so the transparent electrode and the SiO_2 have to be etched to the silicon in these areas. Since the inversion layers only grow beneath the transparent electrode, the transparent electrode should overlap the diffused areas to allow good contact between the inversion layer and the diffusions. Thus, a mask similar in shape to the patterns in Fig. 11, but with narrower widths was

made and used to etch the transparent electrode. If both oxides are etched together, a good possibility that deviations along the periphery will allow the transparent electrode to contact the silicon in small spots and cause leakage problems. Therefore, the silicon oxide is etched to the silicon using a mask with narrower linewidths than even the mask used to etch the transparent electrode. Thus, the silicon oxide extends beyond the tin oxide for better isolation and yet the tin oxide overlaps the diffused n regions to allow inversion to occur up to the diffusion.

Measurements were made on the cell's response to various levels of simulated radiation from a Sylvania FBE light source. A conventional solar cell previously calibrated at JPL was used to estimate the radiation level. The power to the light source was supplied through a variac so that response could be measured at different light intensities. Radiation densities from 72 mw/cm^2 to 178 mw/cm^2 were used.

The first data taken on the cell were measured with electronic apparatus shown in Fig. 12. The short circuit current was measured with a digital voltmeter across a .1 ohm resistor. The data were plotted from the points taken at different bias settings.

Leakage through the transparent electrode was measured with the μ ammeter in series with the power supply and found to be less than 0.3μ ampere at 40 volts.

The results are shown in Fig. 13. The short circuit current change is shown as a function of the change in transparent electrode bias.

At a large negative bias (-40V) the response of the cell will depend on the collection of charges from the long, narrow p-n junctions diffused in the finger pattern. This occurs because any inversion region found there will be swept away by the negative charge on the transparent

electrode leaving the diffused junctions as the only collecting medium. For -40V bias and 142 mw/cm^2 we used, the inversion layer cell responded with 27 ma of short circuit current. At 140 mw/cm^2 the calibrated conventional cell we used will respond with 133 ma of short circuit current. The collection efficiency is obviously low for the long, narrow junctions.

At zero bias on the transparent electrode the cell has a better response due to a small inversion layer normally found on high resistivity p type surfaces.

An enhancement of the response of the cell is found for positive biases. This conforms to the expected action of the cell. As the bias becomes more positive, the inversion layer builds and provides a larger area acting like a p-n junction and, therefore, more charge separation and collection.

These results show that the effect of the inversion layer does enhance the output of the cell.

I-V characteristic curves were also made on this cell showing an increase in the current but not affecting the voltage greatly. A set of curves is found in Fig. 14 for an illustration of 140 mw/cm^2. A block diagram of the apparatus arrangement used to plot the V-I curves is shown in Fig. 15. An objectionable series resistance was found in the current path of the cell, giving a slope to the lines near the zero current axis.

2. Small area cell

One of the problems encountered in the fabrication of cells stems from pin holes that cause shorts and leakage from the transparent electrode to other parts of the cell. Any hole in the oxide can expose the transparent electrode to the silicon surface. Since the density of pin holes is

not large, smaller cell sizes would increase the chance of obtaining a "good"

cell. Information gained from a smaller cell would be just as valuable as a

large 2x2 cm cell, so masks were made to reduce the size of each cell from

2x2 cm to .5 x .5 cm. This allows a matrix of 4x4 cells to be fabricated

simultaneously on a 2x2 cm wafer. Thus, from the sixteen areas some will be

pin hole free and therefore subject to close examination.

Since the area of each cell will be small, there is no need for a

multiple finger contact pattern. One contact area in the center would suf-

fice. A more useful structure can be made, however, by providing two contact

stripes so measurements can be made between them. This arrangement will be

particularly useful in the contaminated oxide and the surface state cells.

The mechanism that creates the inversion regions will be effective only in

the area between the two stripes. Therefore, a conductance measurement

between the two stripes will give an indication of the magnitude of the

inversion layer between them. Metallic contact to the top of the silicon

is made by an evaporated layer of metal (Al) etched into a grid pattern. The

space openings are .4 cm x .4 cm. Within each opening are two stripes of

metal separated by .25 cm. An n type diffusion exists under each metallic

stripe, in the p type wafer creating two p-n junctions, .35 cm long, .075 cm

wide and separated by .25 cm. A .25 cm and .35 cm layer of silicon dioxide

topped by a transparent conducting layer of tin oxide is formed on top of the

silicon between the two stripes and slightly overlapping each stripe. This

configuration is seen in Fig. 16. A cross section of the device is shown in

Fig. 17.

When a positive bias is placed between the transparent electrode

and the wafer, negative charges are attracted to the top of the silicon

between the two n diffusions. Thus, the p type wafer at the surface is converted to n type. The two n diffused stripes are thus connected together by this n layer affording conduction between them. The conductance will depend on the magnitude of the positive bias to the electrode. If a charge already exists on the silicon surface due to filled surface states or contamination, conduction will take place at zero bias. This zero bias conductance can be reduced by applying a negative bias to the transparent electrode, causing the negative charges to leave the surface and convert it back to p type. Once the semiconductor between the two n diffusions is p type, at least one reverse biased junction appears in the current path between the n diffused areas. This limits the current to the reversed bias saturation current I_0.

Thus, a plot of I vs. bias to the transparent electrode will range from I_0 to comparatively large values of current. If I is forced through the circuit with a small constant potential (in this case, .1v), then I will be directly proportional to the conductance of the device.

Such a plot for one of the small cells is found in Fig. 18. Measurements were made in the dark to eliminate any photo voltage that might occur and upset the results. From examination of the plot it can be seen that there is an inversion layer at zero bias occurring near .01 ma. This can be attributed to either a trapped surface charge or an ionic charge in the oxide or some of both. Saturation in this plot occurs at near -20V and levels off at 1 μa. Since the area of the reversed biased n diffusion is .3 cm^2, the saturation current is 3.3×10^{-6} A/cm^2. From -20V bias the curve rises at first in a linear fashion and then bends over as higher bias potentials are applied. Since the current is a direct function of the

electron concentration n, and n is a direct function of the applied potential, we would expect the current to be a linear function of the applied bias. The mobility changes, however, causing the nonlinearity.

The thickness of the silicon oxide between the silicon surface and the tin oxide is 6000 Å in this sample. The electrical breakdown potential of 6000 Å on SiO_2 is 360V. Cells similar to the one reported above broke down at 200 volts so measurements were limited to a maximum applied bias of 150V.

The plot in Fig. 18 illustrates the growth of an inversion region and will give us some indication of the concentration of carriers at the surface.

Now the conductance G is equal to

$$G = \sigma \frac{wt}{\ell}$$

but

$$\sigma = qn\mu$$

so

$$n = \frac{G\ell}{q\ wt\ \mu}$$

G at 50V bias = .32 mili mhos

ℓ = .25 cm, w = .35 cm

μ = .7 x 10^3 cm^2/Vsec

and assuming an inversion layer thickness of .1μ, we obtain

$$n = 1.9 \times 10^{17} \text{ carriers/cm}^3 \quad .$$

This same parameter can be estimated by considering the capacitive action between electrode and silicon. The capacity between the two can be found by

$$C = \frac{\varepsilon A}{S}$$

A is area of electrode

S is thickness of SiO_2

but

$$Q = CV = \frac{\varepsilon AV}{S}$$

so

$$\frac{Q}{A} = \frac{\varepsilon V}{S}$$

but

$$qnt = \frac{Q}{A}$$

so

$$n = \frac{\varepsilon V}{qts}$$

where

$\varepsilon = 3.5 \times 10^{-13}$ farad/cm

$V = 50$ volts

$t = .1 \times 10^{-4}$ cm

$s = 6000$ $\overset{\circ}{A}$

thus, $n = 1.8 \times 10^{17}/cm^3$, in good agreement with the value of n above.

These are simplified determinations of n because other factors such as the nonlinearity of G vs. bias and the surface charge on the silicon were left out; nevertheless, it does show compatability between the two methods

and gives some confidence that the strength of the inversion layer can be determined by a conductance measurement.

This will be important when we try to determine the strength of the inversion layer when no transparent electrode exists such as in the contaminated oxide cell or the surface state cell.

Another cell was chosen from the same wafer (series 6, wafer 1) and a plot made of I vs. bias between the two n diffusions at an applied potential of .1 volt. A plot of this cell is found in Fig. 19.

Although the current for negative values of bias and the current for large positive values of bias is the same for both cells, an important difference exists in the shape of the curve around zero bias. For cell No. 1 a significant inversion layer is apparent but for cell No. 2, no inversion layer exists. Thus, even on the same wafer, one can see the ion contamination and surface state contribution to the inversion layer vary somewhat.

This illustrates that different conditions at the surface or in the oxide can cause different inversion intensities at zero bias. The factors that bring this about will be studied in order to enhance the effect and create strong inversions without the use of a bias on a transparent electrode.

From the data of conductance vs. bias between the two stripes, a determination of the strength of the inversion layer for the contaminated oxide layer can be obtained. This is accomplished by making a conductance measurement between the two n diffusions and relating this to the bias required to obtain the same conductance.

A schematic of the arrangement of equipment used to make these measurements is found in Fig. 20. The p wafer was connected to the n

diffusion on the negative side of the .1 volts so the other pn junction would be reverse biased.

Curves of short circuit current vs. bias on the transparent electrode were made on the two cells from series 6 No. 1 wafer mentioned above. The plot for these cells is found in Fig. 21, cell No. 2 as the upper and cell No. 1 as the lower curve. One of the significant things to be pointed out as the two curves are compared, is that they are essentially the same shape but have been shifted with respect to the vertical axis. For instance, the two curves would be alike if the lower one is shifted about 20 volts to the right. This further illustrates the fact that an inversion region can exist at 0 bias or if no transparent electrode existed at all. Why there is this difference in two cells on the same wafer has not been determined, but variations can occur occasionally in processing especially when the surface is an important factor. If, for instance, during a cleaning operation a slight residue was left on part of the wafer, that part could manifest a different surface phenomena than the other parts on the wafer.

Another significant fact to be gained from Fig. 21 is the increase in cell response as a bias is applied. A ratio of $\frac{2.8}{1.2} = 2.3$ is obtained from +150 volts to -50 volts. The curve bends over into a saturation condition as we would expect. The conductance curves do not saturate, however, as shown in Figs. 18 and 19. This can be explained because as shown by the equations derived above for n and G that G is a linear function of n and n is a function of the applied bias V.

An attempt to determine the sensitivity of the inversion layer cell to the shorter wavelengths, one of the small cells was exposed to a

light source strong in ultraviolet and compared with the conventional n over p cell. A cell from series 6, wafer 1 was chosen and a plot of short circuit current vs. transparent electrode bias was made for an incandescent FBE photoflood lamp at 140 mw/cm^2 as calibrated by a standard cell. This is a normal plot and is found as the lower curve in Fig. 21. This same cell was then exposed to an ultraviolet source consisting of a fluorescent tube designed as a "black light" source. A plot of I_{sc} vs. electrode bias is found in Fig. 22. Several interesting differences are found between the response of the cell when exposed to the FBE lamp as when exposed to the ultraviolet source.

The light intensity of course is much smaller and therefore the maximum current is 2.75 ma for the FBE lamp and 39 μa for the ultraviolet source. The shape of the curve is very interesting. The transition is sharper, and the saturation at positive biases is flatter. The transition takes place at negative values of bias and levels off at a higher negative bias for the ultraviolet than for the FBE source. It will be shown later that the change in flatness and steepness is due to the lower light intensity rather than the difference in spectrum.

An indication of the relative response of the two different cells was obtained by exposing the conventional cell to the FBE source and then the inversion cell to the same source. Then the two cells were exposed to the ultraviolet source in turn. The results are as follows:

	FBE Source	UV Source
Conventional cell (I_{sc})	133 ma	.22 ma
Inversion cell (I_{sc}) (+150V bias)	2.75 ma	.039 ma

The ratio of the short circuit currents for the two cells for the FBE source is 133/2.75 = 48. That is, the conventional cell generates 48 times as much as the inversion cell. However, for the U.V. source the ratio is .22/.039 = 5.7 so the conventional cell does not generate nearly as much in proportion to the inversion cell. Therefore, the power output for this part of the spectrum should be much greater for the inversion cell. The area of one of the small area inversion cells is about 1/40 of the area of a conventional 2x2 cm cell. If we use this factor, a 2x2 inversion cell should produce 2.75 ma x 40 = 110 ma compared to 133 ma for the conventional cell if flooded with 140 mw/cm^2 of incandescent light, whereas if exposed to U.V. light only, the 2 cm x 2 cm inversion cell would produce .039 ma x 40 = 1.56 ma compared with .22 ma of the conventional cell. This result is compatible with the claim that the inversion cell would be more sensitive in the short wavelength because the hole-electron pairs are created at the surface in a strong electric field and this field separates the carriers quickly before they recombine.

To further substantiate this, a 2 cm x 2 cm inversion cell processed before (series 5, wafer 1) was exposed to the FBE lamp at 140 mw/cm^2 yielding 30 ma I_{sc} and to the U.V. source yielding 1.2 ma I_{sc}.

The ratio of a 2 cm x 2 cm conventional cell to 2 cm x 2 cm inversion cell was

$$\frac{133 \text{ ma}}{30 \text{ ma}} = 4.4 \text{ for FBE}$$

and

$$\frac{.22 \text{ ma}}{1.2 \text{ ma}} = .18 \text{ for U.V.}$$

So although the conventional cell is 4.4 times as sensitive as the inversion cell for white light, the inversion cell is five times as sensitive as the conventional cell in the U.V.

Another attempt to observe the affect of a change in spectrum was tried by using still another light source besides the two used above. A mercury vapor source rich in the shorter wavelengths, but containing a spectrum in the visible also, was used on the two cells for comparison.

A plot of I_{sc} vs. transparent electrode bias is found in Fig. 23. Notice the curve is steeper than the FBE high intensity source, but not as steep as the U.V. source.

Again this difference is probably due to the intensity rather than the spectrum. The same analysis is made as before by looking at the ratio of I_{sc} for the conventional cell with respect to the inversion cell.

	FBE Lamp	Hg Source
Conventional cell (I_{sc})	133 ma	17 ma
Small inversion cell (I_{sc}) (150V Bias)	2.7 ma	.49 ma
2x2 cm inversion cell (I_{sc})	30 ma	6.7 ma

The ratios are:

$$\frac{\text{Conv. cell}}{\text{Small inv. cell}} \text{ (FBE)} = 50$$

$$\frac{\text{Conv. cell}}{\text{Small inv. cell}} \text{ (Hg)} = 35$$

$$\frac{\text{Conv. cell}}{\text{2x2 cm inv. cell}} \text{ (FBE)} = \frac{133}{30} = 4.5$$

$$\frac{\text{Conv. cell}}{\text{2x2 cm inv. cell}} \text{ (Hg)} = \frac{17}{6.7} = 2.5$$

Again the evidence shows that a short wavelength rich source will decrease the ratio between the conventional cell short circuit current and the inversion cell short circuit current.

Another attempt to ascertain the affect of spectrum on the relative response of the two types of cells was made by exposing both cells to radiation from the FBE photoflood lamp as the current through the lamp was changed. This change of current would change the temperature of the filament and, therefore, the spectral distribution. The distribution would change from a peak in the infrared to a peak near the visible. A short wavelength tail is present, but small, for the hotter temperature. The temperature was changed by changing the setting of the variac used to power the lamp. The intensity of the radiation also changes, so a plot can be made of cell response (I_{sc}) to variac setting. If there is a difference between the two cells in response to the visible wavelengths, the curves of I_{sc} vs. variac setting would show the difference. In fact, if the inversion cell is more sensitive to the middle of the spectrum, we should see a greater relative output at the higher variac settings where more of this light is found in the spectrum. The upper curve in Fig. 24 shows the I_{sc} response vs. variac setting for the conventional cell and the lower curve the response for the inversion cell at a transparent electrode bias of +150V. The upper curve of Fig. 25 shows the response of the inversion cell at -100V bias to the transparent electrode. The curves look similar and a comparison between the conventional cell and the two parts

of the inversion cell is found in the lower part of Fig. 25. This figure

shows the ratio between the conventional cell output and the inversion cell

output vs. variac setting. If the ratios change, this would indicate that

the spectral distribution could be a factor. From the results of Fig. 25,

it is noted that very little change occurs that could be attributed to a spec-

trum change. This result is not incompatible with the U.V. results because

very little U.V. appears in the FBE lamp even at high current. The conclusion

to be reached, then, is that the inversion cell is not more sensitive in mid-

visible spectrum but only in the shorter wavelengths.

A number of plots of I_{sc} vs. bias for different variac settings

for the FBE lamp were made. Figure 26 shows the curves for variac settings

of 40, 60, and 100. The trend of sharper rises and flatter saturation is

noted as the curves are compared. Each curve was normalized at the negative

bias saturation. To illustrate that the change in shape is due to intensity,

the FBE light source was effectively removed to a greater distance and a plot

obtained for a variac setting of 100. This plot is the dotted plot in Fig.

26, and if it is compared with the other 100 curve, the difference in shape

is obvious. The shape, in fact, corresponds to the shape of the curve with

the same intensity with the lamp closer. Thus, the curve shape changes

with the same variac setting and therefore the same spectral distribution,

but with a difference in intensity.

The antireflection coating on a conventional cell could explain

the reason less response is obtained for this cell rather than the inversion

cell if a strong reflection and, therefore, a weak absorption, occurs at

the shorter wavelengths. The inversion cell has no antireflection coating,

therefore no discrimination due to this coating is possible whereas if the

antireflection coating of the conventional cell is of the proper thickness discrimination in the short wavelengths can occur. To establish that this was not happening, a conventional cell other than the calibrated JPL cell was measured along with the calibrated cell. A plot of I_{sc} vs. variac setting is found in Fig. 27. These cells are very much alike as one can see by examining curve 1 and 2. The antireflection coating was removed from cell 2 and a measurement of I_{sc} vs. variac setting was taken. This appears as curve 3 in Fig. 27. A comparison between the two curves shows that the antireflection coating does not alter I_{sc} for different visible spectral distribution. A test needs to be performed, however, in the U.V. to test the response in the area of interest. For white light, about 140 mw/cm^2, (variac 100) the ratio of the conventional cell before and after removal of the antireflection coating is $\frac{115}{67} = 1.7$. For the mercury vapor source the same ratio is $\frac{15}{10} = 1.5$ and for the ultraviolet source the ratio is $\frac{.46}{.34} = 1.45$. These results show very little rejection of the U.V. due to the antireflection coating and, therefore, substantiates that the greater response of the inversion cell is due to the large electric field at the surface aiding the charge separation.

Another cell on wafer #1, series 6, was chosen to be used to measure a number of interesting things about the inversion cell. A plot of conductance between the n diffusion regions vs. transparent electrode bias for this cell is found in Fig. 28 for a FBE light intensity of 140 mw/cm^2. The plot is similar to the ones on the same wafer.

Figures 29, 30, and 31 show the I_{sc} response vs. bias for white light (FBE), Hg light and U.V. light sources respectively. No new surprises are found in these curves if we compare them with the other curves of series 6.

A new set of data was taken on this cell that was not taken on the others that gives further insight into the effectiveness of the inversion layer as a photon produced charge collector.

Provision was made for a semi-infinite plane with a knife edge to be inserted between the light source and the solar cell surface. The plane was very close to the cell surface so the radiation could be blocked off from a portion of the cell leaving the rest of the cell illuminated. The plane was mounted on a carrier that could be precisely positioned with a micrometer head. Thus, the edge of the plane could be accurately positioned at any point over the cell with respect to an edge of the cell area. The response of the cell as portions of light are prevented from illuminating the cell will indicate how far from the diffusion areas is the cell sensitive to the collection of hole electron pairs generated by photons.

Figure 32 shows the results of cell response (I_{sc}) vs. distance of the knife edge from the edge of the cell area for various values of transparent electrode bias. The edge of the cell area is the edge of the metal grid structure used to contain the p wafer that separates each cell area. The data to plot Fig. 32 was taken by drawing current from only one of the n diffusion areas, the one farthest from the cell edge at 0 inches. The dark bars at the bottom show the n diffusion areas and the dotted lines are the cell edge areas. An outstanding feature of this family of curves is the extension of the sensitive area as the inversion region grows with bias. If the 90% point of each curve is taken, shown by the arrows, it can be seen that as the inversion region becomes stronger, the sensitive area becomes larger and thus will accept more of the charges created by photons. Therefore, the response of the cell becomes greater and the power output more.

At -10V bias the 90% point is .02 inches from the near edge of the diffusion region used to extract power, whereas at +80V bias the 90% point is .03 inches from the edge of the diffusion region. At -20V bias the charges diffuse to the depletion area of the diffused p-n junction and are collected there but when an inversion region exists in this region, the charges can be separated by the induced p-n junction at the surface increasing the probability of a collection before recombination. At distances greater than .03 inches from the diffusion area or distances less than .078 inches from the edge of the cell area no increase of response is observed as light impinges on this area because the hole-electron pairs created there recombine before reaching the n diffusion area even though collected by the inversion layer. The linear response from the near edge of the diffusion region as the light is eliminated over the diffused area is due to the fuzzy edge of light on the cell due to the diffuse nature of the FBE light source and the distance the knife edge had to be above the cell in order to clear probes to the conducting areas.

Nevertheless this region is not affected by the bias and, therefore, not affected by the inversion layer. The diffusion length is about .015 inches for minority carriers in the p wafer.

An interesting parallel to the analysis of Fig. 32 is found in Fig. 33. Here the same type of curves were made but both n diffusion regions were connected together. Since the start of the plot from 0 distance on eliminates light over a diffusion region, as does the end of the plot, the slope at the beginning and the end should be the same. For a -20V bias the photons at middle of the cell generate changes that do not reach either depletion region and thus a flat portion occurs.

For the OV bias curve a flat portion should occur but should be shorter than the -20V curve and shorter at both ends. For the +80V bias there is response across the entire length of the cell as one would expect because of the presence of the inversion layer. At about .06 inches a lump can be noted. This is due to the bending of the curve from the collection of carriers by the left n diffusion and the influence of the collection of carriers by the right n diffusion. The curve could approximate a straight line by placing the two diffusion areas closer together. Placing them very close would cause the diffusion length to overlap and straighten the -20V curve.

Figure 34 shows a similar plot of knife edge vs. I_{sc} response for a mercury vapor light source. This light source is a point source and therefore much less diffuse than the FBE lamp and the shadow edge is much sharper. Therefore, we do not see the characteristic slope at the end of the curve as for the FBE lamp. This curve acts as would be suspected; that is, the curve flattens out as it passes over the aluminum on the active diffusion area and sharply dips at the end as the sharp shadow passed over the exposed area between the n diffusion and the edge of the cell or aluminum matrix. A marked difference in the extent of influence of the light when the inversion layer is present than when it is not, is brought out by comparing the 80V and -20V curves in this figure. The ultraviolet rich source will create holes and electrons near the surface where they can be separated by the strong field there before recombining.

Figure 35 shows this same cell in response to the U.V. source. Only one contact was used. This source is a diffuse source so we have a fuzzy shadow as in the FBE lamp and a slope exists at both ends for the OV to 80V bias. The slope exists at the left end because the collection of

carriers for these wavelengths extends across the cell and the aluminum over the diffusion area blocks out the light. The -20V bias curve collects carriers from a greater distance than for white light but not as much as when the inversion layer is present.

Thus, it has been demonstrated by this set of experiments that the induced p-n junction and associated electric field does indeed separate the hole-electron pairs created by photon irradiation.

Evidence also points to this cell being extra sensitive to the ultraviolet spectrum. It was also pointed out that the separation of the n diffused areas for optimum collection should be closer than the separation of the n diffusion in the test cells.

A curve of solar cell current vs. cell output voltage for the transparent electrode cell is found in Fig. 36. Biases of -20, 0, 40 and 80 volts were used. The illumination of the FBE lamp was adjusted for 140 mw/cm^2. The maximum power at a bias of 80V is about .51 milliwatts, at a bias of 40 about .47 milliwatts, at 0V about .4 mw, and at 0 bias about .3 mw. Since the area of the small cell is about .1 cm^2, the efficiency of the cell at 80V bias is

$$\frac{.51}{140 \times .1} = .036 \quad 3.6\% \quad ,$$

and the efficiency of the -20V bias is

$$\frac{.3}{14} = 2.1\% \quad .$$

The short circuit current - open circuit voltage at 80 volts bias product yields an efficiency of

$$\frac{.48 \times 2.3}{14} = .079 = 7.9\% \quad .$$

An experiment was performed to obtain a comparison of the response of the transparent electrode cell to the sun with respect to an FBE photoflood lamp. The results show a short circuit current increase of about 10% when illuminated by the sun with respect to the photoflood illumination. This result is shown in Fig. 37.

The two curves in Fig. 37 were plotted from data obtained by illuminating the cell with 120 mw/cm^2, which is the sun's intensity at noon in Tucson. The 120 mw/cm^2 figure was obtained by exposing a conventional cell (calibrated at 133 ma short circuit current for 140 mw/cm^2 illumination) to the sun and getting a short circuit current measurement of 110 ma. This corresponds to an illumination of

$$\frac{110}{133} \times 140 = 120 \text{ mw/cm}^2 \quad .$$

The curve labelled "sun illumination" is the curve obtained in the sun as a function of the bias on the transparent electrode.

The intensity of the photoflood light source was set to illuminate the conventional cell so an I_{sc} output of 110 ma was obtained. Data on the transparent electrode were then obtained at this illumination and is plotted as the lower curve labelled photoflood illumination in Fig. 37.

Thus, the transparent electrode is more sensitive to the radiation from the sun than with radiation from an incandescent source when the two sources are adjusted for equal response to a conventional solar cell.

This phenomena can be explained by considering the difference in spectral distribution between the sun and the photoflood lamp. If the conventional cell is not as sensitive as the inversion layer cell to a part of the spectrum, the shorter wavelengths for instance, but both are equally sensitive

to the rest of the spectrum and the two cells are exposed to two different

light sources, one containing the short wavelengths and the other deficient

in short wavelengths, then the inversion layer cell will show a greater out-

put for the spectrum with the short wavelengths. The reason for this stems

from using the conventional cell as a calibrator. The same short circuit

current is demanded of both light sources so the illumination in the spec-

trum that both cells are sensitive to is the same in both but added to this

is the part of the spectrum in the short wavelength source that only the

inversion layer cell can convert to external current. For the tungsten light

source no extra radiation exists that the inversion layer cell is sensitive

to that the conventional cell is not.

It is interesting to notice that as the inversion layer grows,

so does the difference between the response to the two light sources, and

where there is no inversion layer (at negative biases) there is no differ-

ence between the two sources of illumination. This supports the conjecture

that the high field at the surface of the silicon aids the collection of

the hole-electron pairs created at the surface by the short wavelength

part of the spectrum.

III. CONTAMINATED OXIDE CELL

A special furnace was prepared to grow oxide impregnated with ions.

Oxygen and nitrogen gases were metered and valved so combinations of flow-

rates of either or both gases could be passed down the quartz tube heated

by the furnace to 1050°C. An alternate path for oxygen is provided through

a bubbler. If pure water is used in the bubbler, a steam oxide can be grown

on a silicon wafer surface comparatively free of contaminated ions, but if a substance rich in ions, that would serve as positive charge sources in the oxide, was dissolved in the water, some of the substance would carry over with the water vapor and contaminate the oxide. Sodium chloride was used as the substance rich in contaminating ions. It is well known that sodium can act as a source of positive charge from studies made on MOS transistors. Other substances will be tried after NaCl is characterized.

The small cell configuration was used to evaluate contaminated oxide solar cell response. Conventional fabrication procedure was used to form the cell, except the oxide over the area between the n diffusions was grown with a vapor formed by bubbling oxygen through a sodium chloride solution. Thus, the oxide should be interspersed with Na atoms, some of which are positively ionized. This positive charge in the oxide will cause electrons to accumulate at the oxide silicon interface and, if strong enough, produce an inversion layer in the semiconductor.

The steps used in processing the following contaminated oxide inversion cells is outlined here:

1. SiO_2 was grown on wafer for 50 min. at 1100°C. This produced 6000 $\overset{\circ}{A}$ layer of oxide.

2. Grid pattern was etched through the oxide using conventional photoresist process.

3. 15 minute predeposition of n-type dopant (phosphorus) was accomplished using standard procedures.

4. The oxide growth was completely removed from the front and back of the wafer.

5. Using the auxiliary furnace, a contaminated oxide was grown on the wafer. The contaminate was 4 grams of NaCl completely

dissolved in 400 ml. of deionized water in the bubbler.

6. This layer of oxide was etched with the photoresist process to provide a grid pattern on the diffusion areas, but was smaller than the diffusion areas themselves.

7. Vacuum deposited aluminum on front of wafer.

8. Etched aluminum into grid pattern.

10 ohm cm, 2x2 cm, p type wafers were used.

Four wafers were processed with different contaminated oxide thicknesses thinking that if the distribution of Na atoms is uniform in the oxide, the total charge density would be a function of the oxide thickness. Therefore, the inversion layer strength should increase with thickness and, consequently, the response of the cell. Oxide thicknesses of 700 Å, 900 Å, 1250 Å and 3600 Å resulted from subjecting each wafer to the same vapor flow but different lengths of time in the furnace.

The short circuit current for an illumination of 140 mw/cm^3 was averaged over the nine cells on each wafer. The results for the four wafers are shown below.

Wafer	Oxide Thickness	I_{sc} (140 mw/cm^2)
1	700 Å	1.1 ma
2	900 Å	1.15 ma
3	1250 Å	1.25 ma
4	3600 Å	2.12 ma

This data is plotted in Fig. 38.

A definite increase is noted in the thicker oxide showing a larger inversion region. If the curve is extended to zero oxide thickness at the

lower end, a value of about 1 ma I_{sc} is noted. This is compatible with the results found for the transparent electrode cell where, at zero bias, the curve leveled off at about 1.0 ma at 140 mw/cm^2.

Thus, it can be seen that ionic contamination can create an inversion layer of sufficient strength to affect the power output of the solar cell.

IV. SURFACE STATE SOLAR CELL

Different methods of treating the surface of a silicon wafer to create occupied surface states during the fabrication of inversion layer solar cells were tried. Small area solar cell masks described above were used to fabricate cells with different processing procedures. Four 2 cm x 2 cm wafers with the small cell patterns were processed in four different ways.

The first wafer was processed in the following way after the n diffusion:

1. The final oxide was grown for 12 minutes using steam and oxygen.

2. The wafer was pulled slowly from the furnace with steam and oxygen on.

3. Holes in the oxide were etched for aluminization.

4. The wafer was aluminized and etched.

5. The wafer was sintered for 4 minutes at 480°C.

The average short circuit current over the 12 cells on this wafer was 2.08 ma for an illumination of 140 mw/cm^2 from a FBE incandescent light source. Variation of I_{sc} response from cell to cell over the wafer ranged from 1.9 ma to 2.1 ma. 2.08 ma can be compared to the transparent electrode

cell of the same configuration where a bias changed the cell from 1.2 ma to 2.8 ma (+160V). Thus, there is an inversion region created by mechanisms at the surface or in the oxide or both.

The second wafer was processed as the first wafer except the aluminum in Step 4 was sintered before it was etched. Thus, the aluminum over the oxide over the sensitive portion of the cell is allowed to interact with the top surface and reduce the surface states at the Si-SiO$_2$ interface. This annealing effect is probably due to the interaction of the aluminum with a slight trace of water at the top surface. This interaction produces hydrogen and hydrogen diffuses rapidly through the oxide at the sintering temperatures and partially pacifies the surface states at the interface. Thus, the response of the cells on wafer #2 should be less than the response on wafer #1. Such is the case because the average I$_{sc}$ for the cells on wafer #2 is 1.58 ma with a variation across the wafer of 1.5-1.7 ma. This is a significant change compared to wafer #1 and illustrates how a change in processing can effect a change in the strength of the inversion layer.

Another wafer was processed differently than wafer #1 or #2. Whereas in the first two wafers, both steam and oxygen were left on in steps 2 and 3, only oxygen was left on in fabricating wafer #3.

Steps 1, 4, 5 and 6 are the same as wafer #1. The schedule is like this:

1. During final oxidation 7 minutes of oxide was grown using steam and oxygen.

2. The steam was then turned off and the wafer was left in the furnace for 5 minutes with dry oxygen on.

3. Wafer was then pulled out slowly with dry oxygen on.

4. Pre-ohmic holes were cut in oxide.

5. Wafer was aluminized and etched.

6. Wafer was sintered for 4 minutes at 480°C.

The average short circuit current over the twelve cells is 1.66 ma with a spread of 1.2-2.0 ma. The average is significantly less than wafer #1 but the spread is much larger than wafer #1. Thus, there is a difference in I_{sc} between wafer #1 and wafer #3 which indicates that whether steam is present or not, as the wafer cools, does affect the surface states and thereby the magnitude of the inversion region.

Another variation in processing was tried in fabricating wafer #4. The procedure is essentially the same as wafer #3 but nitrogen was used in Step 2 and 3 instead of oxygen. Steps 1, 4, 5 and 6 are the same as wafer #1 and #3. The average I_{sc} for this group of cells was 1.78 ma with a spread of 1.4-2.0 ma.

A summary of the results of this experiment is found below.

	Average I_{sc}	Spread
Both steam and O_2 left on	2.08 ma	1.9-2.1 ma
Al sintered before etch	1.58 ma	1.5-1.7 ma
Only O_2 left on	1.66 ma	1.2-2.0 ma
Only N_2 left on	1.78 ma	1.4-2.0 ma

The results of this experiment show a change in inversion layer is possible with a change in processing. This can be attributed to surface state phenomena since the other source of induction, contamination, should be a minimum.

Another wafer was processed to investigate surface state creation of inversion layers. The following procedure was used to process the wafer:

1. Normal process through diffusion step.

2. All oxide was stripped from wafer.

3. 4500 Å of steam oxide was grown.

4. Wafer was slowly pulled from furnace with steam on.

5. Pre-ohmic holes were cut.

6. Wafer was aluminized and sintered for 4 minutes at 480°C.

All sixteen cells on the wafer responded to illumination from the FBE incandescent lamp. Short circuit current ranging from 1.6 to 2.8 ma were measured. The average over the wafer was 2.14 ma. The individual currents were (all in ma):

2.1, 1.9, 1.6, 1.9, 2.0, 2.1, 2.1, 2.0, 2.1, 2.1, 2.1,

2.0, 2.8, 2.6, 2.5, 2.3.

The response of the last four cells is higher than the average and they were all located along one edge of the cell, showing that a high response can be achieved by proper treatment of the silicon surface during fabrication. What factors of processing led to a high response at the edge has not yet been determined, but will be a point of investigation as an optimum response to the surface state cell is sought.

V. THEORETICAL ANALYSIS

The approach to the determination of the currents and voltages expected with this cell is similar to the approach taken to analyze the conventional diode with a graded junction. The equation

$$J = J_n + J_p = qD_n \frac{\partial n}{\partial x} + qn\mu_n E + qD_p \frac{\partial p}{\partial x} + qp\mu_p E$$

is used to obtain the current density. As a first approximation, the E field is neglected and the diffusion terms retained. Since the p side is similar to a conventional diode, it will be handled similarly.

The n side, however, is due to the distribution of inversion layer electrons and involves equations derived from consideration of phenomena at the surface.

If we combine Poisson's equation

$$\frac{\partial^2 \psi}{\partial x^2} = - \frac{\rho(x)}{\varepsilon_s}$$

with the charge density inside the semiconductor

$$\rho(x) = q(N_D - N_A + P_p - n_p)$$

and considering

$$P_p - n_p = P_{po} e^{-\beta\psi} - n_{po} e^{\beta\psi}$$

then

$$\frac{\partial \psi}{\partial x} = - \frac{2}{\beta L_D} \left[(e^{-\beta\psi} + \beta\psi - 1) + \frac{n_{po}}{P_{po}} (e^{\beta\psi} - \beta\psi - 1) \right]^{1/2}$$

where

$$\beta = \frac{q}{kT} \quad ,$$

when we are interested in the strong inversion region where $\psi\beta \gg 1$ or

$$e^{\beta\psi} \gg \beta\psi \gg 1 \quad .$$

The above equation reduces to:

$$\frac{\partial \psi}{\partial x} = - \frac{2}{BL_D}\sqrt{\frac{n_{po}}{P_{ro}}}\ e^{\beta\psi/2}$$

Integrating over the limits from the surface where the surface band bending potential is ψ_s at $x = o$ to a point within the surface at x, we get:

$$x = L_D\ \sqrt{\frac{P_{po}}{n_{po}}}\ e^{-\beta\psi/2} - e^{-\beta\psi_s/2}$$

but

$$n(x) = n_{po}\ e^{-\beta\psi}$$

and finally

$$n(x) = \frac{n_{po}}{\left[\frac{x}{L_D}\ \frac{n_{po}}{P_{po}} + e^{-\beta\psi_s/2}\right]^2}$$

In order, though, to obtain a reasonable result for the current flowing across the depletion region, the gradients of electrons and holes at the depletion region have to be known. Mathematical expressions exist that can give these relationships but boundary conditions must be determined from judgments made about the onset of strong inversion and weak inversion. Strong inversion occurs at the points where the Fermi level, with respect to the mid-band energy, is equal but opposite to the Fermi level in the bulk. This can be illustrated in Fig. 39. This figure represents the forbidden band of a semiconductor with the bottom of the conduction band on top and the top of

the valence band on the bottom. E_i is in the middle of the forbidden band. E_F is the Fermi level. An indicator of whether a semiconductor is n or p type is whether the Fermi level is above (n) or below (p) E_i. A measure of the magnitude of n or p is the position of the Fermi level with respect to either the valence band for p type or the conduction band for n type. The closer to either band the more heavy is the carrier concentration. Thus, when the bands bend and E_i crosses over the E_F, a semiconductor near the surface can change from p to n as shown. Thus, a p-n junction is formed at the surface.

The shape of the band as it bends toward the surface can be obtained from a theoretical analysis of the inversion process. A plot of ψ vs. x is shown in Fig. 40. This is the shape of the bands near the surface. Of course, the shape depends on the magnitude of the final deviation at the surface ψ_s. Figure 40 is the plot for a ψ_s of .65 volts, Fig. 41 for a ψ_s of .70 volts and Fig. 42 for a ψ_s of .75 volts. These surface potentials correspond to a surface concentration of electrons of 10^{16}, 5×10^{16} and 10^{17} respectively, assuming room temperature and wafers of 10 ohm-cm p type. The equation integrated to obtain these three plots is:

$$\frac{\partial \psi}{\partial x} = \frac{2}{BL_D} \left[e^{-\beta \psi} + \beta \psi - 1 + \frac{n_{po}}{p_{po}} (e^{\beta \psi} - \beta \psi - 1) \right]^{1/2}$$

(See Physics of Semiconductor Devices, Sze, Wiley, p. 431.)

where

$$\beta = \frac{q}{kT}$$

L_D = diffusion length

n_{po} = electron concentration in the bulk

p_{po} = hole concentration in the bulk

The onset of strong inversion is at the point where ψ = .6. From the plot for ψ_s = .75 this corresponds to a point .06 μmeters into the silicon surface and for .65 volts ψ_s about .03 μmeters.

The onset of inversion occurs where $\psi = \psi_\beta$ = .3 volts. For ψ_s = .65 inversion starts at 3 μmeters and when ψ_s = .75 inversion starts about the same. Thus, the boundary points can be determined from these plots.

The surface potential ψ_s was obtained by applying an external potential to the transparent electrode. A plot of the external bias to the transparent electrode vs. the ψ_s it creates is found in Fig. 43. The equation used for this plot is:

$$V_{applied} = \psi_s + \frac{qD_s}{\varepsilon}\left[u_d + u_w\right]$$

where

$$u_w = p_{po}\left[\left(\frac{2\varepsilon\psi_s}{p_{po}}\right)^{1/2} - d\right]$$

and

$$u_d = L_D\, n_i\left(e^{\beta\psi_s/2} - \frac{1}{\frac{d}{L_D}\sqrt{\frac{n_{po}}{p_{po}}} + e^{\beta\psi_s/2}}\right)$$

d is the inversion thickness

n_i is the intrinsic concentration

Figure 44 is an approximate plot of electron concentration vs. depth into the wafer for two values of surface potential .65 and .75 volts. The two vertical lines represent the value at strong inversion. The left one for the lower .65 volt curve and the right one for the .75 volt curve. The equation used to obtain this plot is: (when $\beta\psi \gg 1$)

$$\frac{\partial\psi}{\partial x} = \frac{2}{BL_D} \sqrt{\frac{n_{po}}{P_{po}} e^{\beta\psi}}$$

and $n = n_{po} e^{\beta\psi}$.

Simple theory indicates that conductance, G, between the two stripes of the small cell should be a linear function of the bias applied to the transparent electrode of the transparent electrode solar cell. The equation describing this relationship is:

$$G = \frac{\mu w \varepsilon V}{\ell s}$$

where μ carrier mobility

   w   width of cell

   ε permittivity of dielectric SiO_2

   V   applied bias to transparent electrode

   ℓ length of cell

   s   thickness of dielectric

Thus, if μ, w, ε, ℓ and s are all constants, then G is directly proportional to V and a plot of G vs. V should be a straight line with slope $\frac{\mu w \varepsilon}{\ell s}$.

However, a plot of G vs. V for a small cell is not a straight line but bends over for large values of bias. This is illustrated in Fig. 45. Since w, ℓ and s are physical dimensions, they are not likely to

change and changes in ε will be negligible, so these influences will not cause the change in slope. However, μ does change as the concentration of electrons changes in the inversion layer.

This change in mobility for a change in electron concentration is well known and is explained in the book, "Semiconductors" by H. Wolf published by Wiley. Page 402 in this book contains curves of μ_{eff} vs. carrier concentration for inversion layers.

To obtain a calculated curve of G vs. applied bias, a computer-aided plot of μ_{eff} vs. surface voltage (ψ_s) was made from the equations found in Wolf:

$$\mu_{eff} = \frac{\mu_B \mu_s}{\mu_B + \mu_s}$$

$$\frac{\mu_s}{\mu_B} = 1 - e^{\alpha_s^2} \, efc \, (\alpha_s)$$

$$\alpha_s = \frac{1}{E_s \mu_B} \left[\frac{2kT}{m_n}\right]^{1/2}$$

Curves of E_s vs. surface voltage (ψ_s) were computed so a plot of μ_{eff} vs. ψ_s was possible and is found in Fig. 46. A plot of ψ_s vs. applied bias was also available, so a plot of μ_{eff} vs. applied bias is possible. Since μ is directly proportional to G, a plot of μ vs. applied bias could be applied to the experimental curve of G vs. applied bias.

This experimental curve, however, does not meet the origin at 0 bias because of other sources of charge creating the inversion layer beside the applied bias. To bring the two curves together they were both normalized at 100 volts bias and the experimental curve shifted by 17 volts. Figure 47 shows the results of this comparison. The dotted line is the computer-aided

calculation and the solid line is the experimental curve taken from Fig. 45. A fairly good match is noted. The deviation comes at large values of bias.

Thus the departure from the linearity of G as the inversion layer grows is undoubtedly mainly due to the change of mobility of the electrons as the layer grows. The response of the solar cell is therefore affected by this change in mobility and we should see a "flattening" of the curve for large biases as we do. There are other factors besides the mobility change that flattens the response curve so an exact correlation between the two is not possible.

It has been shown, however, that the change in mobility of the electrons at the surface has a gross effect on the conductivity of the inversion layer and, therefore, a gross effect on the response of the solar cell to illumination.

VI. MEASURING APPARATUS

To enable accurate measurements of current to be made, a temperature controlled cell holder was constructed. The holder was made from a block of aluminum machined to form chambers under the top surface to allow water to circulate in the block. The water is pumped from the tank of a constant temperature bath to the water cooled block. Provision is made for the insertion of the standard solar cell in the circulating path. A thermocouple well was made so a thermocouple could be inserted in the block close to the surface near the cell position. The temperature will be measured by this thermocouple and regulated by adjusting the temperature of the bath water.

Three probes are mounted near the block so an electrical connection can be made to the cell under test. The platform, containing the block and probes, is mounted on an adjustable swivel to allow the cell to be oriented normal to the sun rays. The entire apparatus including the constant temperature bath can be used on a movable cart for easy transportation in

and out of the building for a choice of illumination from an inside tungsten source or the outside sun source. The inside tungsten source is a FBE daylight flood light (650W).

Four conventional solar cells were calibrated against the standard cell supplied by JPL. These four cells will be used as substandards to calibrate the inside light source and to determine the sun's intensity when measuring outside.

The standard cell was set in place in the measuring apparatus and one of the substandards set on the aluminum block as mentioned above. The circulating water bath temperature was adjusted to 28°C and a measurement made on the short circuit current of the standard cell. A value of 40.81 ma was obtained. At 28°C and 140 mw/cm^2 the standard cell will supply a short circuit current of 47.88 ma. Therefore, the sun's intensity at the time of measurement was 119 mw/cm^2. The substandard cells produced short circuit currents of 122.4 ma, 125.5 ma, 122.4 ma and 123.4 ma all at 28°C. The calibration current of these four substandards with respect to an illumination of 140 mw/cm^2 is 143.6 ma, 147.2 ma, 143.6 ma, and 144.8 ma. The substandards were 2x2 cm cells whereas the standard cell was 1x2 cm.

VII. RECOMMENDATION OF APPROACHES TO FUTURE INVESTIGATION

A. Transparent Electrode Cell

The transparent electrode inversion layer solar cell has essentially served its purpose. That the induced p-n junction can act as a collector of photon created hole-electron pairs has been demonstrated. An indication of the strength of the inversion layer has also been garnered from this cell which will be useful in determining the strength of the inversion layers for the other types of cells under investigation.

This has been done by observing the response of the cell to illumination and to conduction between the n^+ diffusions.

The successful transparent electrode cells, however, have been the small cell variety and large cells should be fabricated for testing. Thus, several of the large 2x2 cm cells will be produced.

Measures to obtain a much better curve factor on the inversion layer cells will be attempted. Of prime importance is the titanium-silver contacts that might decrease the series resistance somewhat and thereby increase the curve factor. A vacuum station is currently being prepared to allow evaporation from two independent sources and to allow the thickness to be monitored. When this station is available, evaporation of titanium-silver contracts will be possible.

The transparent electrode cell will be helpful in investigating the things mentioned above.

B.   The Contaminated Oxide Cell

The ionized atoms introduced into the oxide as the oxide is grown will, supposedly, distribute uniformly throughout the oxide thickness. To investigate this, a contaminated oxide cell will be subjected to a step incremental removal of the contaminated oxide and measurements of the response to illumination taken between each increment. A plot of oxide thickness vs. cell response can then be obtained. This plot will indicate how effective the distribution of ions is to the creation of an inversion layer.

If all of the ions distributed in the oxide could be forced to lie at the interface between the oxide and the silicon, a stronger inversion layer could result. In order to investigate this possibility, a

contaminated oxide cell will be fabricated with a transparent electrode layer deposited on top of the contaminated oxide. If a negative bias is applied to the transparent electrode with respect to the silicon wafer in the presence of heat, the positive ions should migrate through the silicon oxide to the oxide silicon interface. If the bias is left on while the wafer cools, the ions should be trapped at the interface. This is especially true of sodium contamination and will be tried to evaluate its possibilities.

A variety of contaminating substances will be used in the bubbler in an endeavor to optimize the contamination. Other sodium compounds besides NaCl, such as NaOH, Nabr, NaI and other will be used. Other ions from the sodium family such as potassium and lithium will be tried also.

Another interesting experiment might be to contaminate the surface of a non-contaminated oxide and try to drive the ions in toward the interface by applying heat or an electric field or both. A thin layer of the contaminate could be supplied by painting the surface with a solution of the contaminating substance.

Measurements of the response of the contaminated cell to a dark edge as was done for the transparent electrode cell will be done. An indication of the extent of sensitivity of the cell to illumination can thus be realized. This information will be used to design a future contact pattern for the large 2x2 cm cells.

C. Surface State Cell

An investigation of processing variations that might affect the surface states will be continued. These variations might include the removal of all oxide from the surface rather than leaving an oxide that

passivates the surface. To keep the natural thin oxide from building up when exposed to the air, substances such as photoresist will be used as an isolation layer. A spin on oxide will be used to cover the raw silicon surface in an endeavor to affect the charge at the surface captured by states at the interface.

Measurements of both conductance between n^+ diffusion regions and dark edge illumination will be part of the methods used to evaluate the response of the cell to radiation.

D. Theoretical Investigation

Currently under investigation is the comparison of theory with experimental results with respect to the conductance through the inversion layer between the n diffusions in the transparent electrode cell. The conductance changes with transparent electrode bias linearly for small biases and nonlinearly for large biases. The simple theory predicts a linear relationship between conductance and applied bias but for heavy inversions the mobility of the carriers in the layer decreases and thereby produces a nonlinear relationship.

A theoretical V-I plot for the inversion layer cell will be considered, using equations derived from fundamental equations relating to the p-n diode and the surface phenomena of semiconductors. At first, series resistance of the inversion layers and contact patterns will be neglected but will be added later to establish a more clear comparison of theory and practise.

VIII. CONCLUSIONS

A transparent electrode inversion layer cell has been fabricated and shown capable of producing power from intense light sources. The affect on the production of power that the inversion layer has, has been illustrated.

Curves of short circuit current vs. transparent electrode bias have been taken and analyzed.

Small cells whose inversion layer was induced by ionic contamination of the oxide layer have been fabricated and a plot of oxide thickness vs. short circuit current resulted. Further work to enhance and optimize the contamination will be attempted.

Several small cell arrays have been fabricated to emphasize the creation of a charged layer at the interface of silicon and oxide due to donor states at the interface. The creation of an inversion layer was obvious, especially for one small cell whose output was much larger than the rest. Work will continue to better understand the ways to create surface states and to study their affect on the response to solar cells.

Some progress has been made in comparing theory to experimental results. A look at the theoretical properties of surface phenomena of semiconductors has been made and further work is planned.

Typical I-V Curve

for Photovoltaic Cell

n over p   2 ohm-cm

$140 mw/cm^2$ illumination

2 x 2cm

current
(ma.x20)

Figure 1

Voltage (volts)
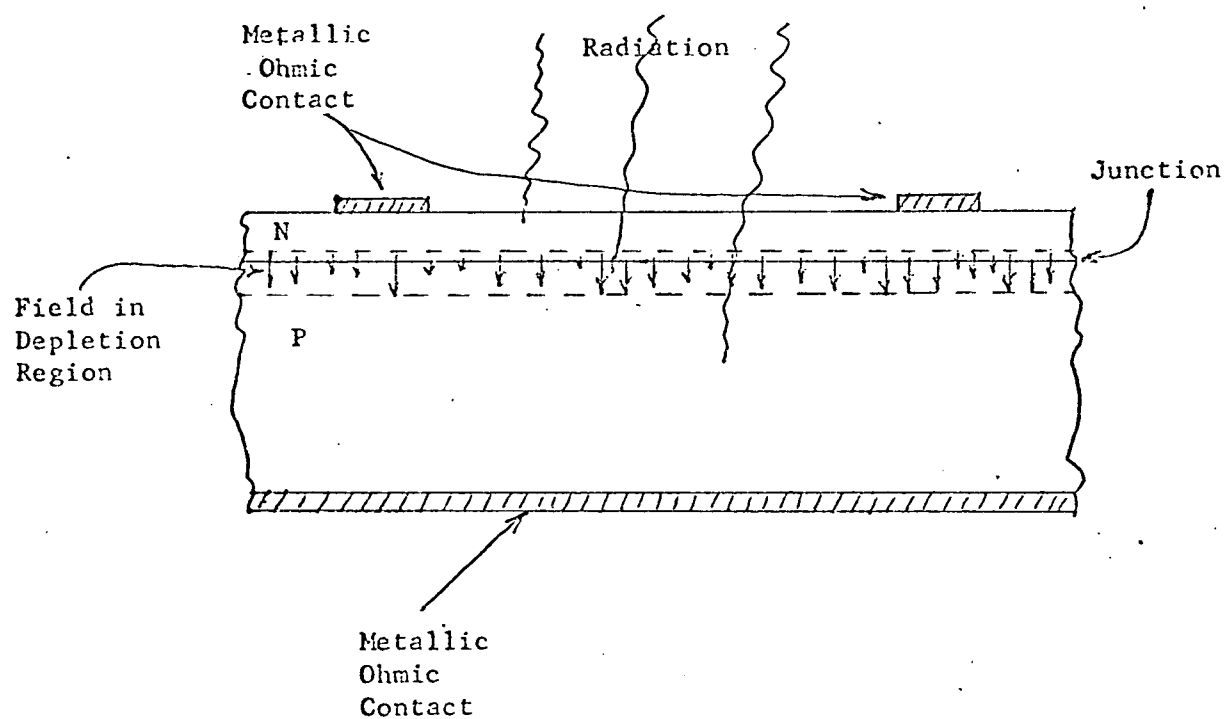
Figure 2.

Standard Solar Cell Construction
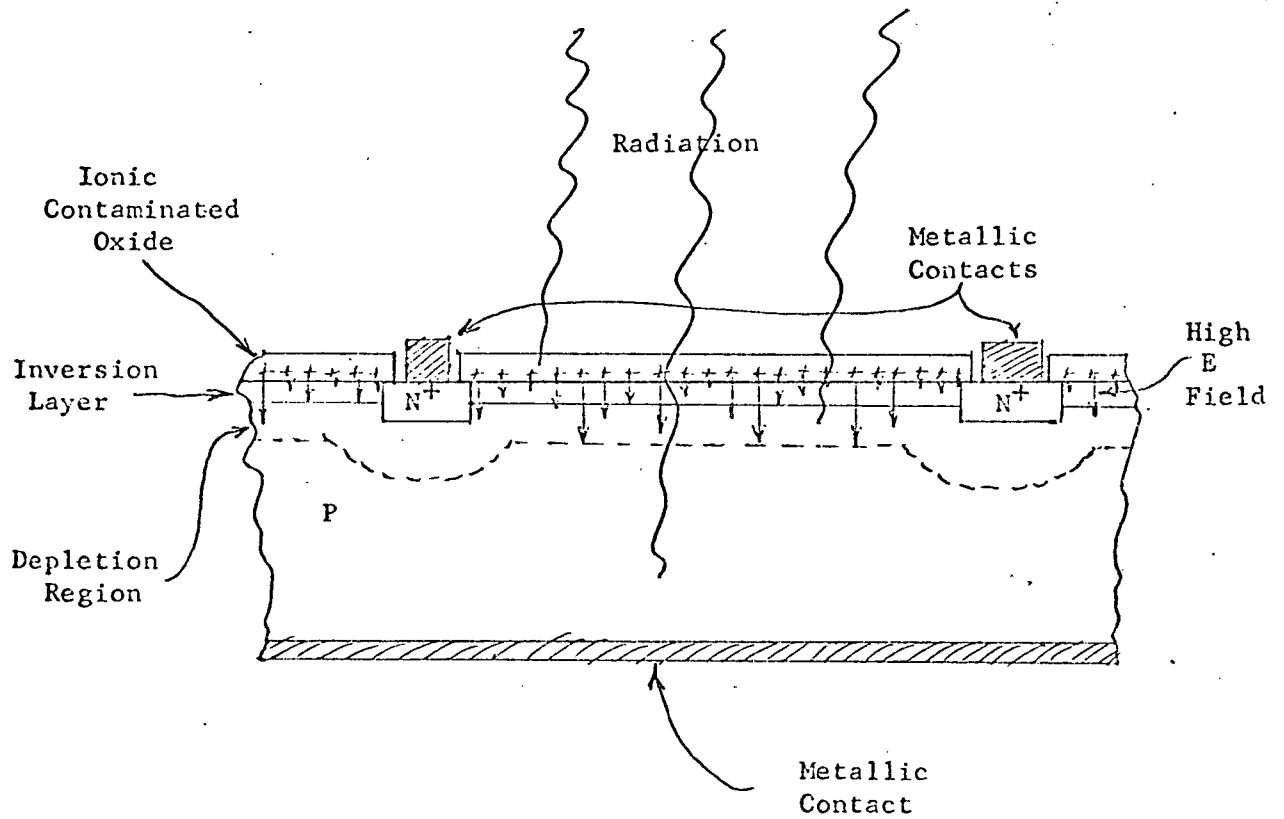
Figure 3

Inversion Layer Solar Cell
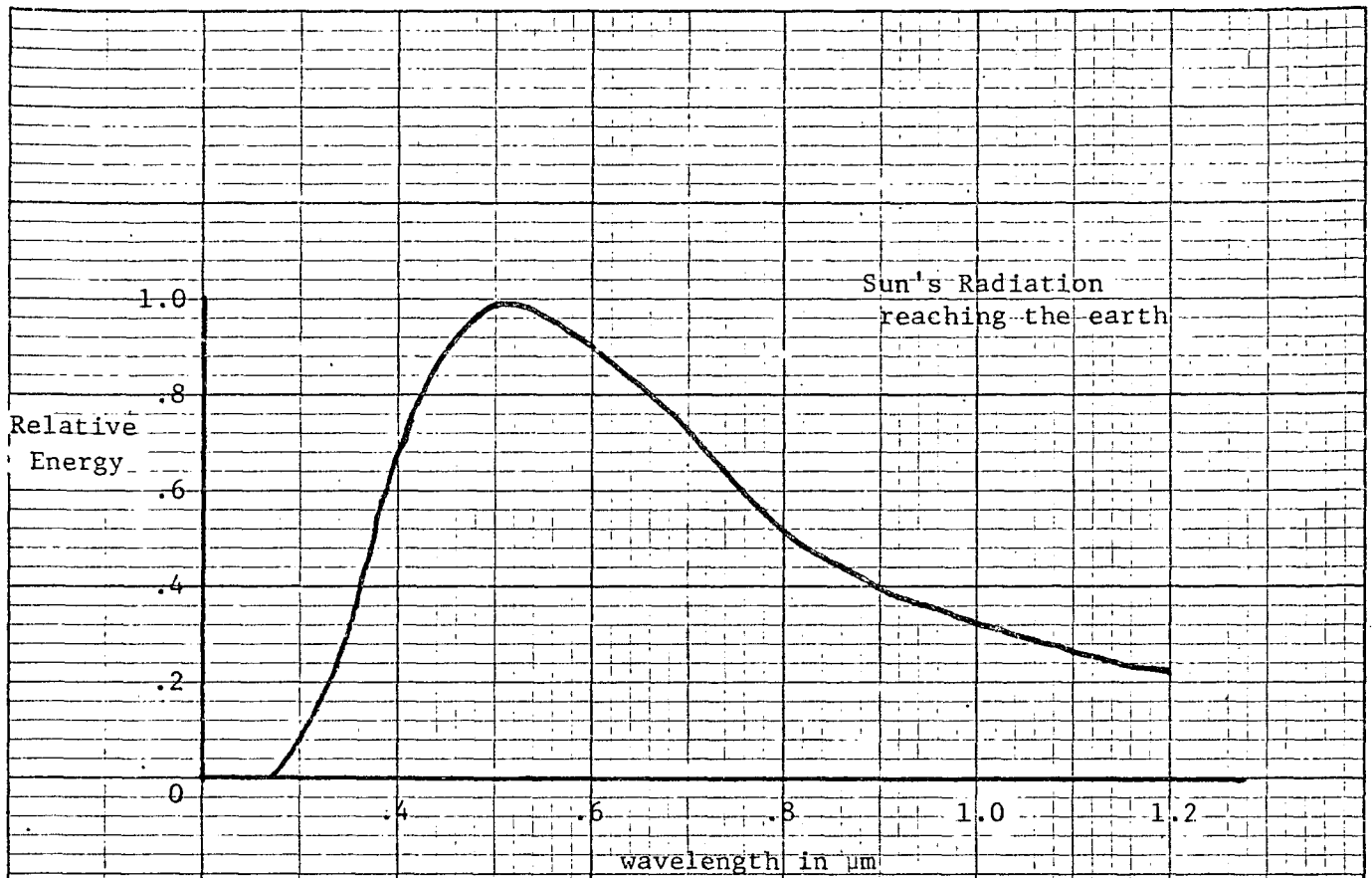
Figure 4a
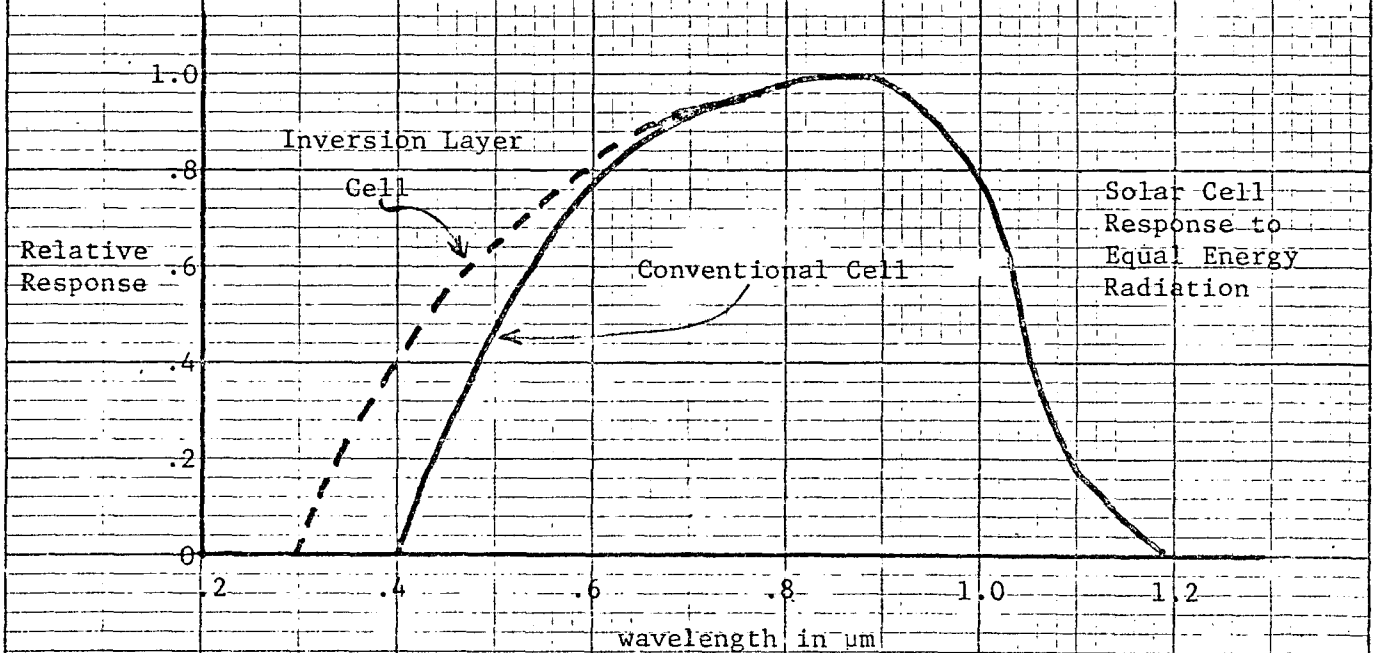
Figure 4b
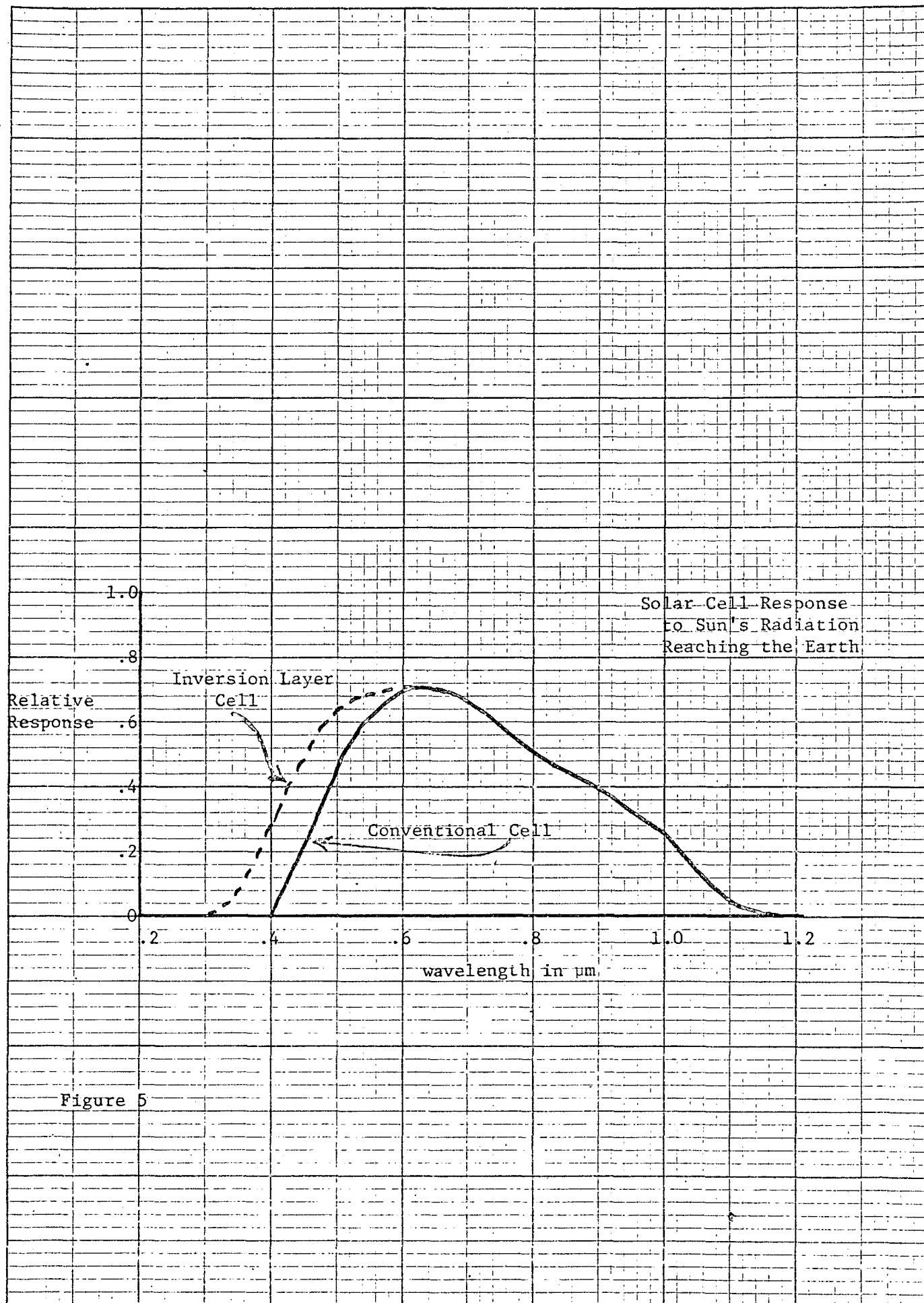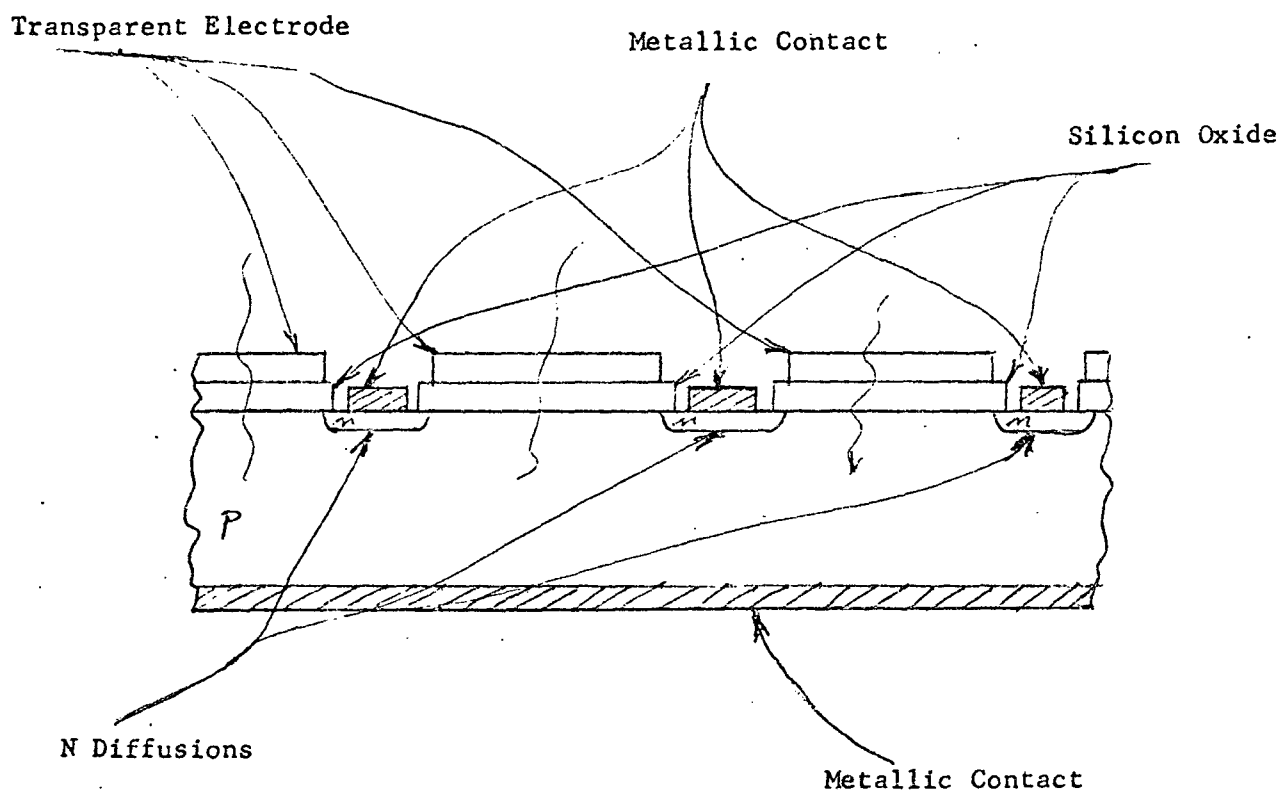
Figure 5

Figure 6

Transparent Electrode Cell

O_2 in

valve

flowmeter

Bubbler

H_2O

Furnace Tube

flowmeter

valve

N_2 in

valve

$SnCl_2$

flowmeter
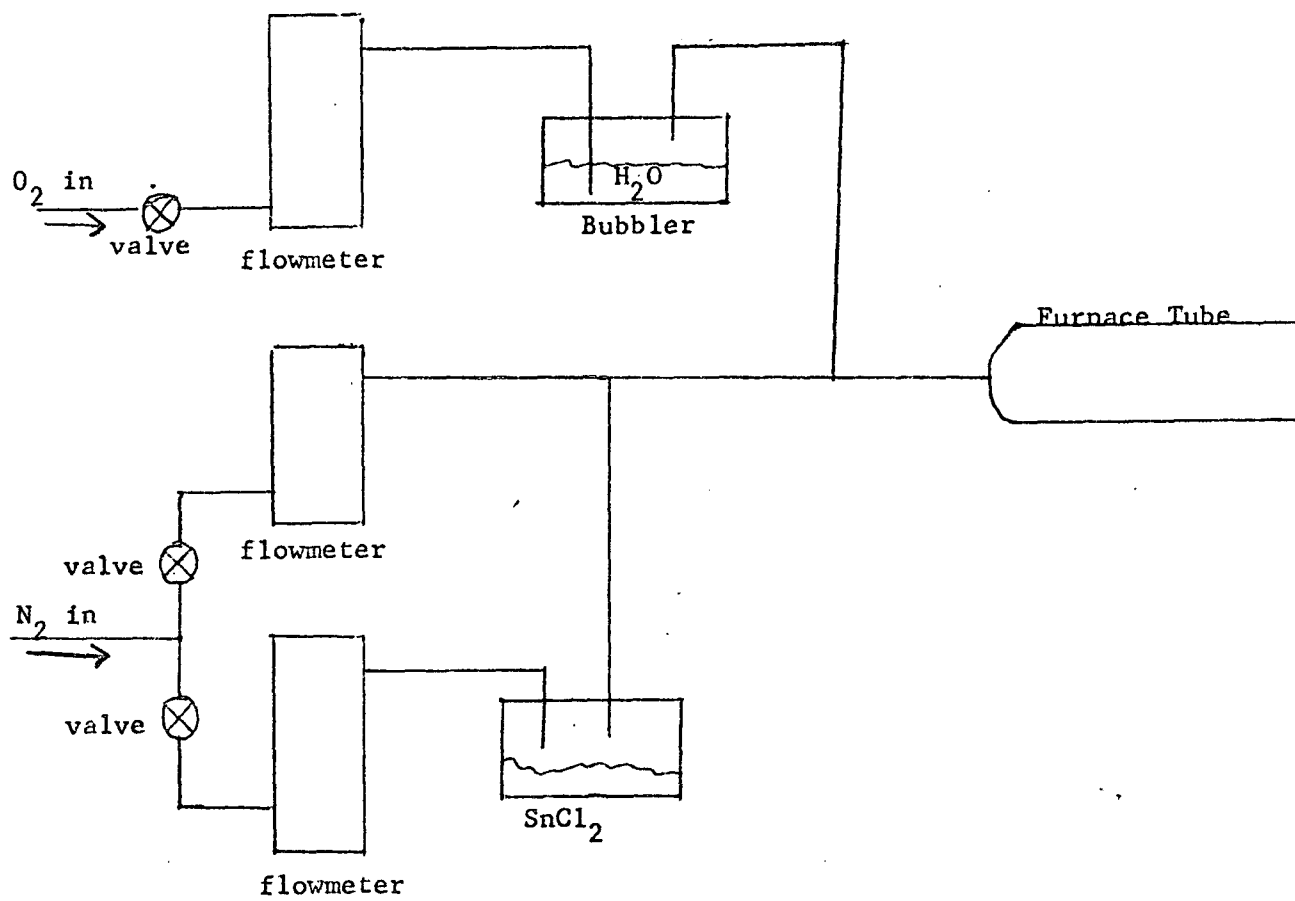
Apparatus for Depositing Tin Oxide

(the transparent electrode)

Figure 7

Figure 8

Tin Oxide Sheet Resistance vs. Time of Deposition furnace at $530^{\circ}C$
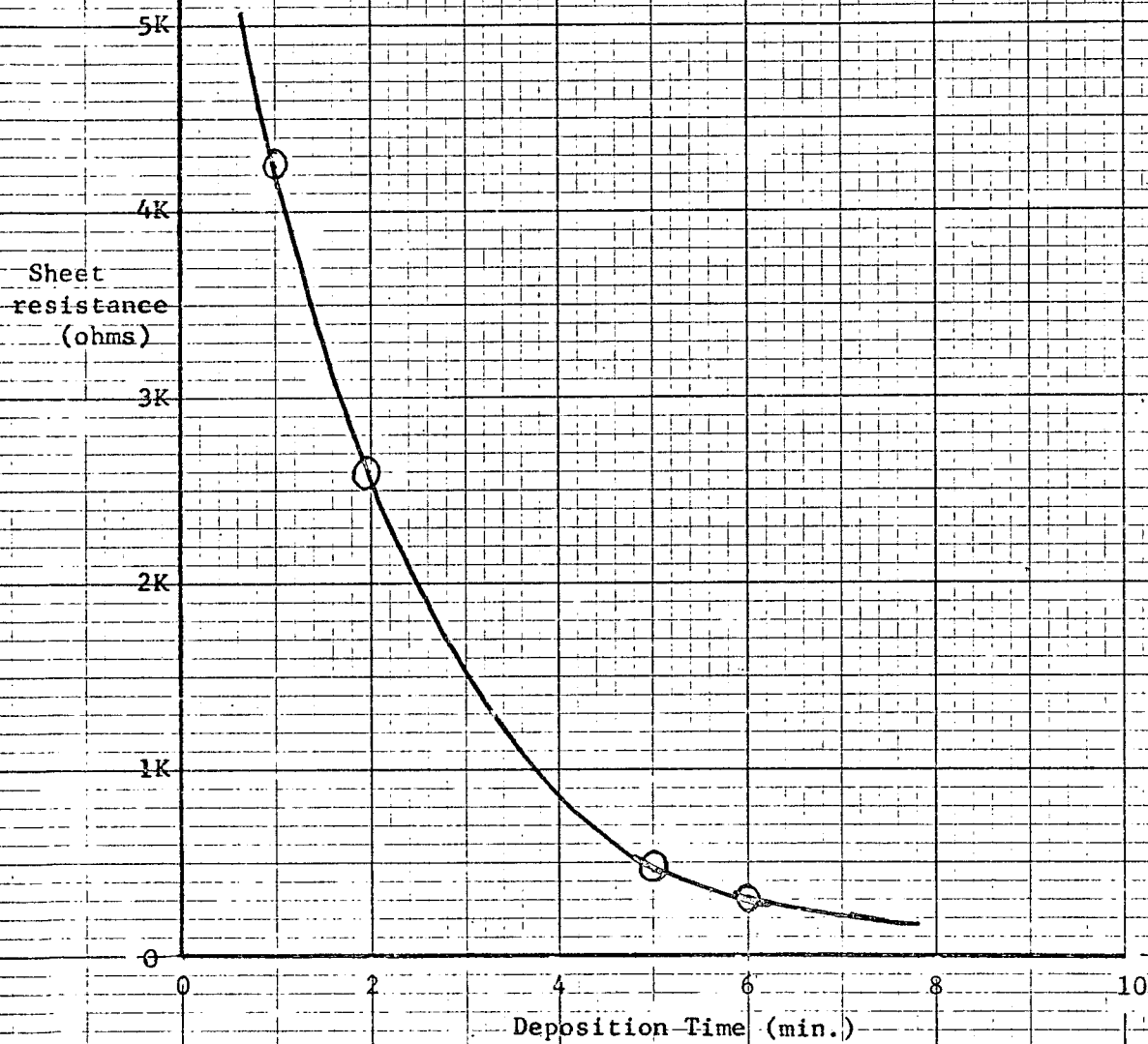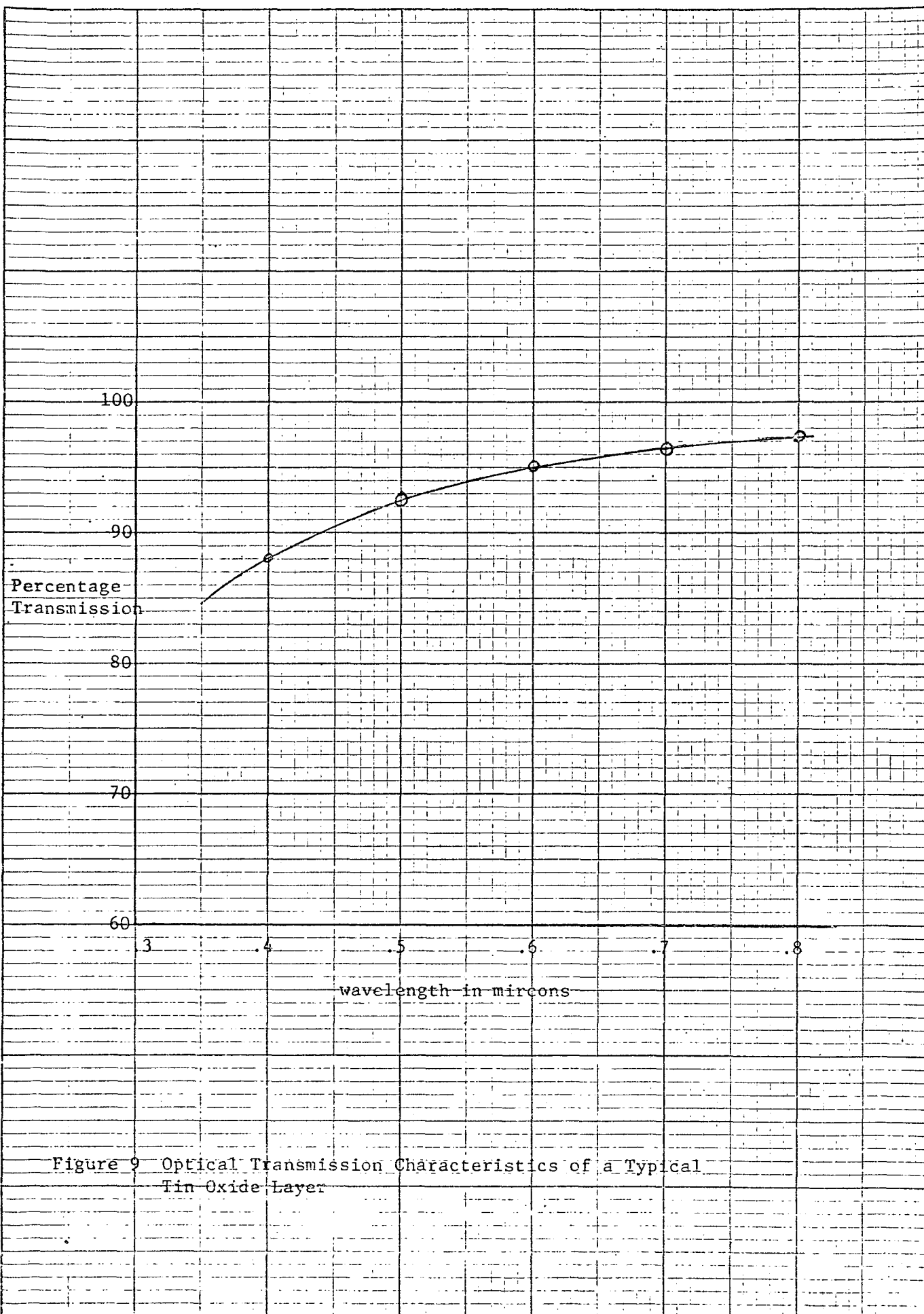
Figure 9 Optical Transmission Characteristics of a Typical Tin Oxide Layer
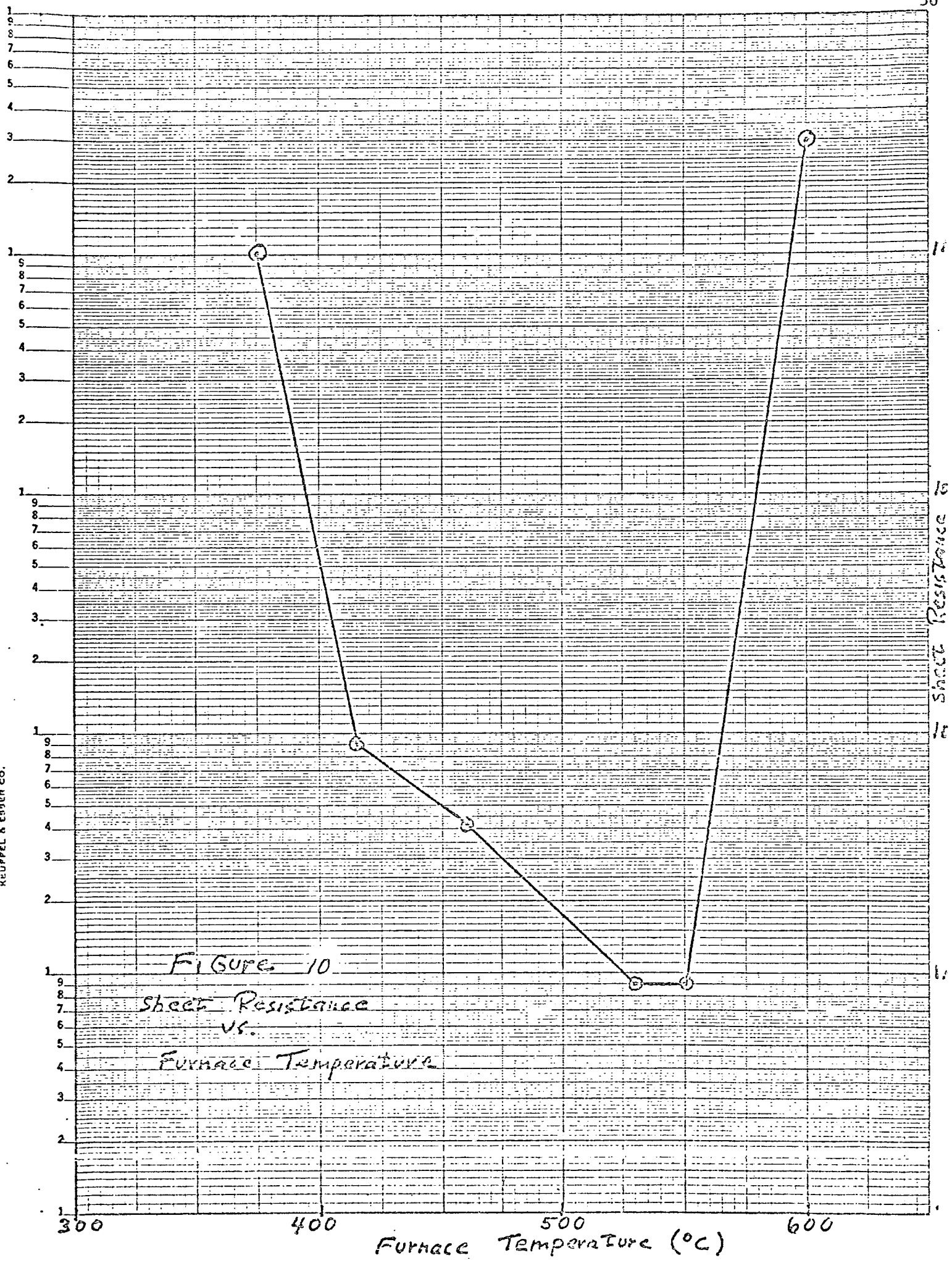
Figure 10
Sheet Resistance
vs.
Furnace Temperature

Sheet Resistance

Furnace Temperature (°C)
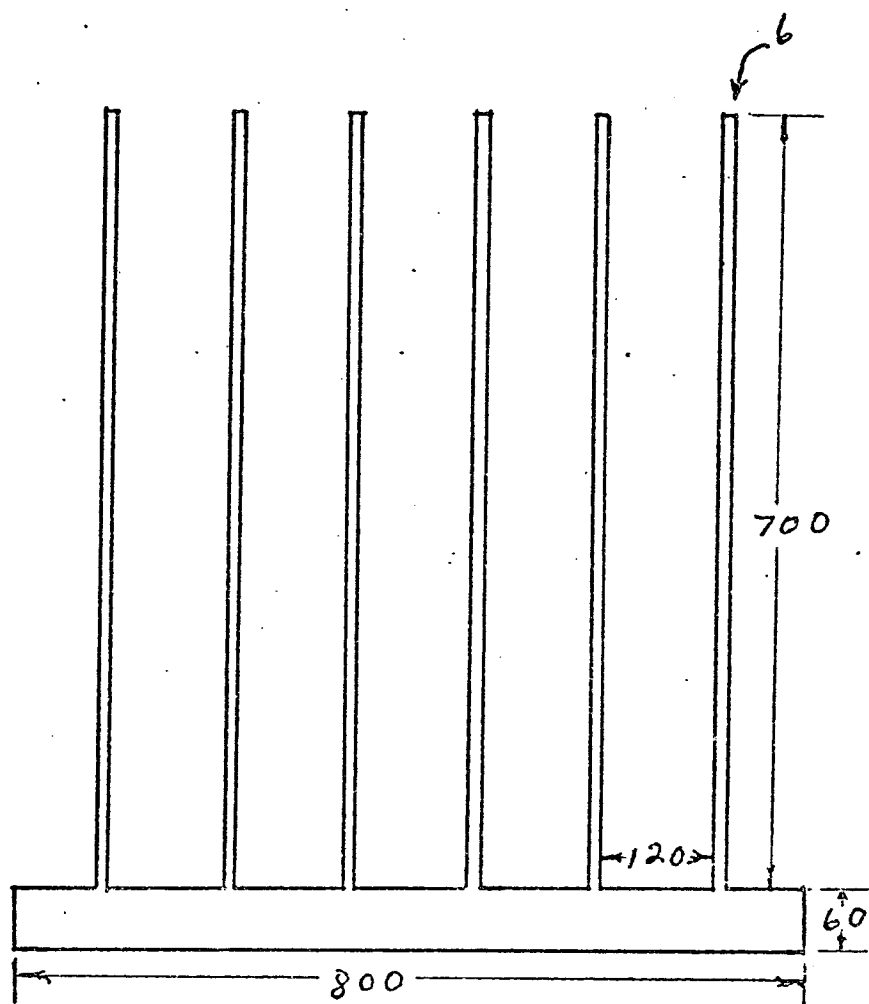
Figure 11   Cell Grid Pattern
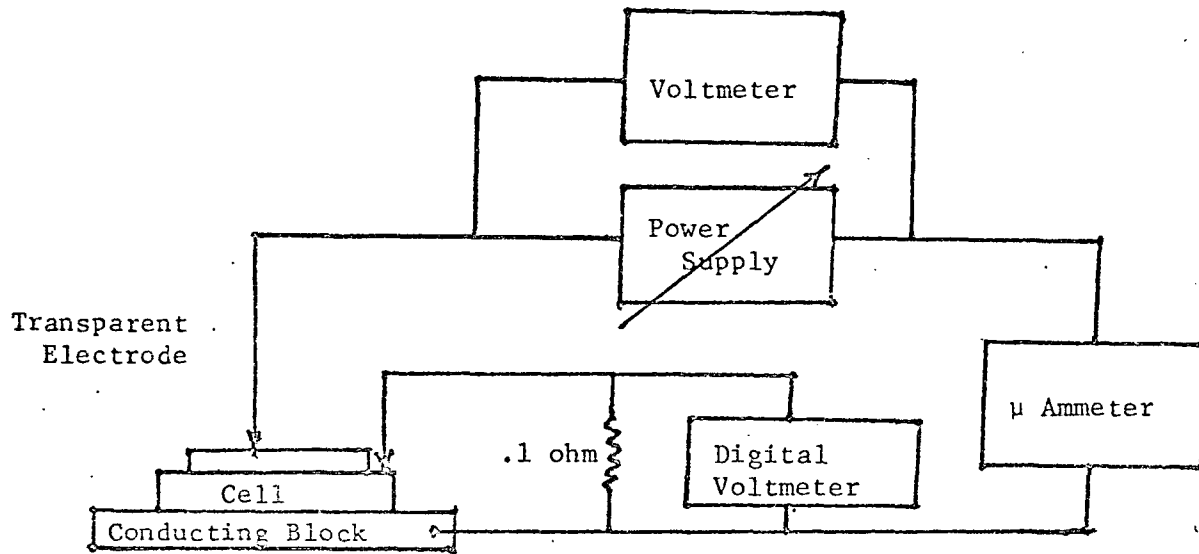
Figure 12

Block Diagram of Measuring Apparatus

178 mw/cm^2

142 mw/cm^2

110 mw/cm^2

72 mw/cm^2

Short
Circuit
Current

Transparent Electrode Bias vs.
Short Circuit Current

Data taken 9-9-72
Cell: Inversion cell
     Series #5, Cell #3
Test Temp. 20°C
Simulator Sylvania FBE

Illumination obtained by comparing
with solar cell calibrated by JPL

BIAS ON TRANSPARENT ELECTRODE

volts

Figure 13
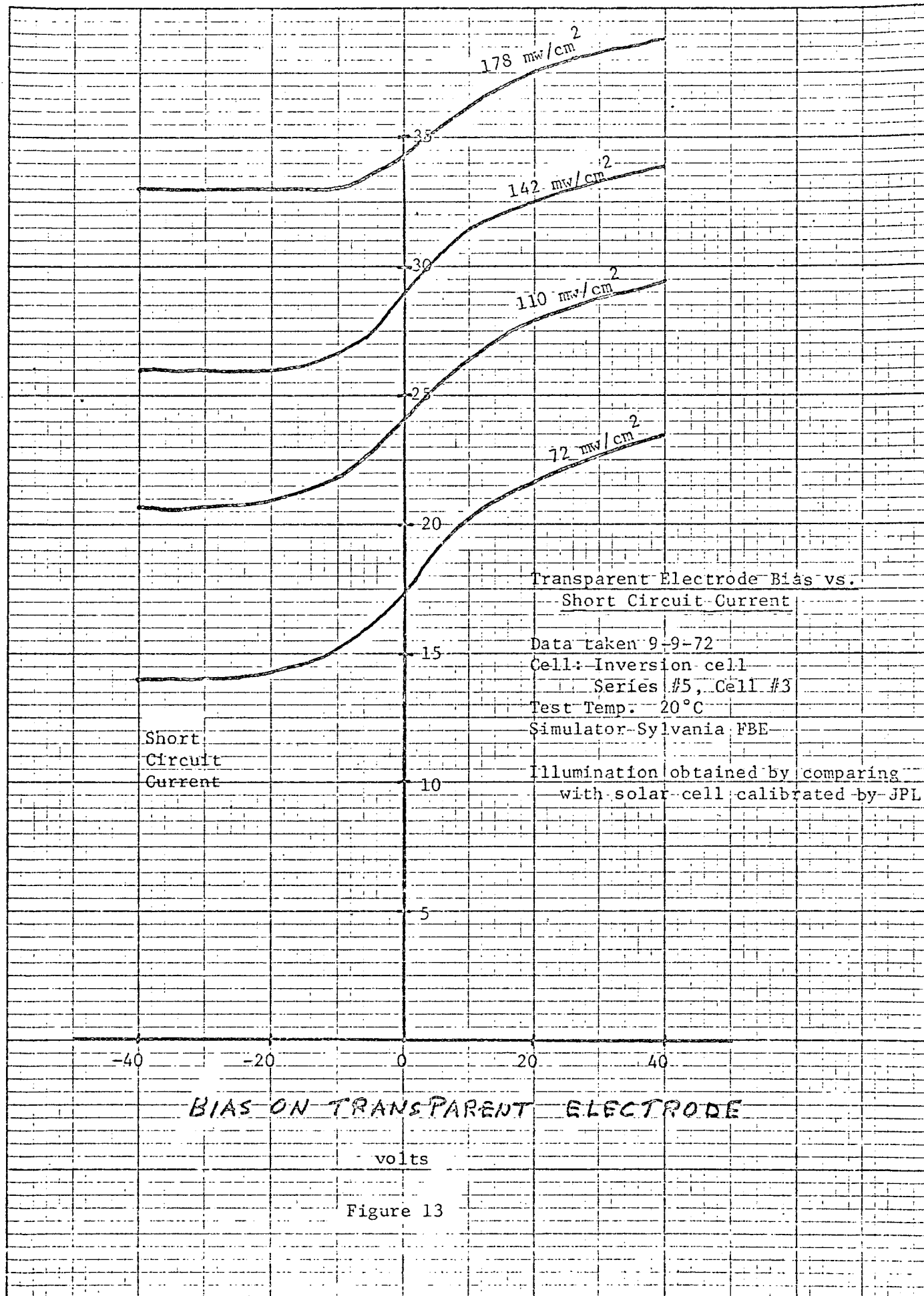
I-V CHARACTERISTIC CURVE
BY: R. Adams   DATE: 9/9/72
CELL: Inversion Cell Series #5, Cell #3
TEST TEMP: 20°C
ISC PER JPL STD.: 134.5 ma.
SIMULATOR: Sylvania FBE
VARIC SETTING: 90
BIAS FOR CURVES FROM TOP TO
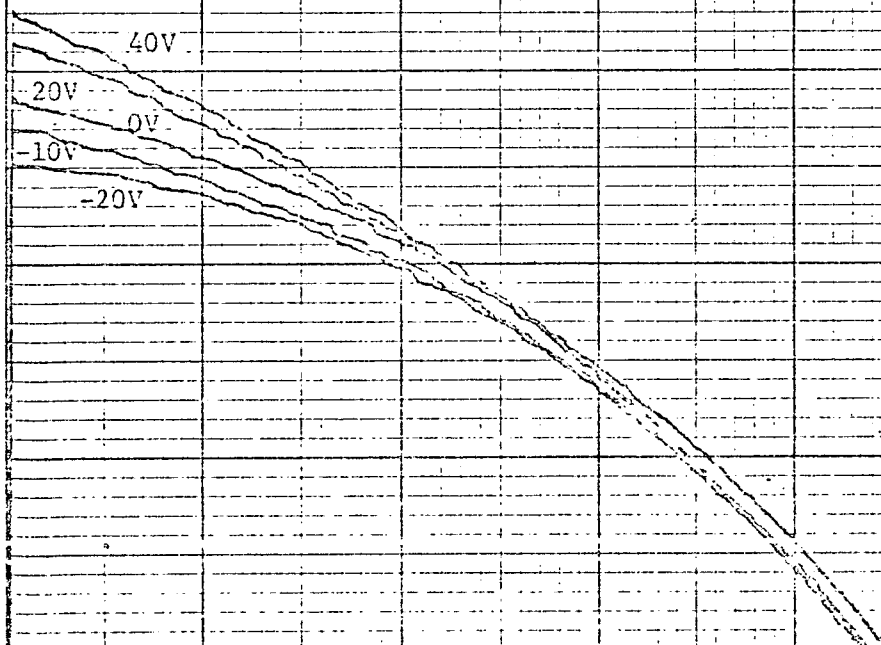BOTTOM RESPECTIVELY: 40V, 20V, 0V, -10V, -20V
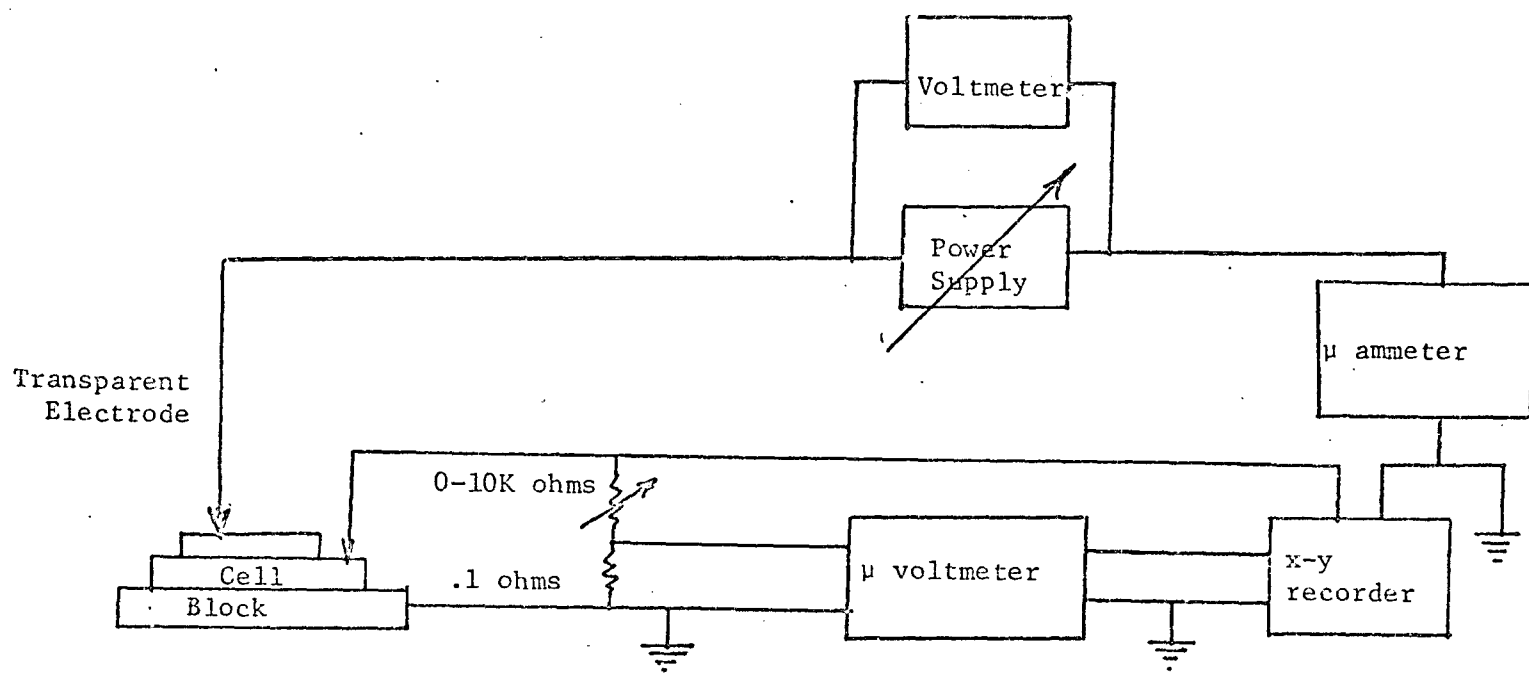
Figure 14

CURRENT (20 ma./in)

VOLTAGE (200 mv./in)

40V
20V
0V
-10V
-20V

Figure 15

Block Diagram of I-V Plotter

.5 cm

.5 cm

.35 cm

.25 cm

Transparent
Electrode

n Diffusions

Metal Ring

2 cm.

2 cm.
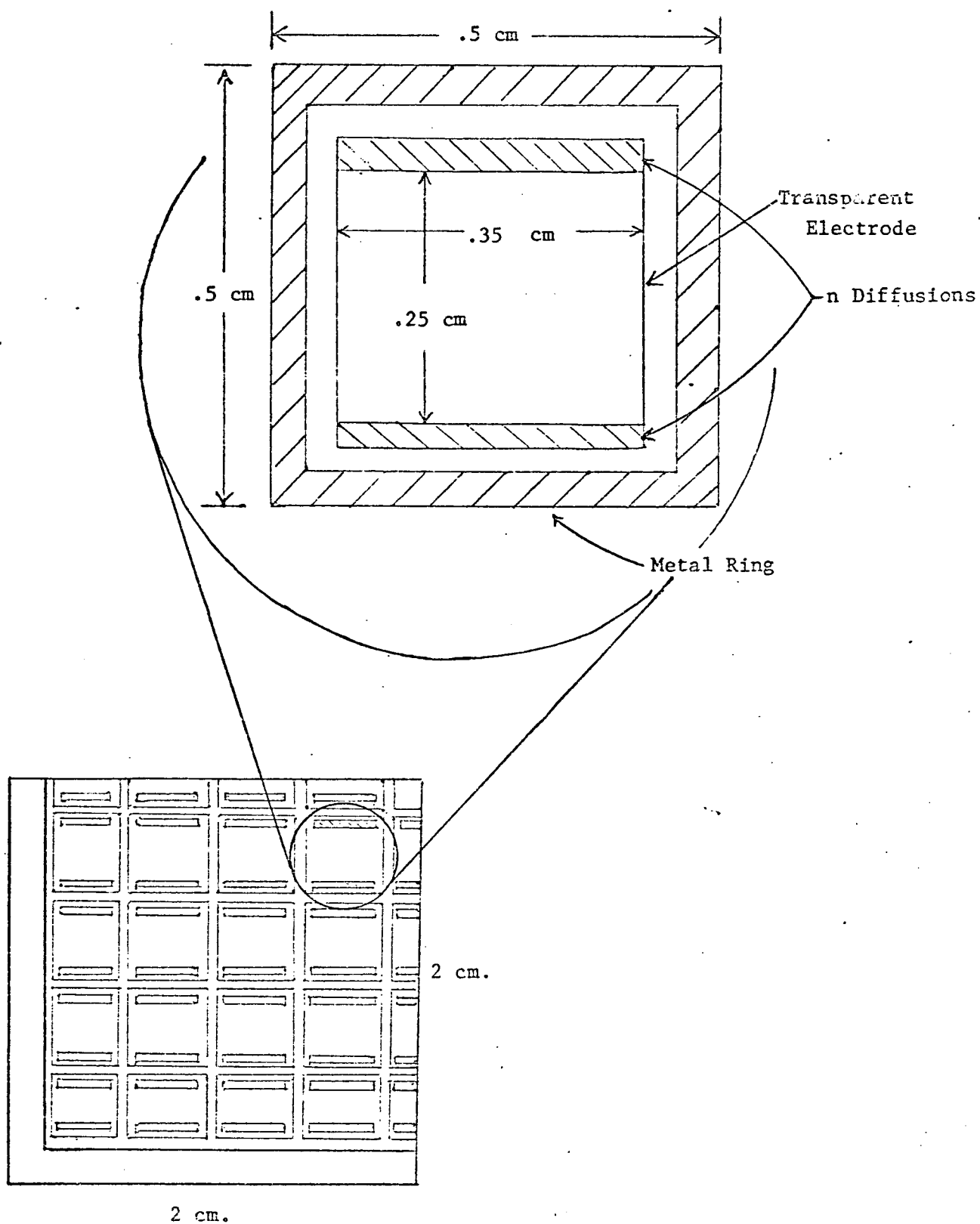
Figure 16

New Cell Configuration

Metal   Transparent Electrode

                                                                    SiO$_2$

n   n

p

Diffused Stripes
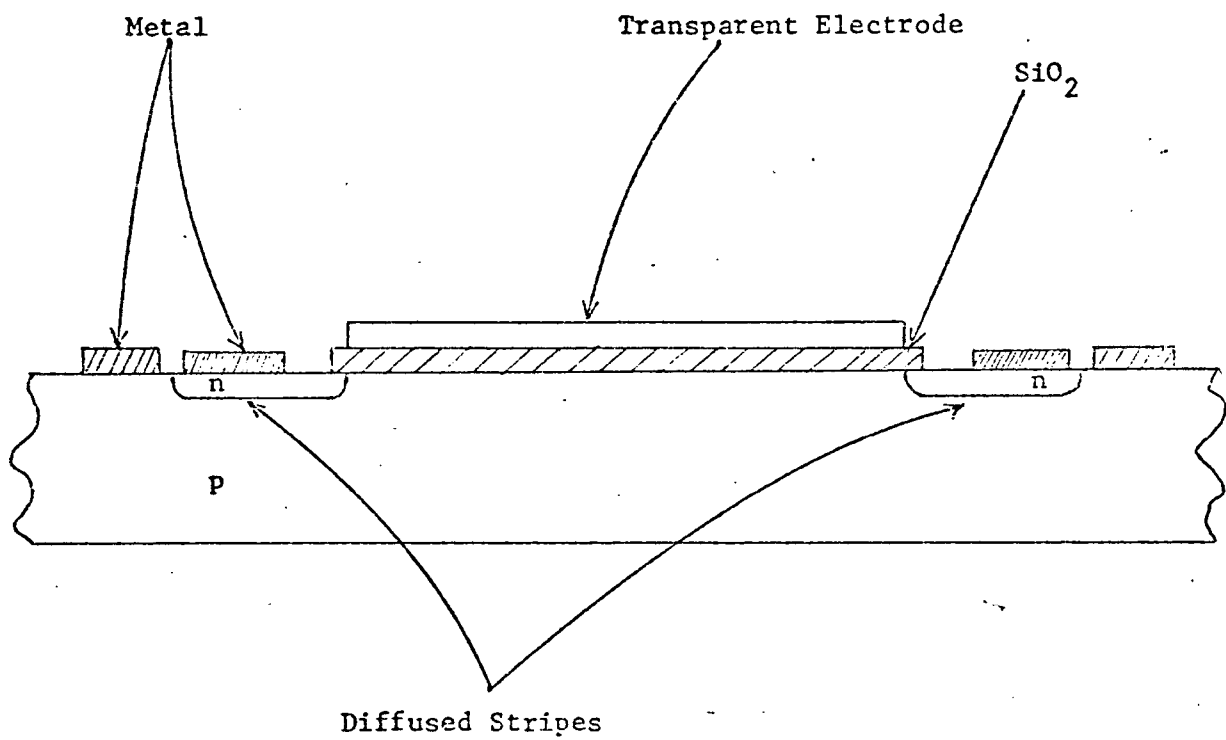
Figure 17

Cross-section of New Cell Configuration

Figure 18

Current between

n diffusion

(ma)

I vs. Bias
(.1 volt between
n diffusions)

Series 6
No. 1 (small cell)

Room Temperature

No Illumination
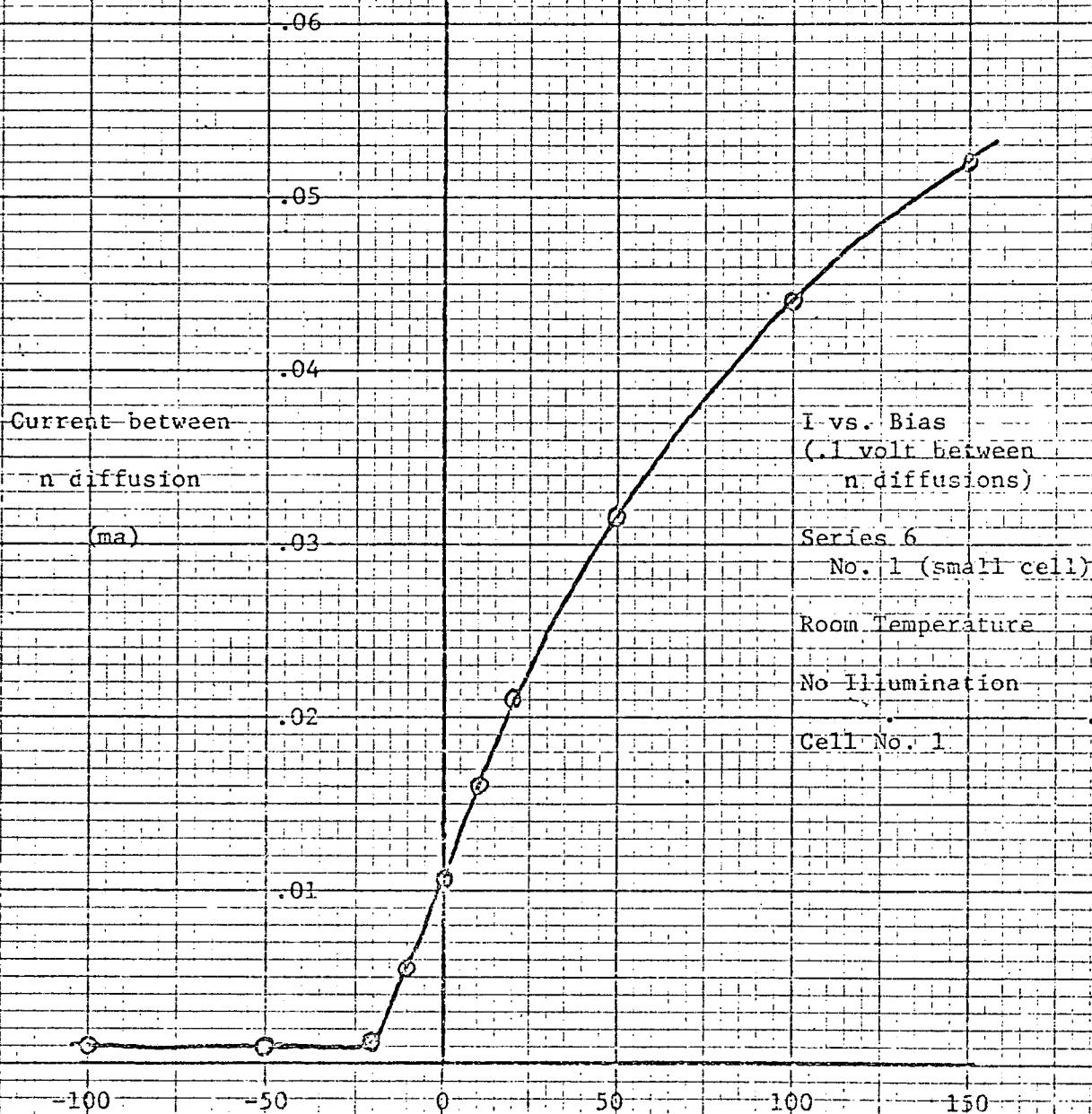
Cell No. 1

Volts bias on transparent electrode, Cell No. 1

Figure 19

I vs. Bias
(.1 volt between
n diffusions)

Series 6
No. 1 (small cell)

Room Temperature

No Illumination

Cell No. 2

Current between n diffusion (ma)
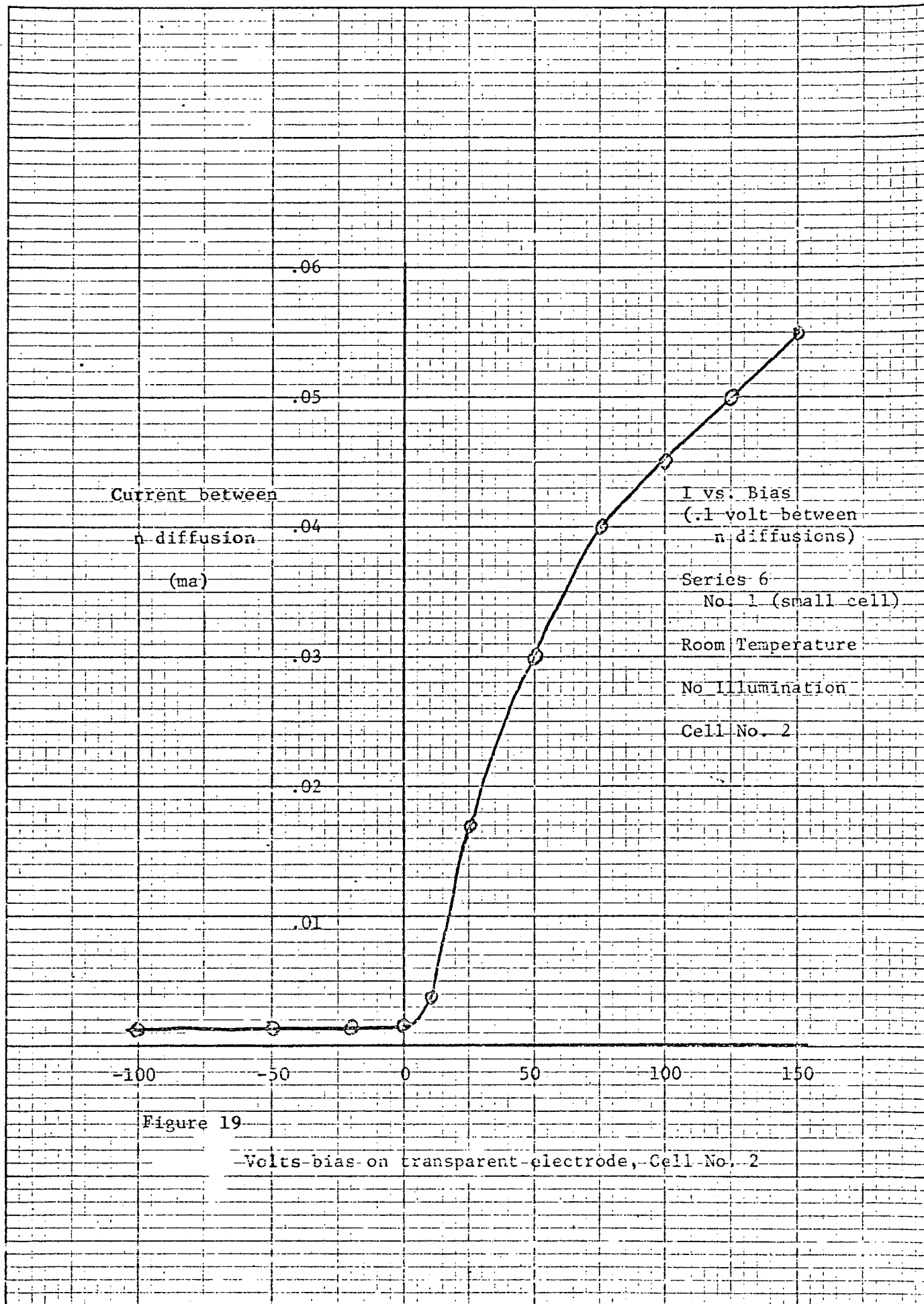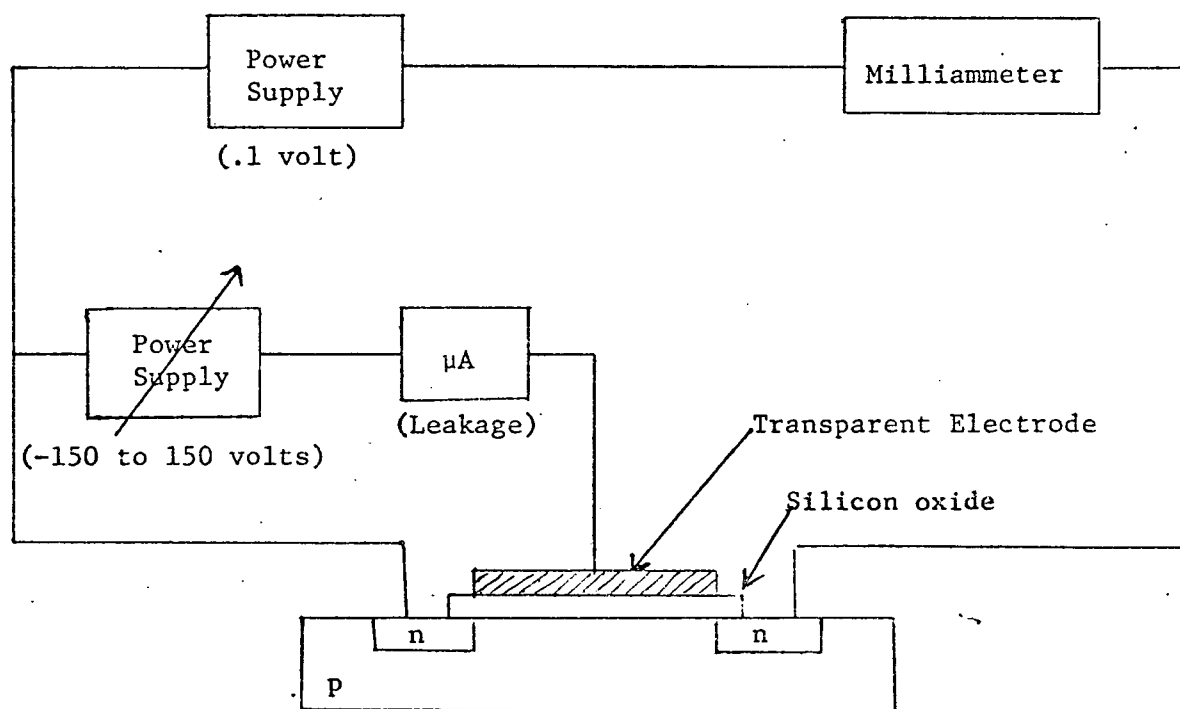
Volts bias on transparent electrode, Cell No. 2
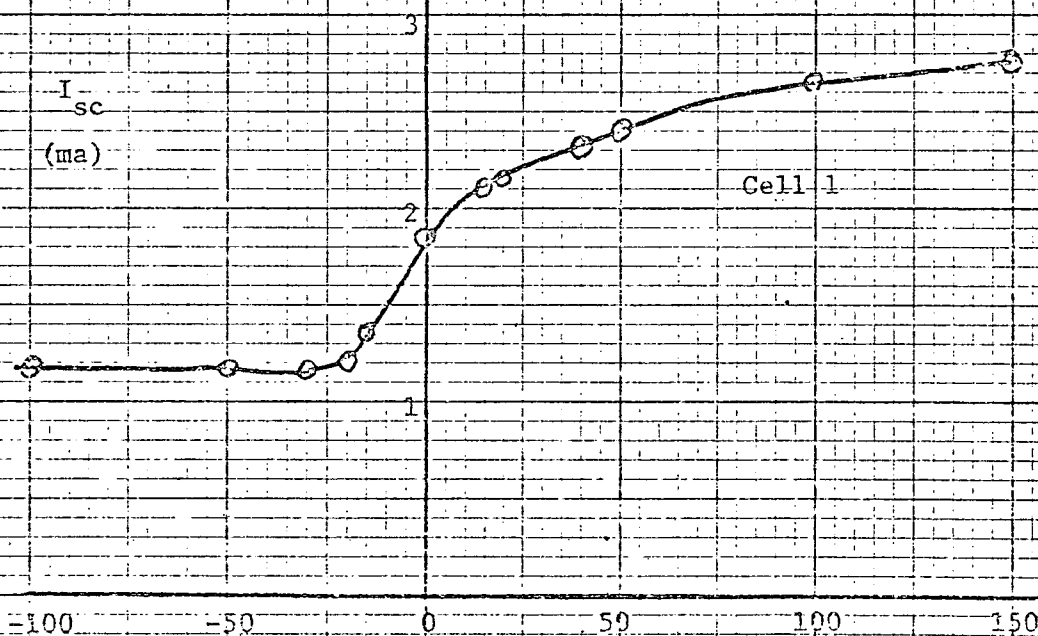
F

Figure 20

Circuit Used for Conductance Measurements
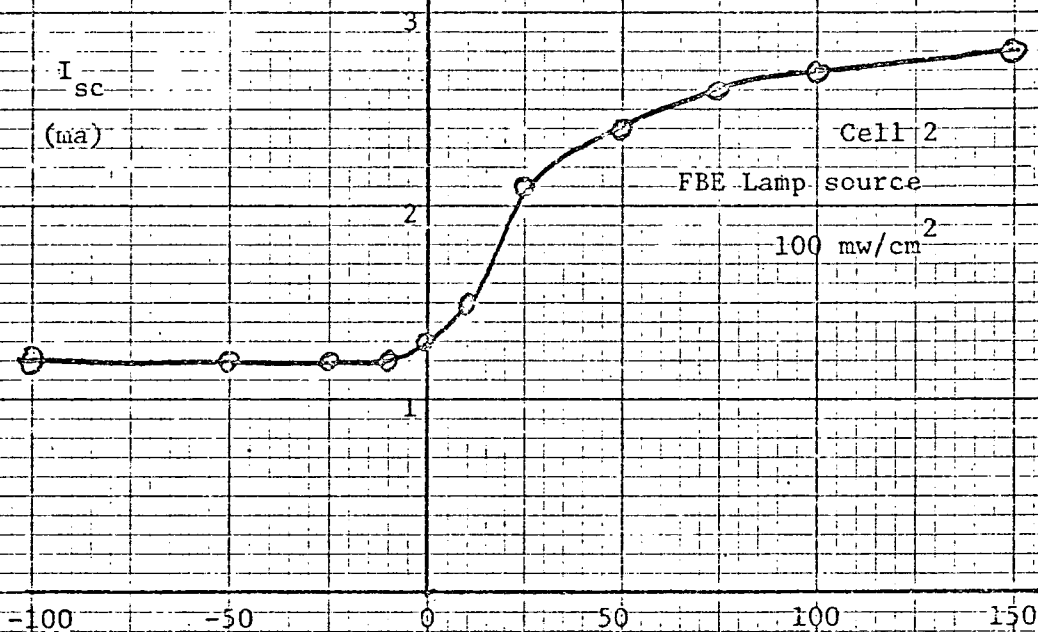
Figure 21

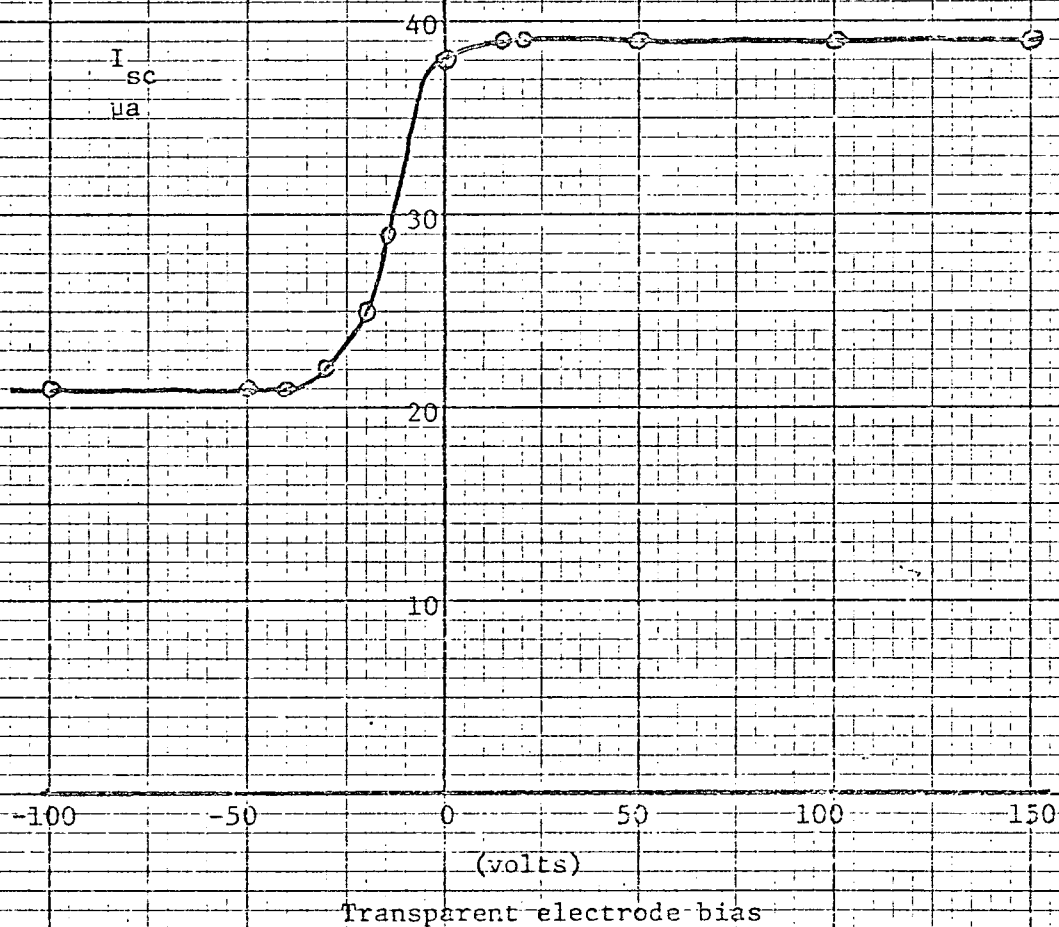Transparent-electrode bias vs. I_{sc} for small cell, Series 6, wafer 1

Figure 22

Transparent electrode bias vs. I_{sc} for series 6, wafer 1, cell 1.
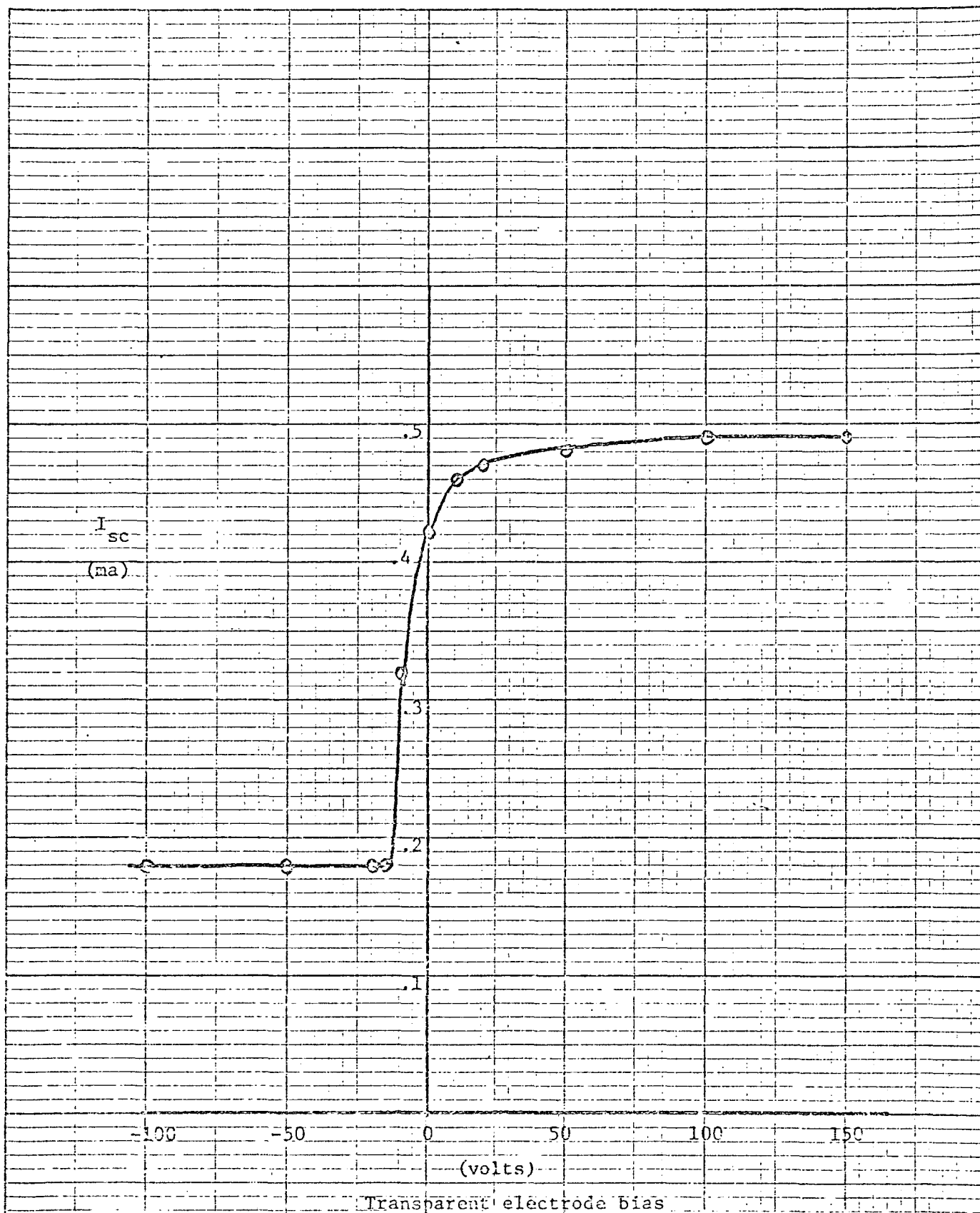Exposure to an ultraviolet source.

Figure 23

Transparent electrode bias vs. I_{sc} for series 6, wafer 1, cell 1. Exposed to mercury vapor source.

Figure 24

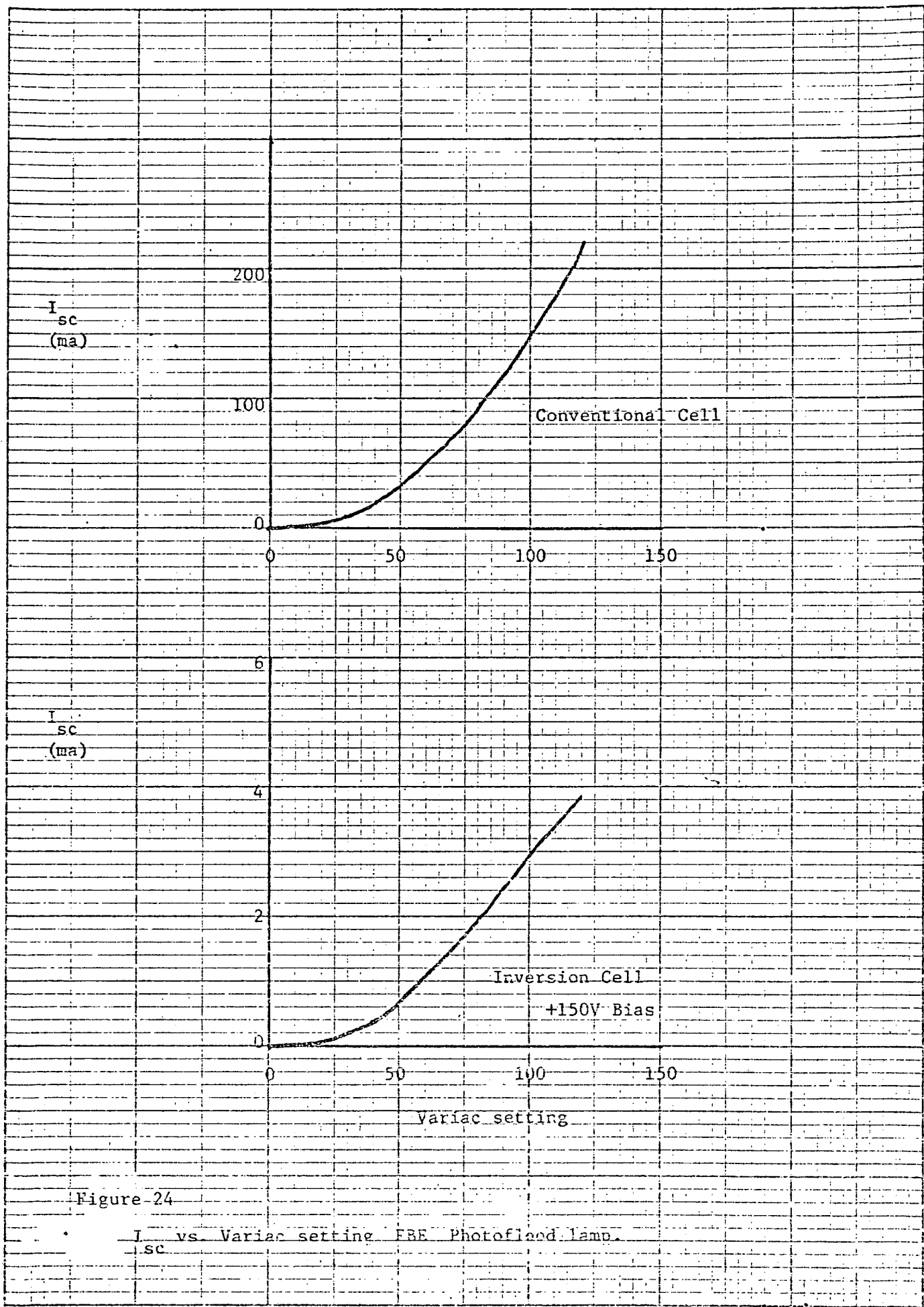I_{sc} vs. Variac setting FBE Photoflood lamp.
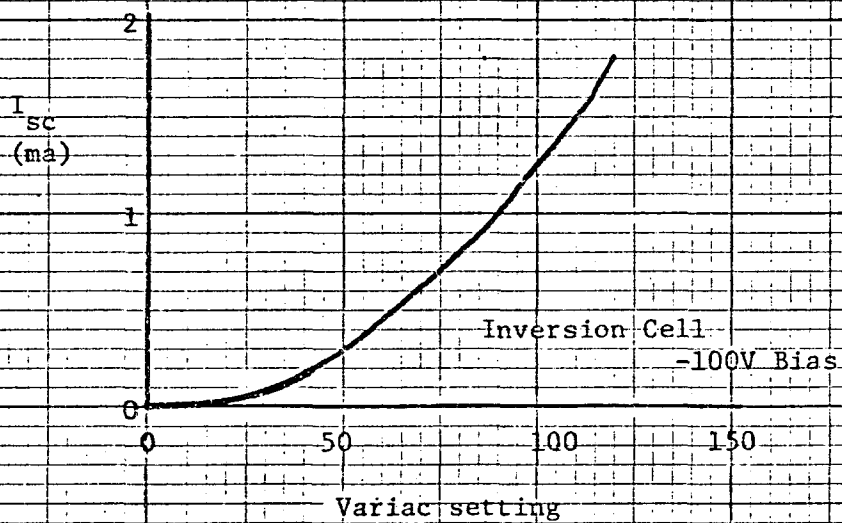
Figure 25

Ratio of conventional cell I_{sc} and inversion cell I_{sc} vs. variac setting
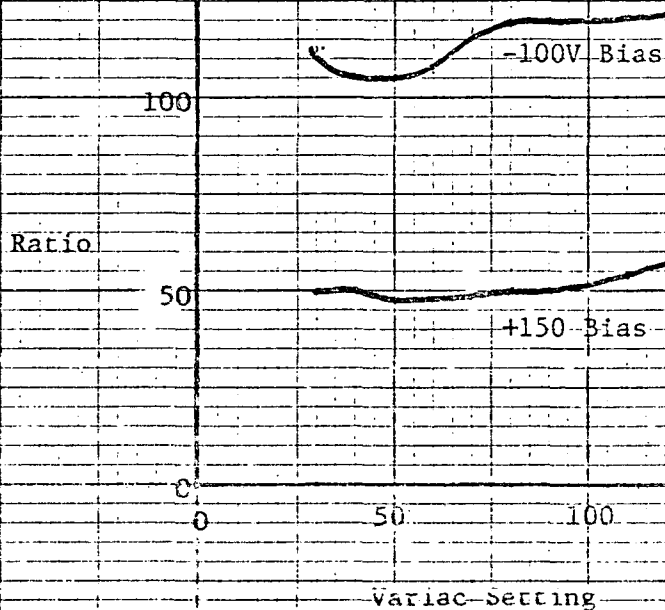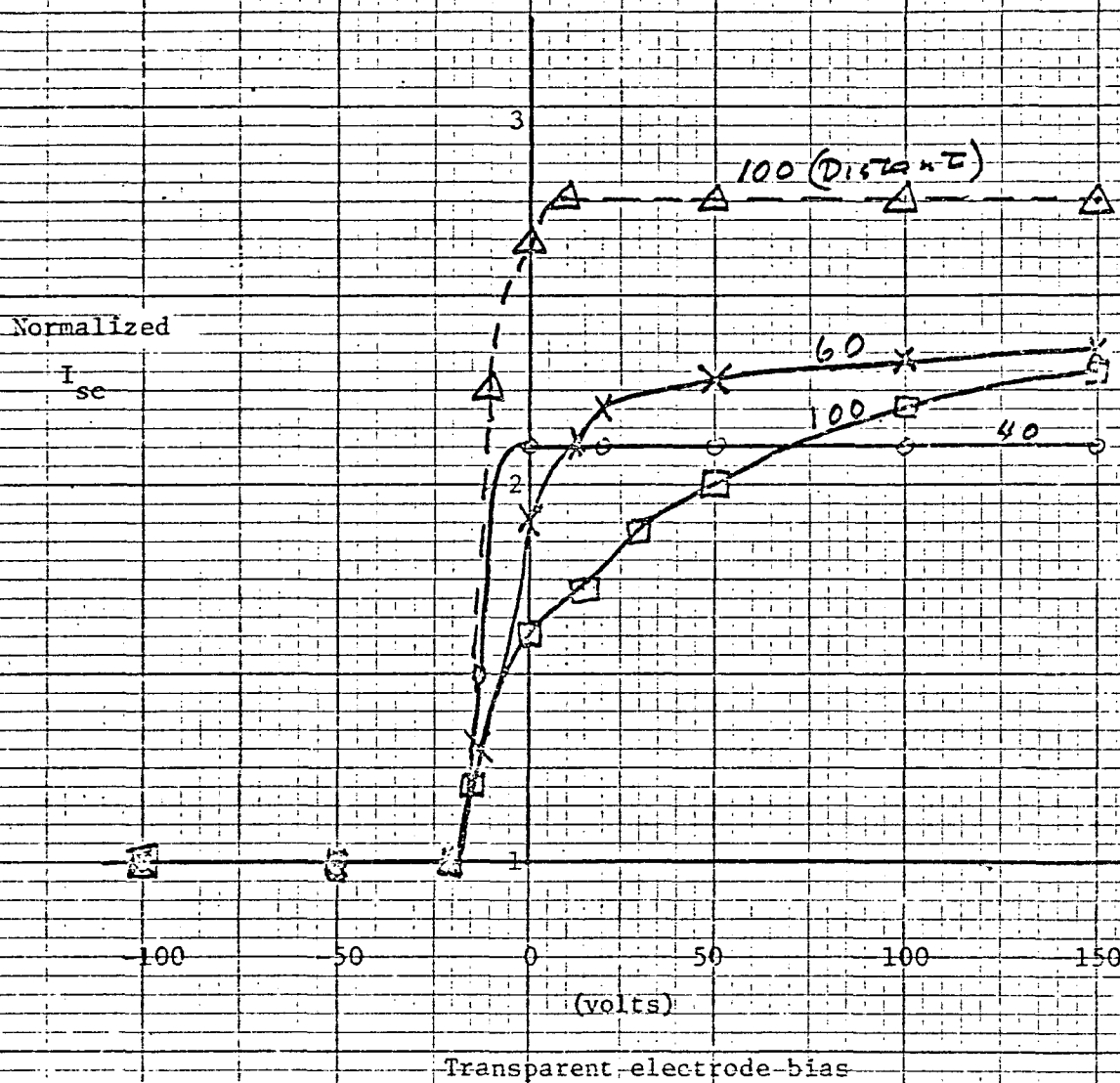
Figure 26

Normalized I$_{sc}$ vs. Transparent electrode bias for inversion cell, series 6, for various variac setting.

R. Adams 11/4/72

Isc vs. Variac Setting for:
1. JPL std. Cell
2. JPL Cell #1
3. JPL Cell #1 with Antireflective Coating Removed

Source: Sylvania FGE

Figure 27

	Isc (Merc. Vapor Source)	Isc (Ultraviolet Source)
1.	15 ma.	.25 ma.
2.	15 ma.	.46 ma.
3.	10 ma.	.34 ma.

CHAMPION LINE NO. 642 – CROSS SECTION · 10 SQUARES TO INCH

Conductance Between
N Diffusions vs. Transparent
Electrode Bias

Small Cell
Room Temperature
No Illuminations

Conductance
(millohms)

Transparent Electrode Bias
(volts)
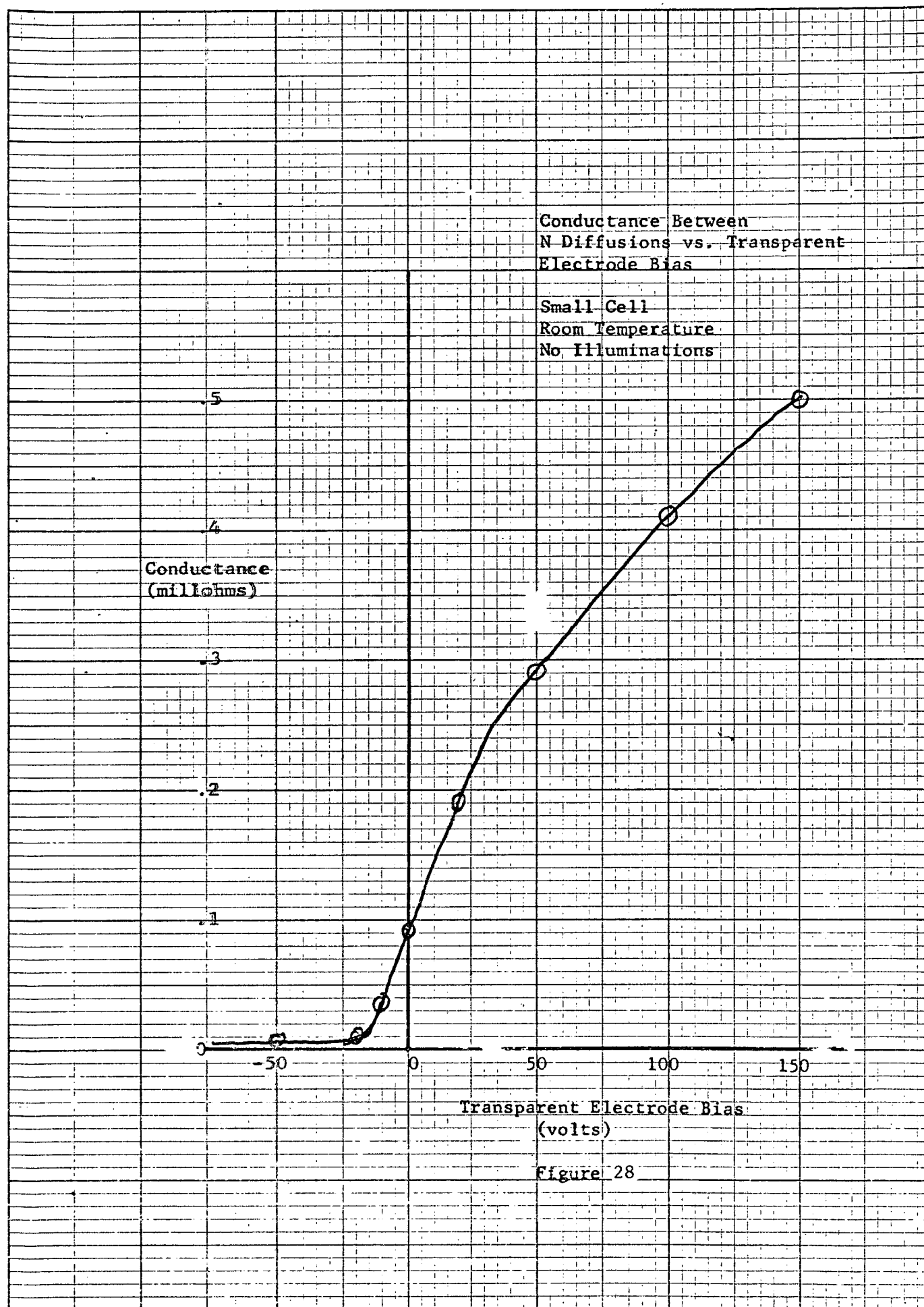
Figure 28

R. Adams 11/8/72

Isc vs. BIAS
SUBCELL (4,2) Wafer #1 Series #6
Source: Sylvania FBE (140 mw/cm²)

Figure 29

Isc (ma)

3.0

2.0

1.0

0

-20   0   20   40   60   80   100   120   140   160

TRASPARENT ELECTRODE BIAS (VOLTS)

CHAMPION LINE NO. 642 – CROSS SECTION · 10 SQUARES TO INCH

ISc VS. BIAS
SUBCELL (4,2) Wafer #1 Series #6
SOURCE: Mercury Vapor

Figure 30

Isc (ma)

TRANSPARENT ELECTRODE BIAS (VOLTS)
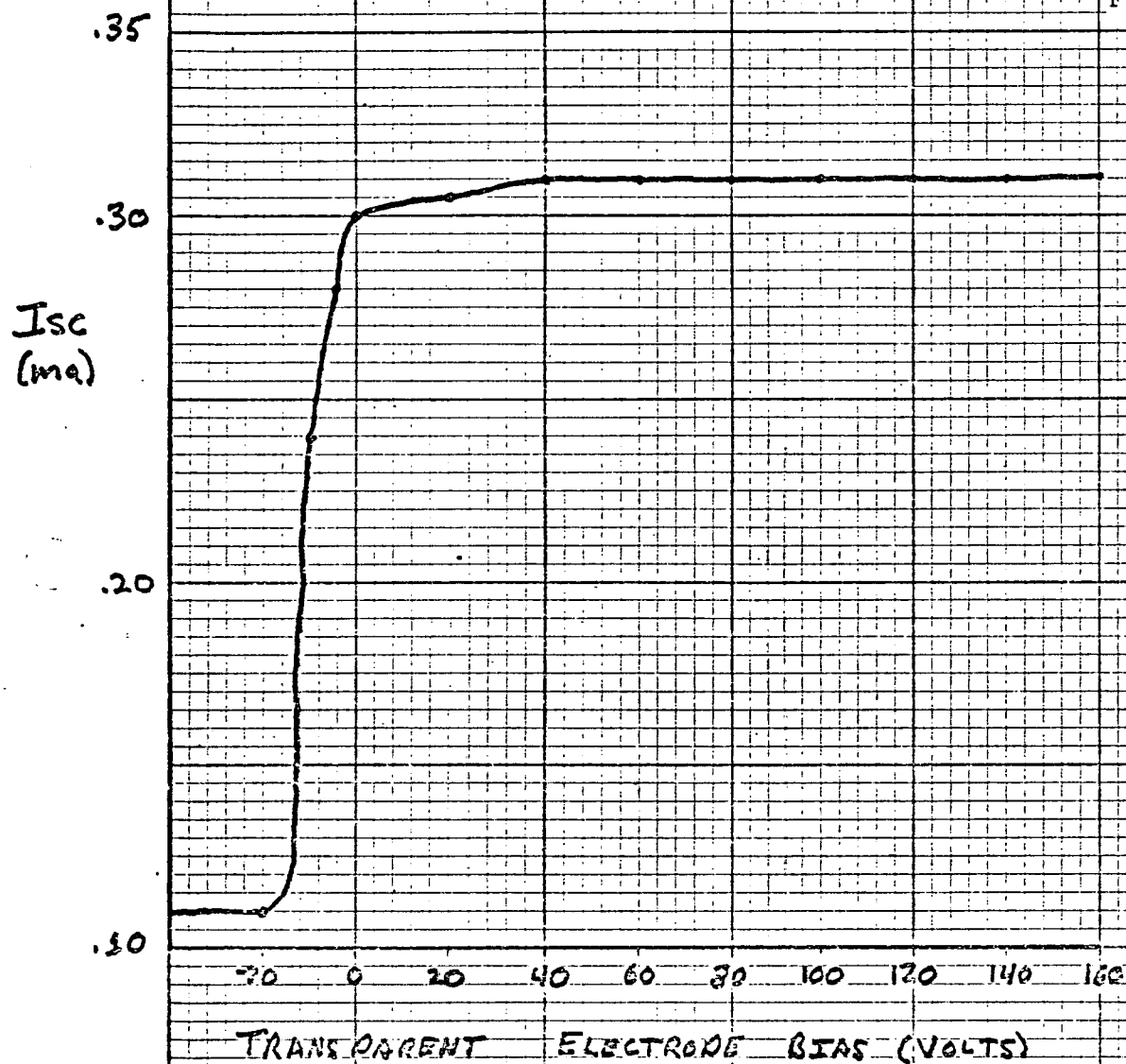
R. Adams   11/9/72

Isc vs. BIAS
SUBCELL (4,2) Wafer #1 Series #6
SOURCE: Ultraviolet

Figure 31
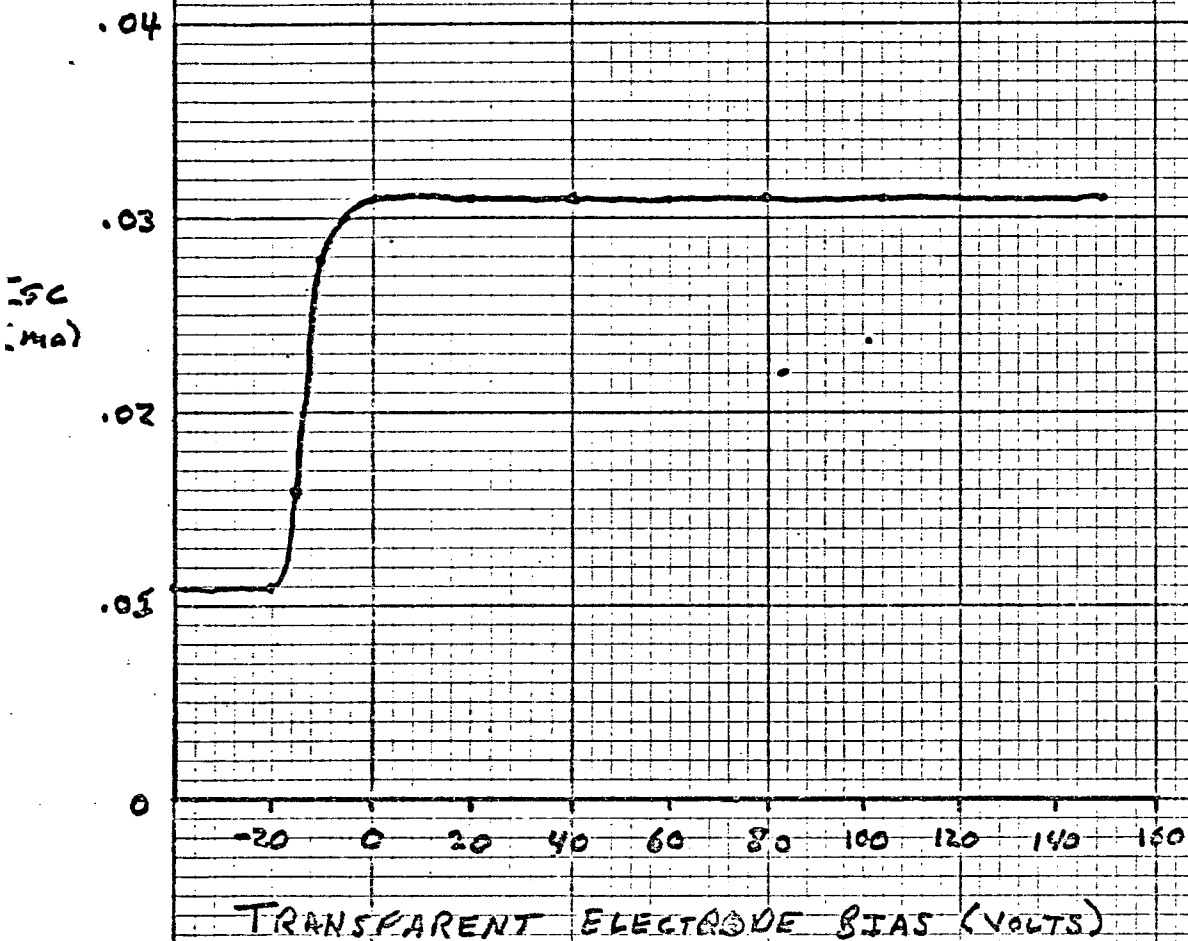
Isc (ma)

TRANSPARENT ELECTRODE BIAS (VOLTS)

.04

.03

.02

.01

0

-20   0   20   40   60   80   100   120   140   160

Isc vs. Distance of Knife Edge over Subcell
with one contact connected to test
circuit.

Subcell (4,2) Wafer #1 Series #6
Source: Sylvania FBE (140 mw/cm²)

Figure 32

Isc (ma)

BIAS: 80V
40V
20V
0V
-10V
-20V

Distance of Knife Edge over Subcell in Inches

R. Adams 11/8/72

ISC VS DISTANCE OF KNIFE EDGE OVER SUBCELL
WITH BOTH CONTACTS CONNECTED TO TEST
CKT.
SUBCELL (4,2) WAFER #1 SERIES #6
SOURCE: Sylvania FBE (140 $^{mw}/_{cm^2}$)
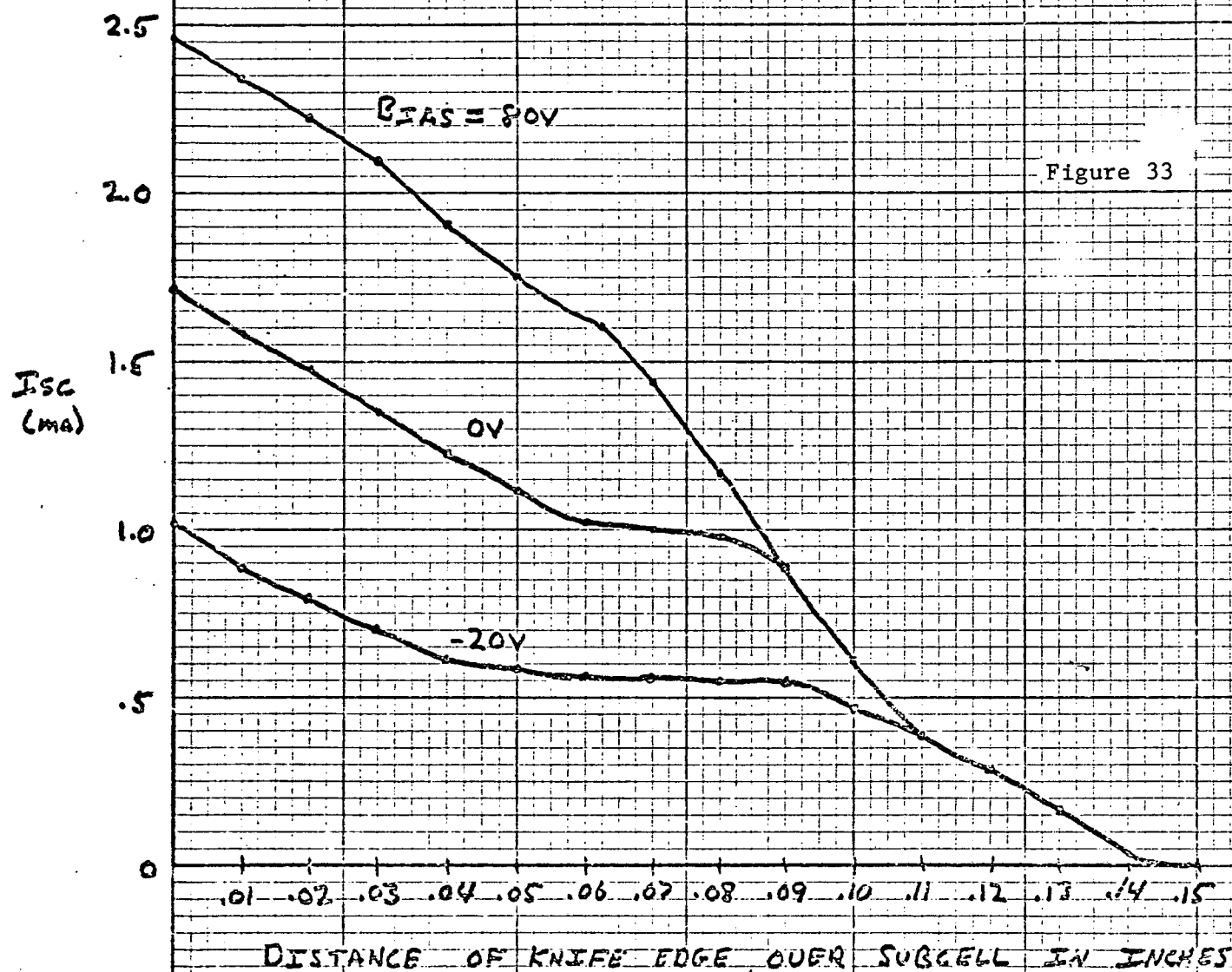
Figure 33

ISC (ma) vs DISTANCE OF KNIFE EDGE OVER SUBCELL IN INCHES

BIAS = 80V
0V
-20V

CHAMPION LINE NO. 642 - CROSS SECTION - 10 SQUARES TO INCH

G

Isc vs. Distance of Knife Edge over Subcell
with one contact connected to test
circuit
Subcell (4,2) Wafer #1 Series #6
Source: Mercury Vapor

Figure 34

Isc (ma.)

Bias = 0V

-10V

-20V

.4

.3

.2

.1

0

.01 .02 .03 .04 .05 .06 .07 .08 .09 .10 .11 .12 .13 .14 .15

Distance of Knife Edge over Subcell in Inches

R. Adams   11/9/72

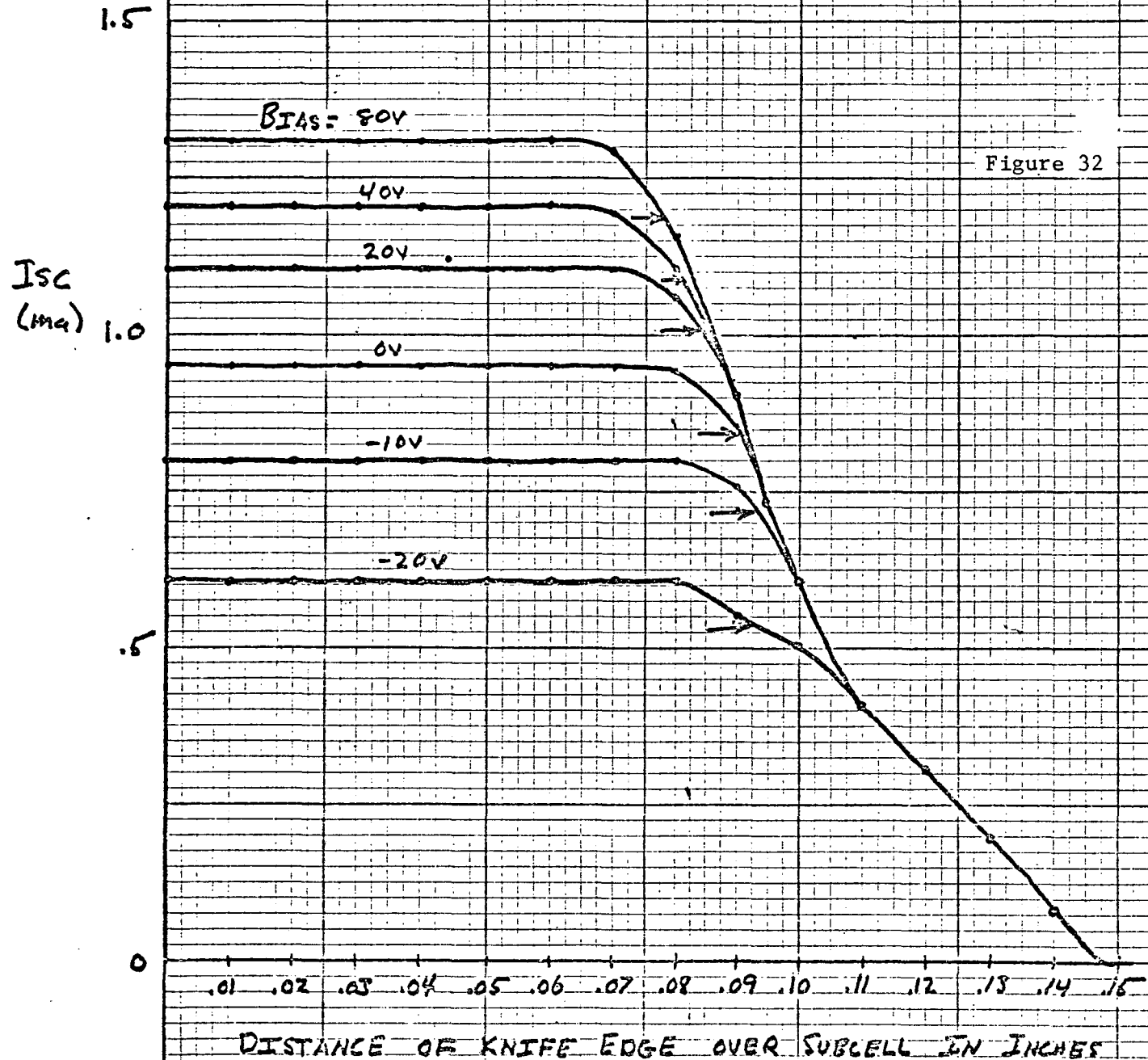ISC vs. DISTANCE OF KNIFE EDGE OVER SUBCELL WITH ONE CONTACT CONNECTED TO TEST CIRCUIT
SUBCELL (4,2) WAFER #1 Series #6
SOURCE: Ultraviolet

Figure 35

BIAS = 0V - 90V

-10V

-20V

DISTANCE OF KNIFE EDGE OVER SUBCELL IN INCHES

ISC (ma)

CHAMPION LINE NO. 642 - CROSS SECTION - 10 SQUARES TO INCH
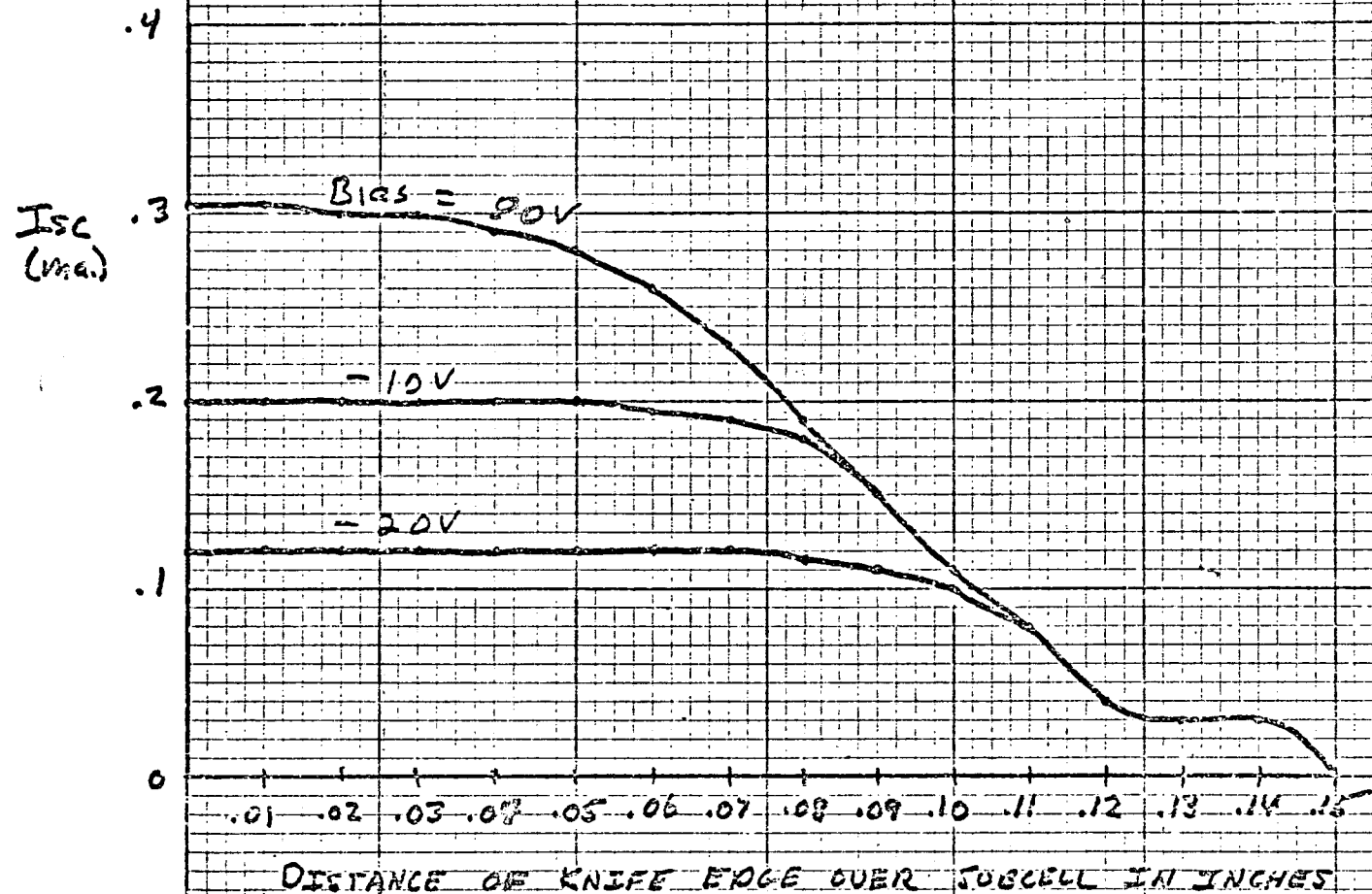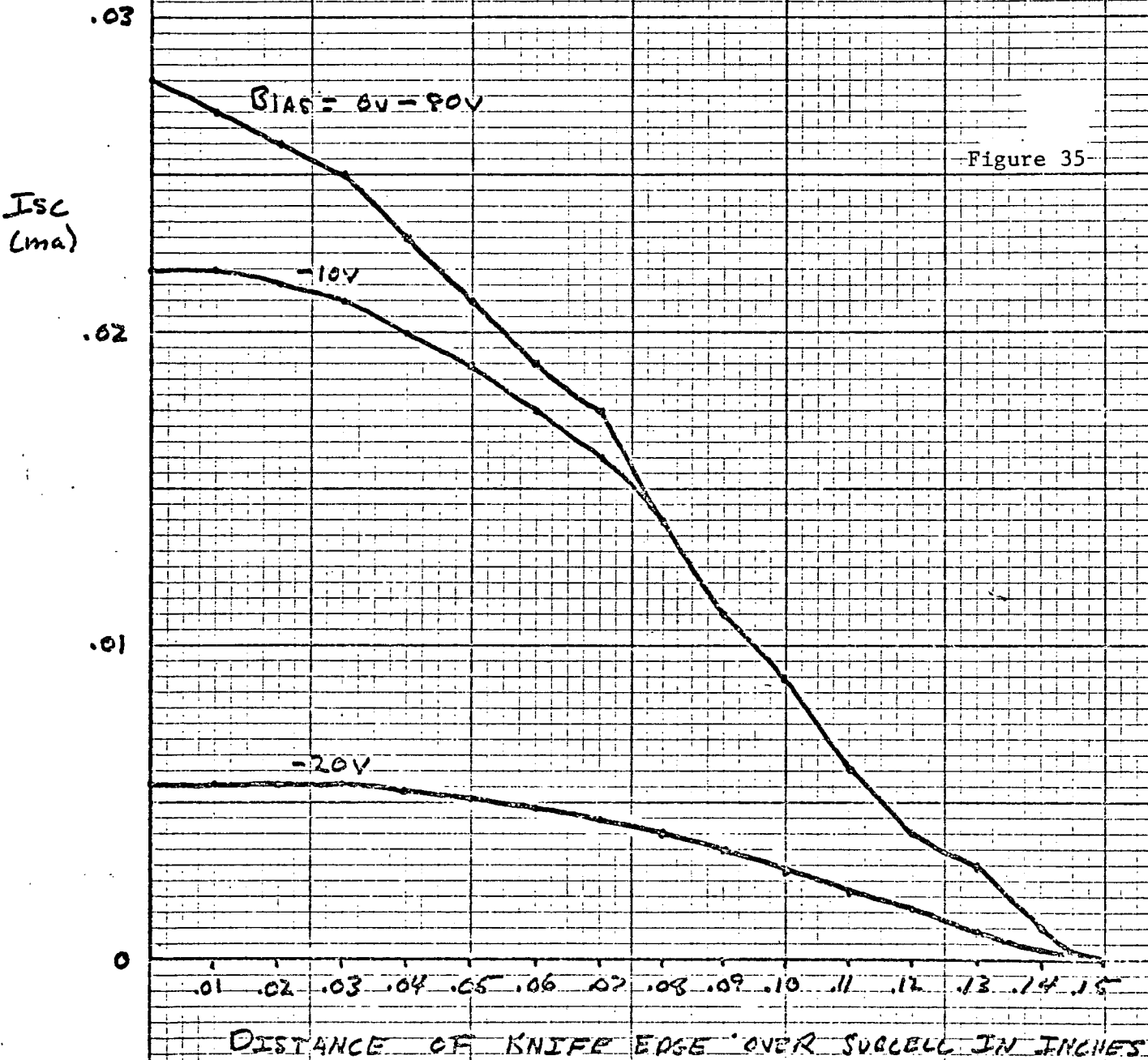
CELL: Series #6, Subcell (4,2) Wafer #1

TEST: I-V curves for blases of 80,40,0,-20 volts.

SOURCE: Sylvania FBE @ Sun Intensity (140 $\frac{mw}{cm}$

Figure 36

Sun Illumination

Photoflood Illumination

(FRE)

I_{sc} vs. Transparent Electrode

Bias for two different light sources.

Small cell. Room temperature.

120 mw/cm^2 illumination.

I_{sc} ma

volts

Transparent Electrode Bias

Figure 37

Average I_{sc} vs. contaminated oxide thickness for arrays of small solar cells
Room temperature
140 mw/cm^2
FBE incandescent illumination
NaCl contamination

Contaminated Oxide Thickness
Å
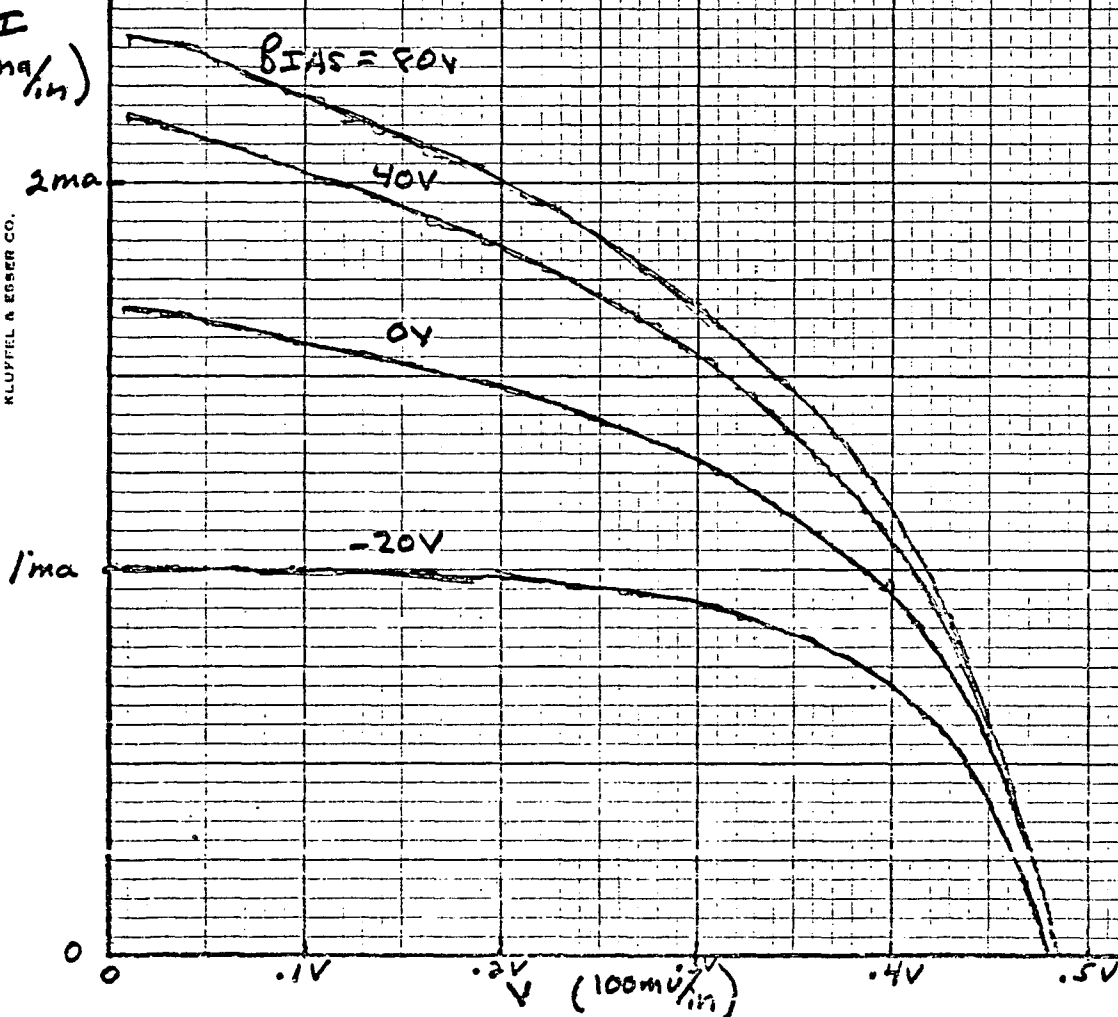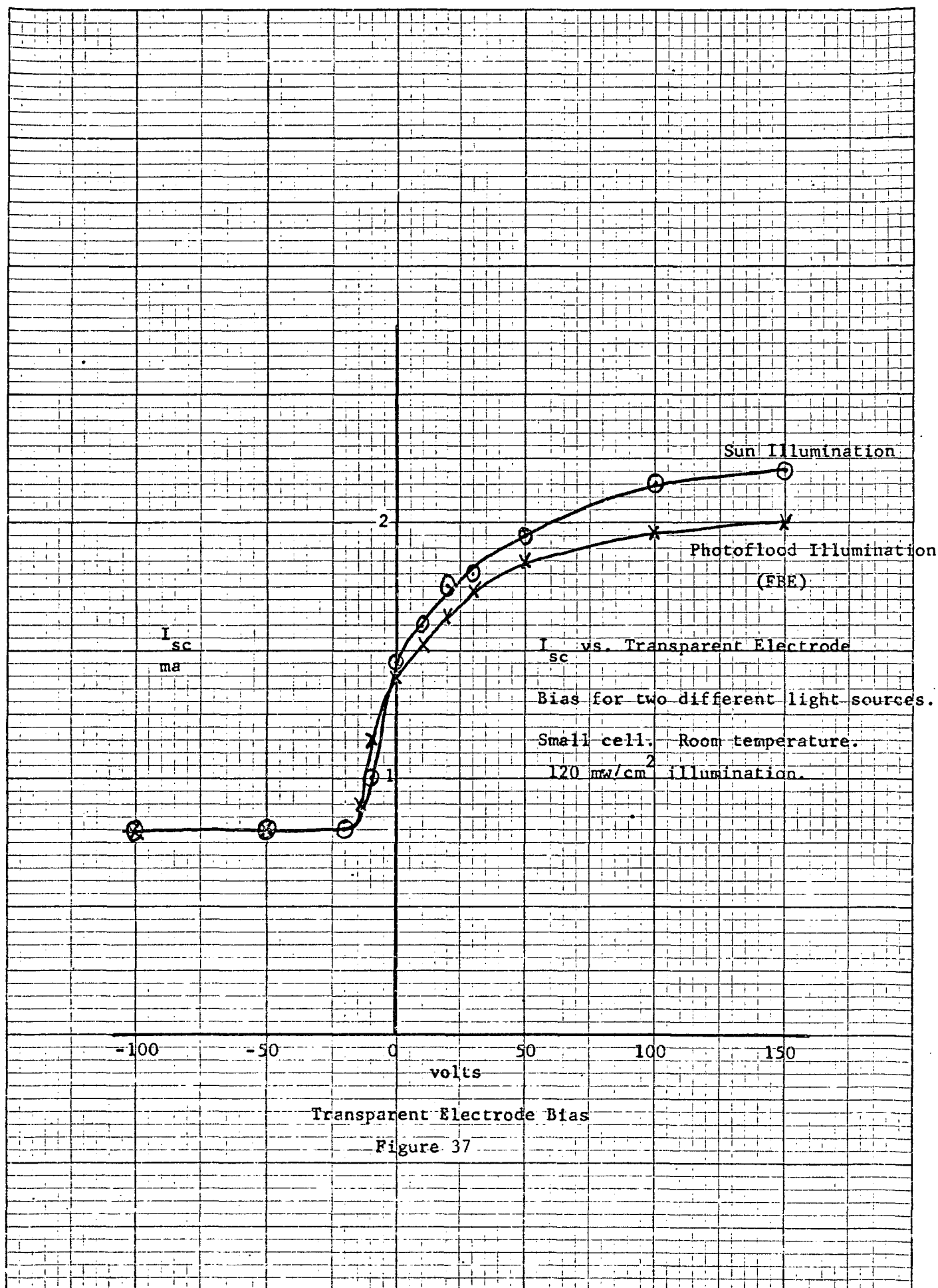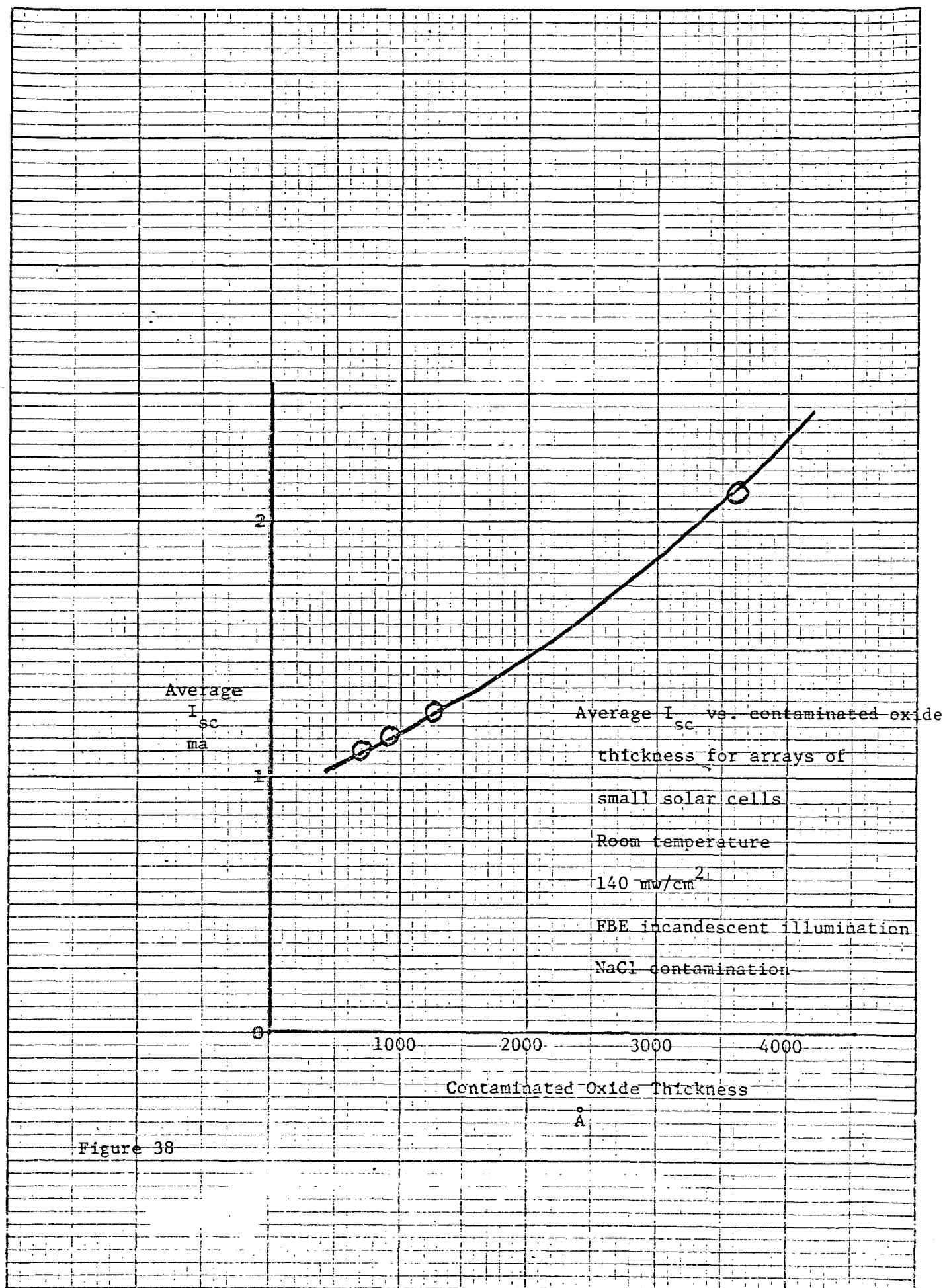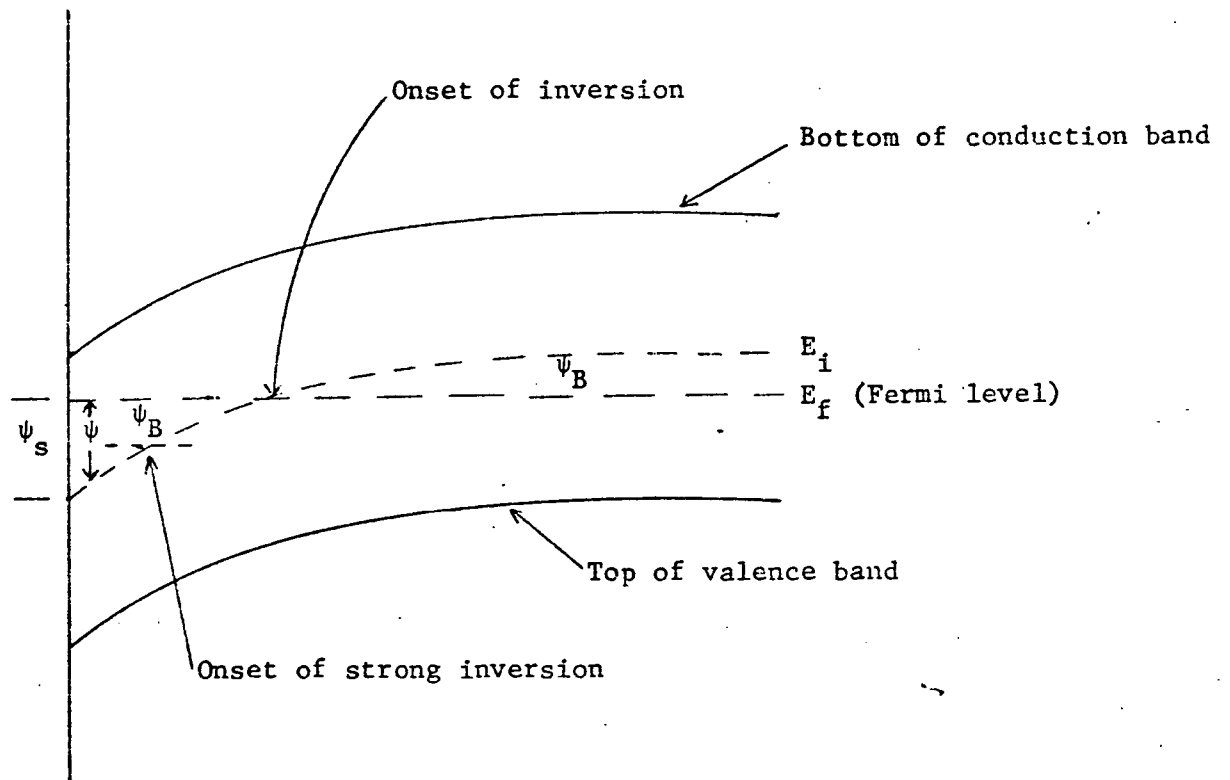
Figure 38

Figure 39

Band Structure of Semiconductor Surface
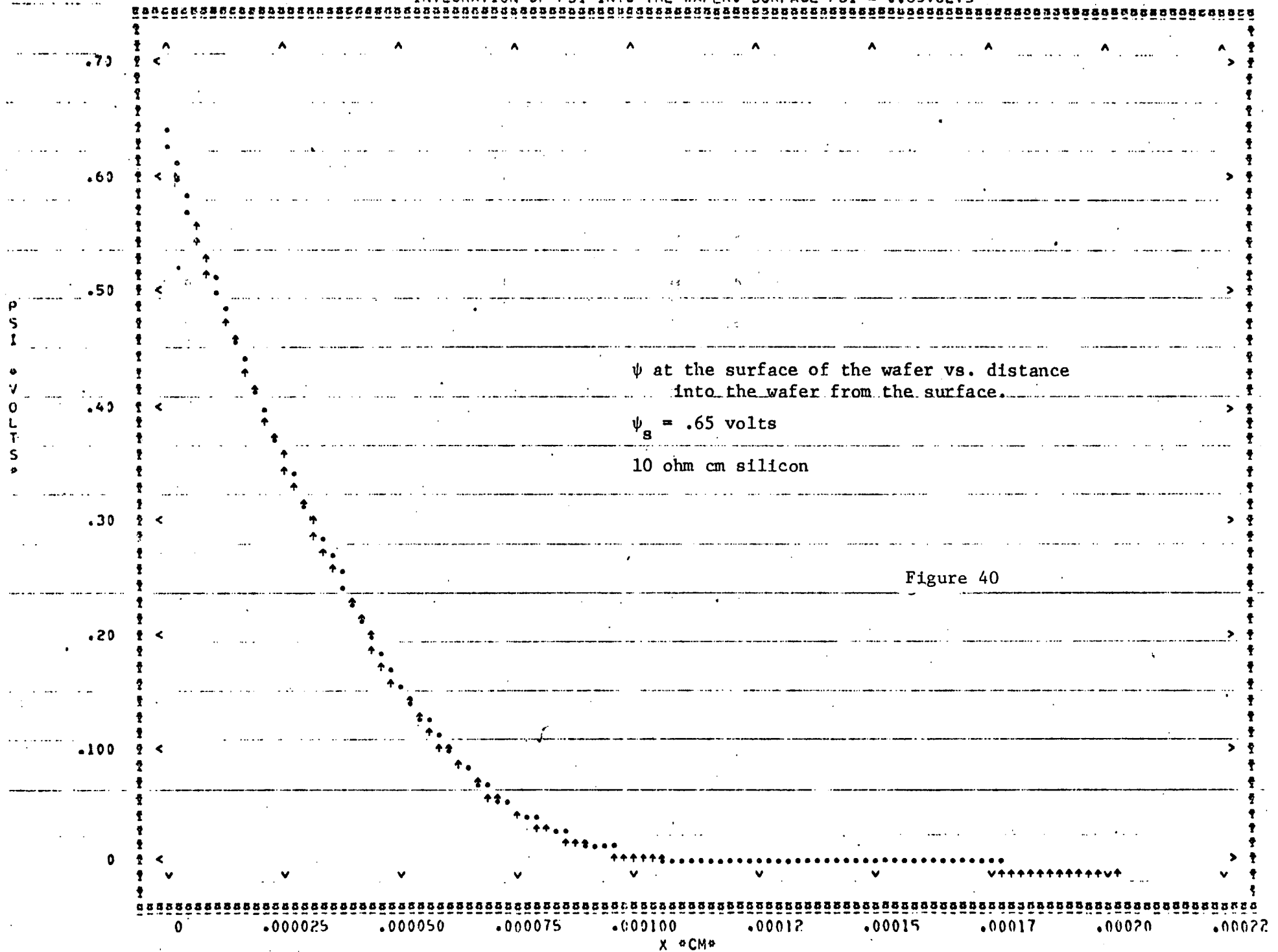
ψ at the surface of the wafer vs. distance
into the wafer from the surface.

ψ_s = .65 volts

10 ohm cm silicon

Figure 40

X *CM*

201 POINTS

ψ at the surface of the wafer vs. distance
into the wafer from the surface.

ψ_s = .7 volts

10 ohm cm silicon

Figure 41

201 POINTS

ψ at the surface of the wafer vs. distance
into the wafer from the surface.

ψ_s = .75 volts

10 ohm cm silicon
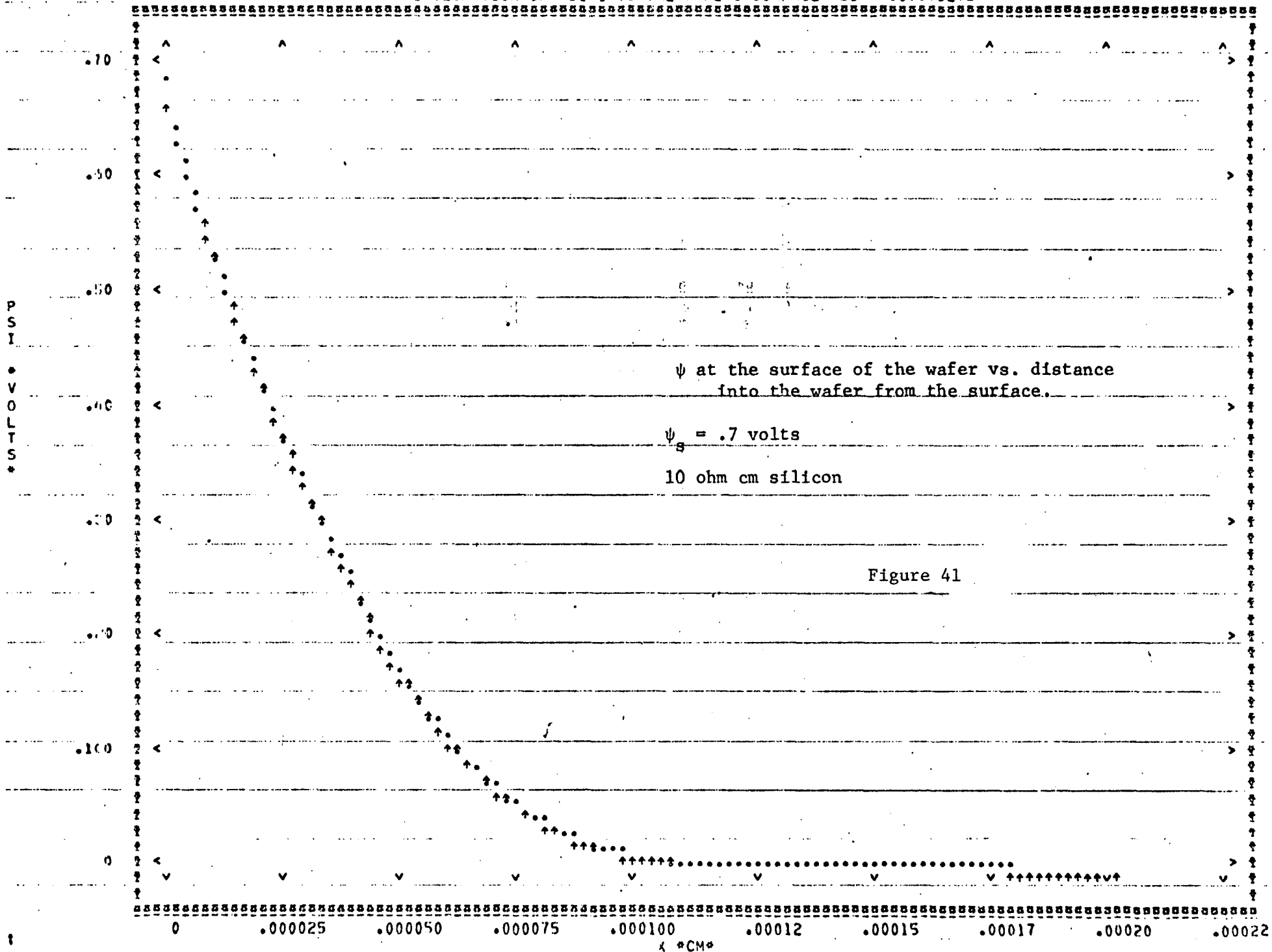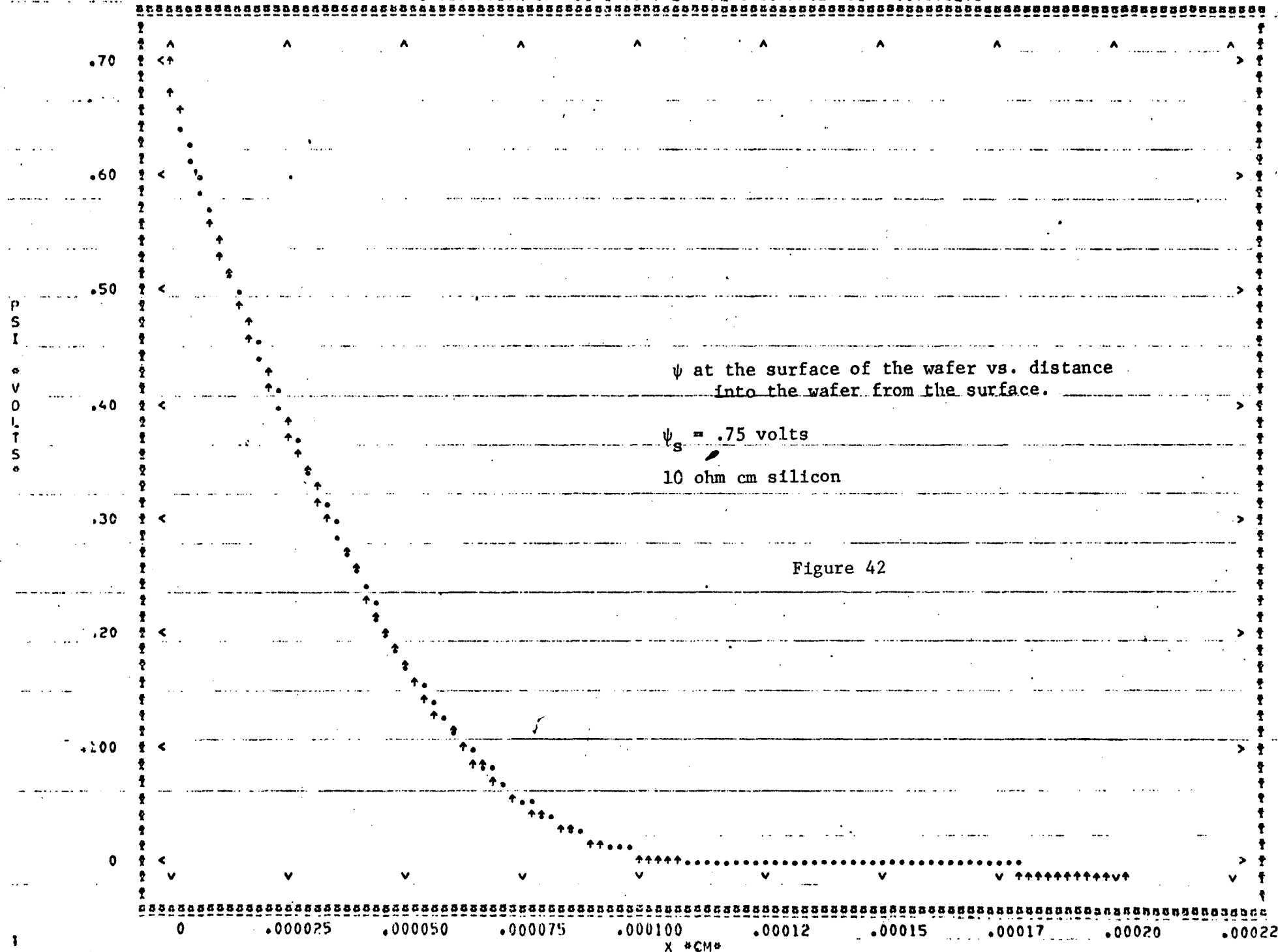
Figure 42

Curve of transparent electrode bias vs. surface potential Ψ_s for an oxide thickness of 6000Å. Points obtained from computer.

Figure 43

ELECTRON CONCENTRATION

```
        18.0    < 3

    L           3
    O           3
    G   17.5  < 3
                3
    1           3
    0           3
                3
    ^           33              Electron concentration vs. distance into the wafer
    C           3
    O   17.0  < 3
    N           3                        from the surface.
    C           33
    E           33
    N           333                           Figure 44
    T           33
    R                                                              Strong inversion points
    A   16.5  < 33    .75
    T               33
    I               33
    O       11      333
    N       111       333
    V       111      33                        ↓            ↓
            111    .65   333                   ↓            ↓
    o   16.0 <  111          33                ↓            ↓
    P          111         3333                ↓            ↓
    E           1111       3333                ↓            ↓
    R           1111     3333                  ↓            ↓
                11111      333                 ↓            ↓
    C           11111        33333   ↓         ↓            ↓
    C           11111       33333              ↓            ↓
    3   15.5 <    111111    ↓ 33333            ↓            ↓
                  111111      333333           ↓            ↓
                    111111  ↓      333333       ↓
                     111111  ↓        333333  ↓
                    ↓ 1111111   ↓     3333333  ↓
                        1111111   ↓      3333333
        15.0 <            111111111  ↓   333333333
                            ↓   111111111      333333333   333333
                                    111111111111
                                        11111111
        14.5 <
```
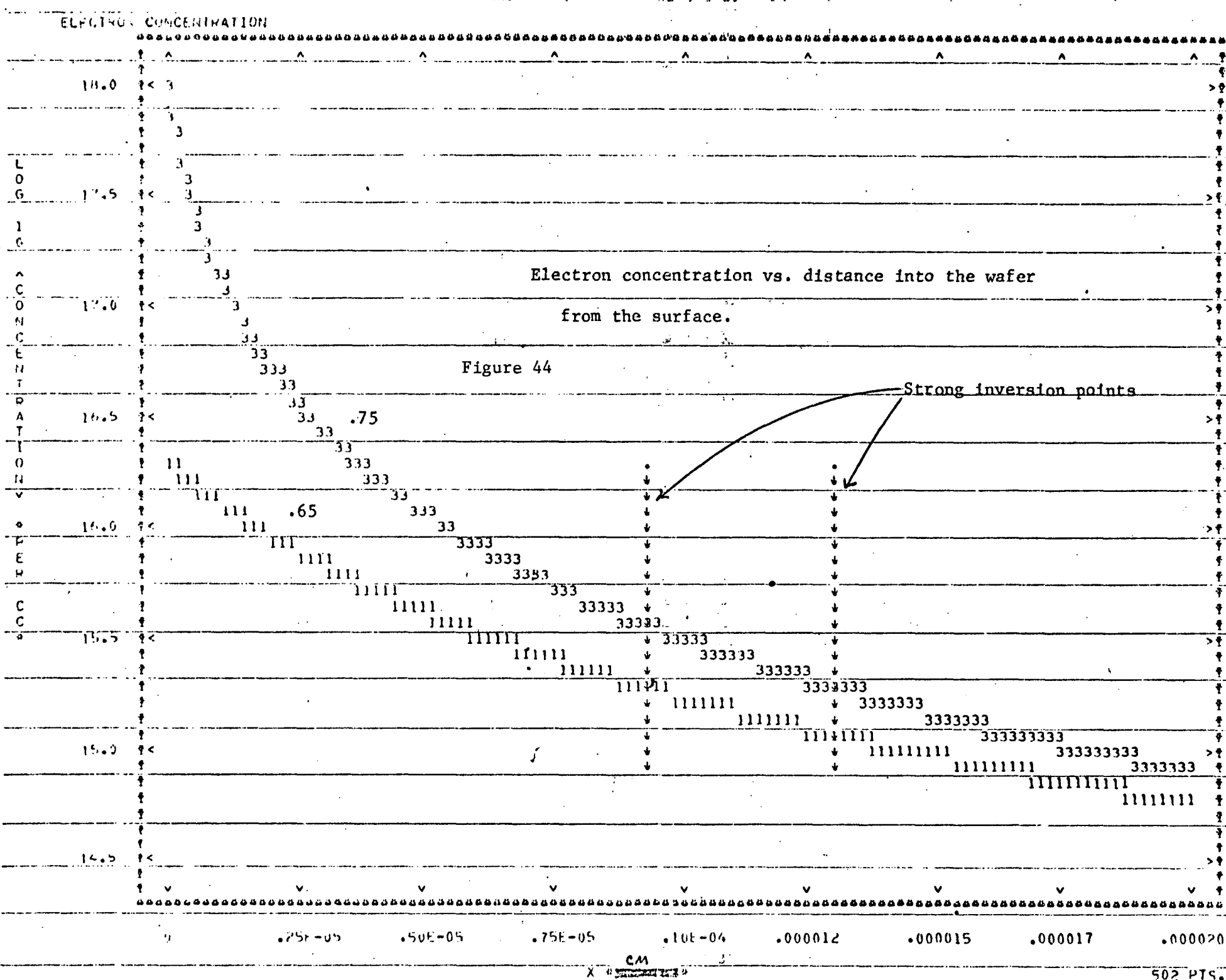
.25E-05   .50E-05   .75E-05   .10E-04   .000012   .000015   .000017   .000020

CM
X

502 PTS.

90

Conductance Between
N Diffusions vs. Transparent
Electrode Bias

Small Cell
Room Temperature
No Illuminations

Conductance
(milliohms)

Transparent Electrode Bias

Volts

Figure 45

Theoretical computer aided curve of effective mobility of electrons in the inversion layer vs. potential at the surface (ψ_s).

Figure 46

Conductance vs. transparent electrode bias for a small cell.

⊙ solid line - experimental points

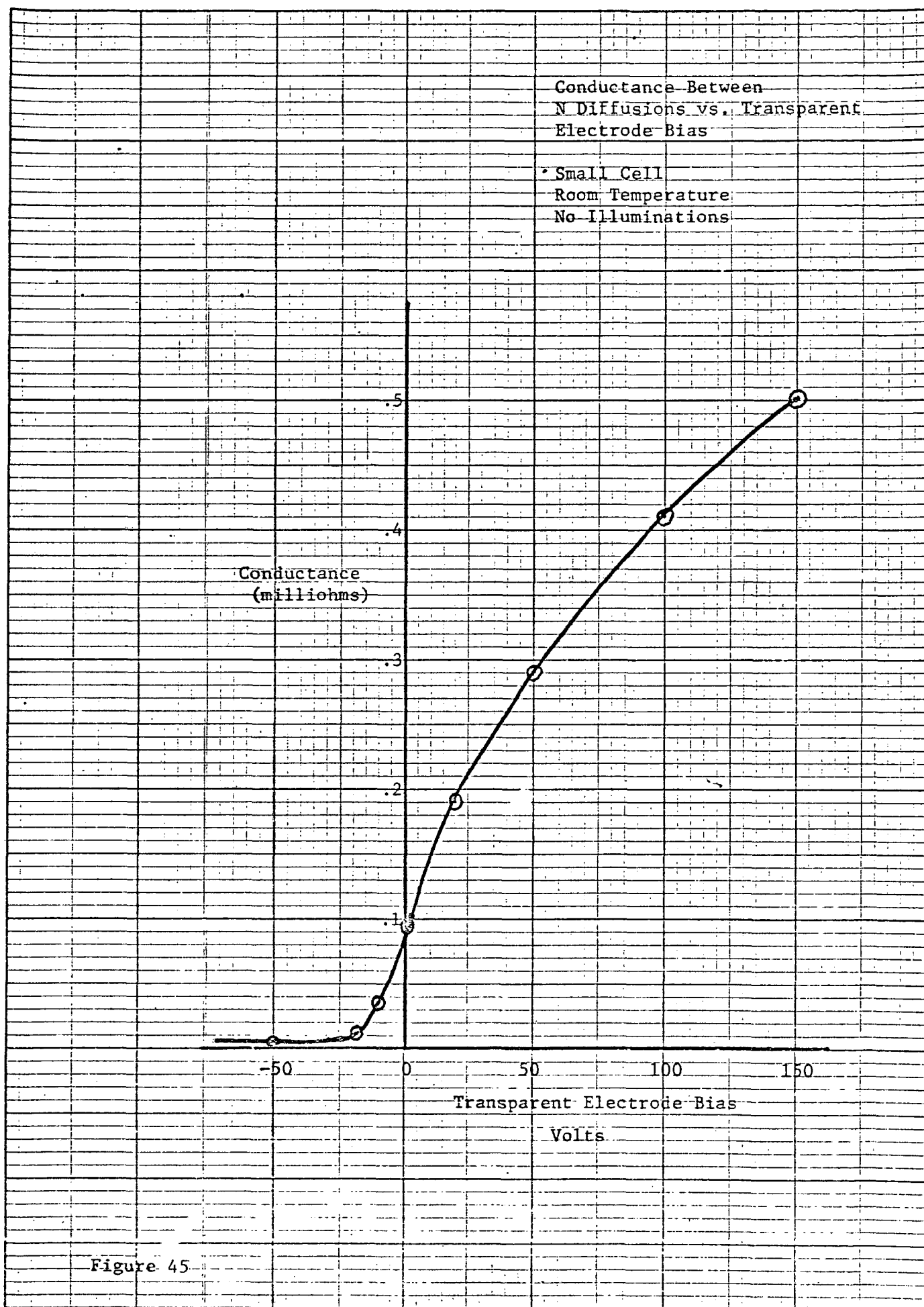+ dotted line - calculated points

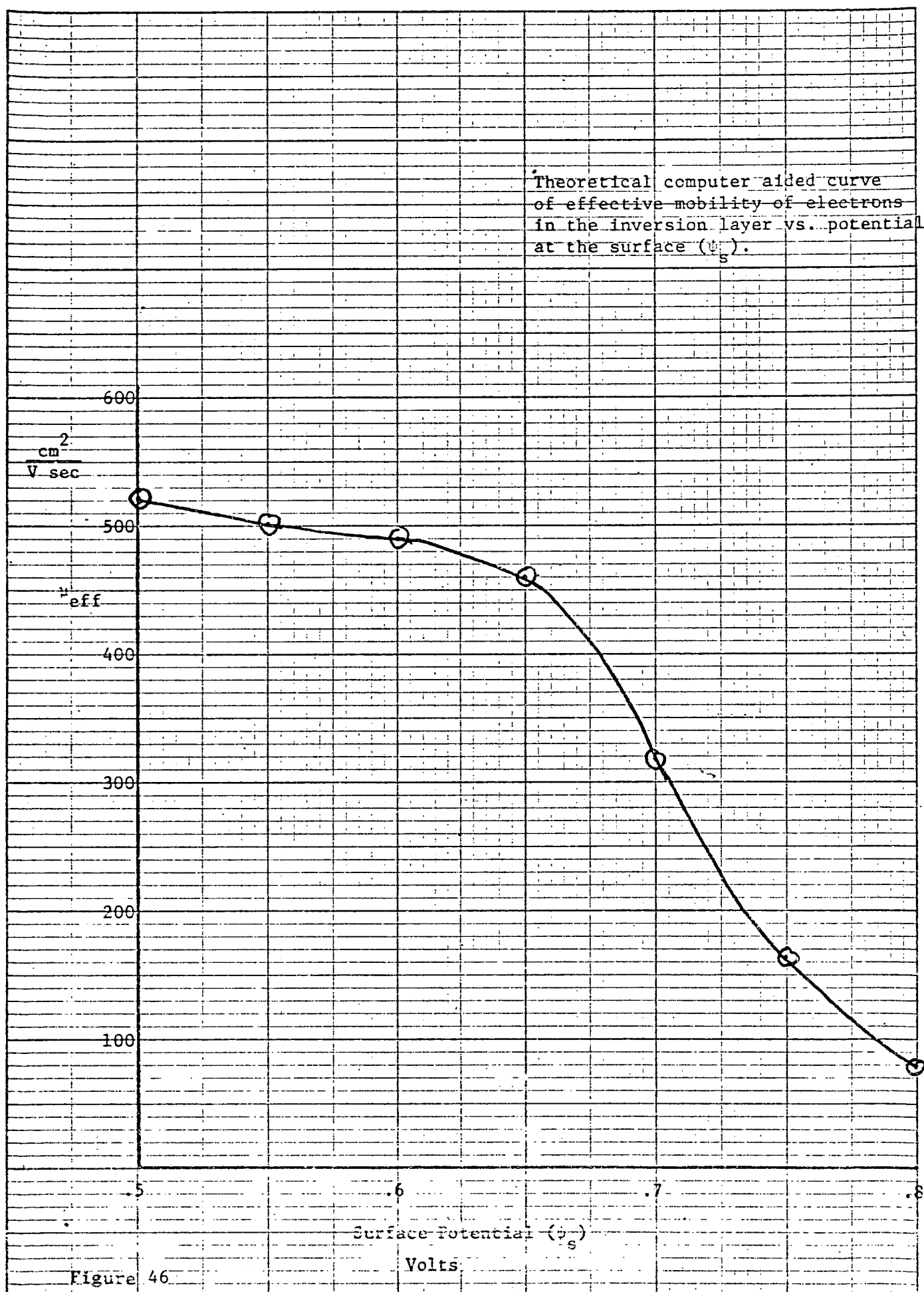Conductance (arbitrary scale)

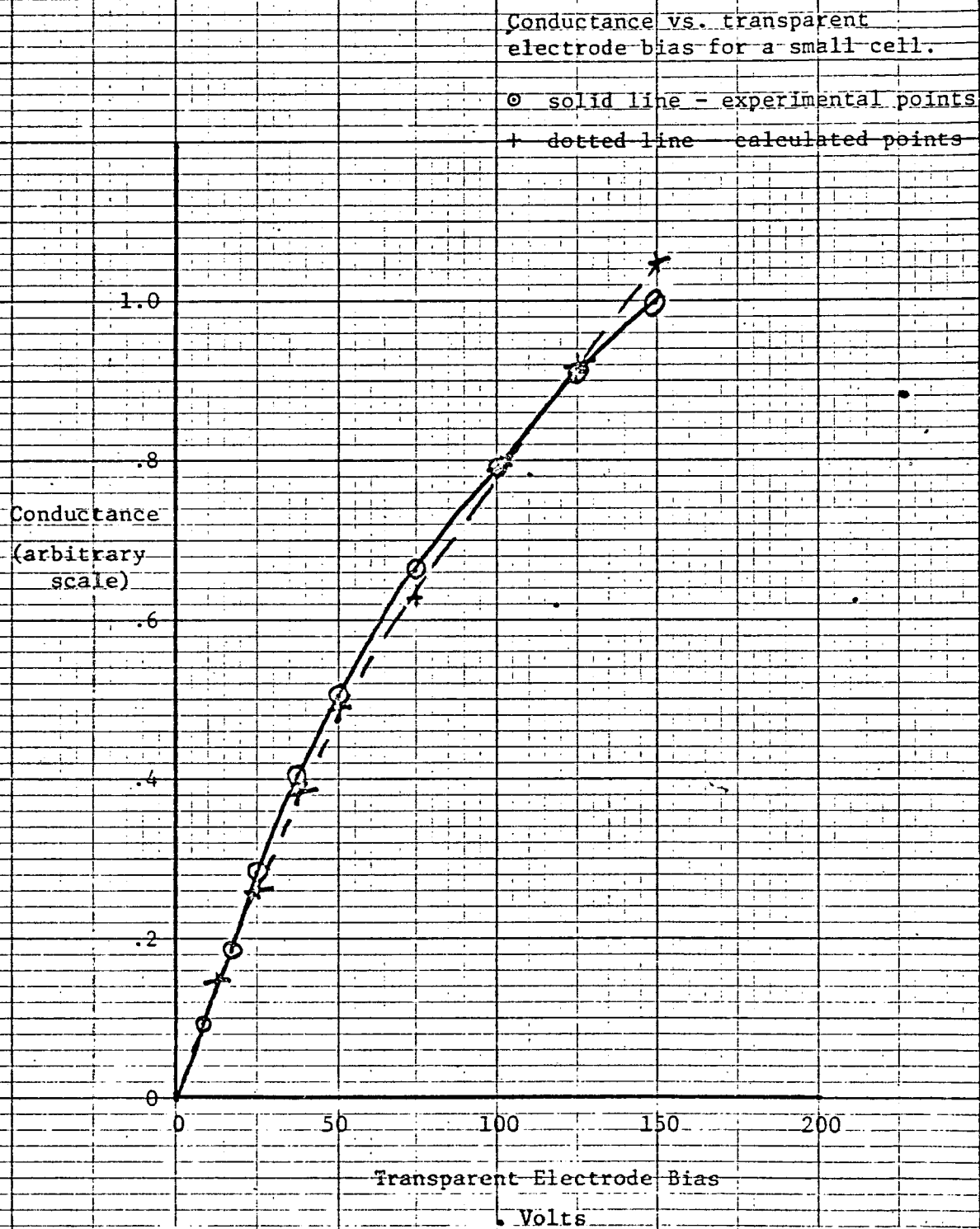Transparent Electrode Bias
Volts

Figure 47

C2

APPENDIX I

STANDARD PROCESSING SCHEDULE FOR
TRANSPARENT ELECTRODE CELLS

1. Clean wafer with chromic and nitric acids, organic solvents and short HF dips.

2. Grow 6000 $\overset{\circ}{A}$ of steam oxide.

3. Using photoresist techniques, etch oxide for diffusion.

4. Phosphorus predeposition at 1050°C.

5. Strip all oxide.

6. Drive in n type dopant (phosphorus) and grow silicon oxide to desired thickness at 1100°C.

7. Deposit transparent oxide (SnO_2) in special furnace apparatus.

8. Photoresist and etch SnO_2 to SiO_2 surface.

9. Photoresist and etch SiO_2 to Si surface.

10. Evaporate metal on wafer. (Aluminize)

11. Photoresist and etch metal.

12. Sinter.

13. Test.